

AD-753 397

AN INVESTIGATION OF NOISE GENERATION ON
A HOVERING ROTOR, PART II

H. Sternfeld, et al

Boeing Company

Prepared for:

Army Research Office (Durham)

November 1972

DISTRIBUTED BY:

NTIS

National Technical Information Service
U. S. DEPARTMENT OF COMMERCE
5285 Port Royal Road, Springfield Va. 22151

Unclassified
Security Classification

DOCUMENT CONTROL DATA - R & D

(Security classification of title, body of abstract and indexing annotation must be entered when the overall report is classified)

1. ORIGINATING ACTIVITY (Corporate author)		2a. REPORT SECURITY CLASSIFICATION	
The Boeing Company, Vertol Division		Unclassified	
		2b. GROUP	
		NA	
3. REPORT TITLE			
An Investigation of Noise Generation on a Hovering Rotor, Part II			
4. DESCRIPTIVE NOTES (Type of report and inclusive dates)			
Final Report: 1 Feb 71 - 31 Jul 72			
5. AUTHOR(S) (First name, middle initial, last name)			
H. Sternfeld		T. Fukushima	
C. Bobo		R. Spencer	
D. Carmichael			
6. REPORT DATE	7a. TOTAL NO. OF PAGES	7b. NO. OF REFS	
November 1972	100 106		
8a. CONTRACT OR GRANT NO.	9a. ORIGINATOR'S REPORT NUMBER(S)		
DAHCO4 69 C 0087	NA		
b. PROJECT NO.	9b. OTHER REPORT NO(S) (Any other numbers that may be assigned this report)		
c.			
d.			
10. DISTRIBUTION STATEMENT			
Approved for public release; distribution unlimited.			
11. SUPPLEMENTARY NOTES		12. SPONSORING MILITARY ACTIVITY	
None	Details of illustrations in this document may be better studied on microfiche.	U. S. Army Research Office-Durham Box CM, Duke Station Durham, North Carolina 27706	
13. ABSTRACT			
<p>This study is a natural extension of the program to investigate noise generation on a hovering rotor reported in Reference 1. That program acquired data on a large (60 ft.) diameter rotor operating on a whirl tower, and evaluated that data in the light of established analytical procedures. The work described in this report compares available data in order to investigate the effects of variations in rotor design. This data, which was available from other test programs included variations in number of blades of similar airfoil, airfoil, and planform. Also included is an evaluation of model testing by comparison of the results of the full size helicopter rotor with a one-eleventh scale model.</p>			
14. KEY WORDS			
Rotary Wings Shock waves Rotor Noise Planforms Helicopter noise Vortices			

I a

FORM 1473
NOV 68

REPLACES DD FORM 1473, 1 JAN 64, WHICH IS OBSOLETE FOR ARMY USE.

Unclassified

November 1972
D210-10550-1

AN INVESTIGATION OF NOISE
GENERATION ON A HOVERING ROTOR
PART II

by

H. Sternfeld
C. Bobo
D. Carmichael
T. Fukushima
R. Spencer

Prepared by

THE BOEING COMPANY, Vertol Division
Boeing Center, P.O. Box 16858
Philadelphia, Pennsylvania 19142

for

U.S. ARMY RESEARCH OFFICE - DURHAM
Durham, North Carolina

under

Contract DAHC04-69-C-0087

Approved for public release; distribution
unlimited.

I h

FOREWORD

This program was conducted as part of Contract DAHC04-69-C-0087 from the U.S. Army Research Office, Durham, North Carolina, under the technical cognizance of Mr. James Murray. The work was performed by the Boeing-Vertol Acoustics and Aerodynamics Research Staffs. The principal investigator and prime author was Mr. Harry Sternfeld, Jr., Supervisor of Acoustics. Individual contributors to each section were:

Rotor Noise Prediction:	D. Carmichael
Model Scaling:	T. Fukushima, H. Sternfeld
Effects of Rotor Design:	R. Spencer, H. Sternfeld
Impulsive Noise:	C. Bobo, T. Fukushima

TABLE OF CONTENTS

	<u>Page</u>
FOREWARD	iii
1.0 ABSTRACT	1
2.0 ROTATIONAL NOISE PREDICTION METHODS	2
2.1 INTRODUCTION	2
2.2 DEVELOPMENT OF A COMPUTER PROGRAM	3
2.3 SENSITIVITY STUDIES OF AERODYNAMIC LOADINGS	4
2.3.1 Radial Distribution of Loads	5
2.3.2 Harmonic Distribution of Loads	6
2.3.3 Phasing of Loading Harmonics	6
2.4 MODIFICATION OF COMPUTER PROGRAM TO USE SIMPLIFIED INPUTS	6
2.4.1 Basic Approach	6
2.4.2 Assumed Loading Laws	7
2.4.3 Computational Simplifications	8
2.5 CONCLUSIONS	9
3.0 COMPARISON OF FULL SCALE AND MODEL ACOUSTICAL DATA	22
3.1 ROTATIONAL NOISE	22
3.1.1 Theoretical Development	22
3.1.2 Comparison of Measured and Predicted Data	25
3.2 BROADBAND NOISE	26
4.0 EFFECT OF ROTOR DESIGN	43
4.1 INTRODUCTION	43
4.1.1 Description of Rotors	43
4.2 EFFECT OF AIRFOIL SECTION	44
4.3 EFFECT OF PLANFORM	44
4.4 EFFECT OF COMBINED PLANFORM AND AIRFOIL EFFECTS	44
4.5 COMPARISON OF WAVEFORMS	45
4.6 EFFECT OF NUMBER OF BLADES ON ROTATIONAL NOISE	46
5.0 HOVERING SINGLE ROTOR IMPULSIVE NOISE	67
5.1 SUMMARY	67
5.2 CRITERIA FOR HOVERING SINGLE ROTOR IMPULSIVE NOISE GENERATION	68
5.3 MECHANISM OF VORTEX INTERACTION	70
5.3.1 Sound Pressure Level	74
5.3.2 Calculation of Sound Pressure Level	74

TABLE OF CONTENTS (Continued)

	<u>Page</u>
REFERENCES	94
APPENDIX WHIRL TOWER FREQUENCY CALIBRATION	96

1.0 ABSTRACT

This study is a natural extension of the program to investigate noise generation on a hovering rotor reported in Reference 1. That program acquired data on a large (60 ft.) diameter rotor operating on a whirl tower, and evaluated that data in the light of established analytical procedures. The work described in this report compares the Reference 1 information with other available data in order to investigate the effects of variations in rotor design. This data, which was available from other test programs included variations in number of blades of similar airfoil, airfoil, and planform. Also included is an evaluation of model testing by comparison of the results of the full size helicopter rotor with a one-eleventh scale model.

A separate portion of the original test program evaluated the effect of tip vortex strength and trajectory on the impulsive (or "banging") noise generated by a hovering rotor. It was found that although intersections between the generated vortex and a following blade occurred over a wide range of operating conditions, this condition, by itself, did not result in the generation of an impulsive acoustical signature. Reference 1 hypothesized that this noise might be associated with an attached shock wave which, under certain conditions, might undergo rapid chordwise displacement thereby radiating sharp pressure disturbances. This concept is further examined in Section 5 of this report.

2.0 ROTATIONAL NOISE PREDICTION METHODS

2.1 INTRODUCTION

The problem of predicting helicopter rotor rotational noise has been treated by numerous investigators, one of the most comprehensive studies of the subject being that of Lawson and Ollerhead (Reference 2). After carefully deriving the equations governing rotor noise generation, they develop two different calculation methods. The first, code named HERON I, is designed to do very exact calculations using high speed digital computers. The limitation of this method is that it requires extensive aerodynamic blade loading data for input, which is generally not available, or at best, exists for only several harmonics of the rotational frequency. On the other hand, in their HERON II method, they make a variety of blade loading assumptions and computational simplifications to come up with a series of design charts which are quite simple and convenient to use. Reference 1 shows that noise predictions based on the HERON II method agree quite well with measured data for the first 3 or 4 harmonics of noise, after which the method progressively underpredicts.

The primary objective of the present study is to develop a method which produces accurate predictions for more noise harmonics than HERON II does, without requiring a great body of aerodynamic loading data, as required by HERON I. In particular, there is a need to determine if the inaccuracies of HERON II are due to the blade loading assumptions used, or to the computation simplifications used, or to both. With these objectives in mind, the following plan of work has been followed:

- (1) Develop a versatile computer program which would perform the same basic functions as HERON I but without requiring a large computer with disk storage. This program would have advantages over HERON I such as fast turnaround time and the facility for multiple and frequent changes, and would thus be a useful tool for performing parametric studies to evaluate the influence of each variable on noise generation.
- (2) Perform sensitivity studies to evaluate the importance of planform loading distributions, phasing of blade loading harmonics, etc., on noise generation.
- (3) Modify the computer program to have the capability of assuming a generalized blade loading distribution, so that only basic operational parameters (thrust, RPM, dimensions, velocities) need be used for input.

2.1 INTRODUCTION (Continued)

(4) Check out Lawson and Ollerhead's computational simplifications by comparing exact with simplified calculations.

(5) Adjust blade loading assumptions to make noise predictions agree with measured data, thus empirically deriving blade loadings from noise data.

It was found that Lawson and Ollerhead's computational methods are generally quite accurate, and that greatly improved correlation with measured data is possible through small changes in the assumptions of blade loading harmonic decay. Noise predictions were found to be very sensitive to the precise blade loading harmonic assumptions used. This fact helps to explain the large scatter observed in the measured data, since blade loadings are undoubtedly affected by wind conditions, interaction with the wakes of other blades, and other random phenomena.

2.2 DEVELOPMENT OF A COMPUTER PROGRAM

A computational tool such as HERON I was needed to carry out the desired studies, but HERON I was found to be rather awkward to use because of the large computational requirements. Therefore, Lawson and Ollerhead's basic equations were re-programmed using a much simplified calculation procedure requiring less storage and calculation time, and thus suitable for a WATFOR compiler system of FORTRAN IV, which has the advantages of simplified input formatting and very fast turnaround time. In addition, this system allows for program changes by simply switching or adding cards. Thus, various assumptions of rotor aerodynamic loading could be built into the program, while maintaining a high degree of mathematical accuracy. Ultimately, after many modifications, this program was used as the framework for the desired prediction method.

The heart of this program (as well as HERON I and HERON II) is equation 21 of Reference 2, which can be written in the following form:

$$P = \frac{X_i - Y_i}{4\pi a_c r^2 (1-M_r)^2} \left(\frac{\partial F_i}{\partial t} + \frac{F_i}{1-M_r} \cdot \frac{\partial M_r}{\partial t} \right)$$

2.2 DEVELOPMENT OF A COMPUTER PROGRAM (Continued)

where p is the instantaneous pressure at a point x_i due to a force disturbance F_i at a point y_i which occurred at some previous time. Lowson does not use this equation directly, but develops other equations from it, employing retarded times, Bessel functions, and a variety of coordinate systems. The newly developed program, however, does use the above equation directly. For each of a predetermined number of azimuthal positions of the most outboard radial station, the program calculates and stores sound pressures and propagation times to produce a pressure-time history, adds the effects of the other radial stations to produce a pressure-time history for one blade, and then adds in the effects of the other blades, taking into account the appropriate phase shifts. Finally, after the program has produced the pressure-time history for one blade passage period, it performs a Fourier analysis to get the level of each sound harmonic.

2.3 SENSITIVITY STUDIES OF AERODYNAMIC LOADINGS

One of the most fundamental requirements of any rotor noise computational program is aerodynamic blade loading data as a function of position and time. Aerodynamicists have learned to predict with varying degrees of accuracy such parameters as lift and drag coefficients, aerodynamic angles of attack, and local velocity components at various locations over the rotor disk. From such data, aerodynamic forces (lift and drag) can be calculated. A number of questions arise, however, regarding the suitability of such data for calculating noise. Certain parameters, which may need to be specified with great accuracy to calculate rotor performance can perhaps be ignored in calculating noise, while other parameters which have a significant effect on noise generation may be to a large extent unknown because there never has been a need to define them. Therefore, the major objective of this section is to evaluate the sensitivity of noise generation to a number of different aspects of aerodynamic blade loadings.

Radial distribution of airloads is fairly well understood. Figure 2.1 shows a typical distribution of lift and drag on a blade as predicted for a hovering rotor. In this case, the lift forces are defined as being those which are parallel to the rotor shaft, and the drag forces are defined as being in the plane of the rotor. Only a small part of the drag shown is due to form drag; most of the drag is from the induced forces in the drag direction. The radial lift and drag distributions can be varied

2.3 SENSITIVITY STUDIES OF AERODYNAMIC LOADINGS (Continued)

somewhat by varying twist, RPM, airfoil shape, etc., according to the performance requirements of the helicopter. Such changes can have quite significant effects on performance. On the other hand, performance is relatively insensitive to minor perturbations of blade loading as the blade rotates, since these effects tend to cancel each other and have little or no net effect on aircraft performance. However, it is believed that these azimuthal perturbations have a great deal of effect on noise generation. To more fully understand the situation, numerous hypothetical blade loadings as a function of position and time have been used as input to the computerized prediction method, and the results are presented below.

2.3.1 Radial Distribution of Loads

Noise calculations were made for the steady blade loadings presented in Figure 2.1, for incremental 1 ft. blade sections. Both incremental and cumulative effects are presented in Figure 2.2. It is to be observed that the areas near the tip are by far the most important. In fact, ignoring the inner two-thirds of the blade produces an error of less than 1 dB. It was suspected that within practical limits the shape of the spanwise loading distribution has a relatively minor effect on noise. Partly to evaluate this hypothesis, noise was calculated for several spanwise loading approximations shown in Figure 2.3. Table 2-I compares calculated noise levels of these simplified loadings with the levels of the complicated loading shown. It is apparent that such complicated loadings can indeed be approximated by simplified geometrical patterns without serious error. Section 4 discusses the effects of blade design on a spanwise loading distribution. Since spanwise loading differences are normally rather small between helicopter rotors (because of design restraints imposed for performance and structural reasons), only very minor differences would be expected in noise generation. However, if major design differences exist, such as would be found between a helicopter rotor and the highly twisted configuration used for tilt rotor vehicles, perhaps the effects on noise would be noticeable, since the center of lift could be moved inboard, where the velocity is less.

2.3.2 Harmonic Distribution of Loads

To evaluate the sensitivity of noise generation to the order of blade loading harmonics, noise spectra were calculated for individual harmonics, one at a time. The results are shown in Figure 2.4 for a load of 1000 lb. (peak) exerted at the tip. It is noteworthy that noise generation sensitivity increases with blade loading harmonic number. This is undoubtedly because there is a frequency term in the force derivative, $\partial F/\partial t$, appearing in the above equation of Lawson and Ollerhead. In reality, blade loading harmonics drop off rapidly with frequency, but are still very important for noise generation, not only because of the above reason, but also because for the higher noise harmonics in particular, many loading harmonics can have a large cumulative effect, even though no particular loading harmonic is likely to be very important by itself.

2.3.3 Phasing of Loading Harmonics

A study was performed to determine if the phasing of any one loading harmonic with respect to the observer has a significant effect on the observed noise. Harmonic loads of varying phase angle were fed into the computer program. The results are shown in Table 2-II. The conclusion is that any phase angle can be used without serious error.

Another study was performed to see if the relative phasing of two or more loading harmonics with respect to each other is important. In this case, very large differences in noise level were observed, Table 2-III, apparently because of localized cancellations and additions. Since precise harmonic phasing of the airloads cannot be determined (being to a large extent a function of wind and other random factors), the most logical assumption is that each loading harmonic is randomly phased with respect to the others. Of course, such an assumption is not necessarily true for a specific situation. Relative phasing of loading harmonics could certainly be a factor in the large observed scatter of experimental data.

2.4 MODIFICATION OF COMPUTER PROGRAM TO USE SIMPLIFIED INPUTS

2.4.1 Basic Approach

The level of each noise harmonic in the non-rotating system is made up of contributions from a number of different blade loading harmonics. If it is assumed that these loading harmonics are phased randomly with respect to each other, then the level of each noise harmonic can be ob-

2.4.1 Basic Approach (Continued)

tained by adding incremental contributions from the significant loading harmonics on an energy (pressure squared) basis. Therefore, a decision was made at the end of the sensitivity study to modify the program to have the computer perform such a function, while at the same time making generalized assumptions about the spanwise loading distribution and the blade loading harmonic decay, thus producing a program which would serve the same function as HERON II.

Starting with the steady loading component, the program calculates the noise spectrum for each blade loading harmonic, the total number of which is a function of the number of blades and the number of noise harmonics desired. Values of pressure squared are stored in a two-dimensional array as a function of blade loading harmonic number and noise harmonic number. Finally, these values are sorted and the level of each noise harmonic is obtained by adding the incremental contributions from the various loading harmonics.

2.4.2 Assumed Loading Laws

The program was initially modified to assume six radial loading positions on each blade, using the distribution described by curve C of Figure 2.3. Later, it was found that computer time could be saved, without serious loss of accuracy, by assuming a concentrated load at a single point on each blade. The critical assumption turned out to be the decay rate of the loading harmonics. Figure 2.5 shows the markedly different noise spectra that were calculated using loading laws which differed only slightly from each other. Curve A is based on the same loading law used for HERON II. Here, the first loading harmonic has a peak value equal to the steady, and the other harmonics decay at a rate proportional to $\lambda^{-2.5}$, λ being equal to 1 for the first loading harmonic, 2 for the second, etc. Curve B shows the effect of assuming a λ^{-2} decay rate. Curve C shows the additional effect of beginning the decay with the first rather than the second loading harmonic. (In other words, the first loading harmonic has a peak value of 1/4 of the steady, the second, 1/9, etc.). This latter choice appears to produce excellent agreement of calculated with test data, as can be seen in Figures 3.7-3.9.

2.4.2 Assumed Loading Laws (Continued)

It is interesting to note that Lowson and Ollerhead recommend a λ^{-2} decay rate, based on data of Scheiman. The reason they use a $\lambda^{-2.5}$ decay rate for HERON II is to account for assumed random phasing (lack of correlation) of noise generated at different stations along the span of the blade. However, it is quite likely that correlation is actually good, since most of the noise is generated over a relatively small part of the blade near the tip.

2.4.3 Computational Simplifications

Lowson and Ollerhead use several computational simplifications which deserve closer investigation, although they seem reasonable. One of their more basic assumptions is that drag forces are equal to 1/10 of the lift forces. Figure 2.1 indicates that this is a fair assumption. To further check on the validity of this assumption, a comparison has been made between noise levels calculated using the actual lifts and drags shown in Figure 2.1 and noise levels calculated using the same lifts but drags equal to 1/10 of the lifts. The maximum error, occurring in the plane of the rotor, where only the drag forces are of significance, is still less than 1 dB. At large angles from the rotor plane, the drag forces have very little influence at all on the noise radiation.

Another assumption used by Lowson and Ollerhead is that the lift and drag forces are concentrated at the 80% radius position on the blades. To check out this assumption, noise calculations were performed with the loads concentrated at several radial positions (90%, 85%, 80%, 75%). In Table 2-IV, these noise levels are compared with noise levels calculated using six radial loading positions, based on the distributions of Figure 2.1 and Curve C of Figure 2.3. The 80% choice appears to be quite good for some of the higher harmonics, but the predictions seem to be a bit low for the lower harmonics. The errors are not very great for any of the cases, however, so this seems like a reasonably good assumption.

Lowson and Ollerhead discuss the matter of the number of loading harmonics needed to calculate a given noise harmonic, and come up with the following relationship for the range needed:

$$m B (1 - M) < \lambda < m B (1 + M)$$

2.4.3 Computational Simplifications (Continued)

where m is the order of the noise harmonic, B is the number of blades, M is the tip Mach number, and λ represents the range of loading harmonics needed. Thus, to calculate the tenth noise harmonic for a three bladed rotor with a tip mach number of .76, loading harmonics number 7-53 would be needed. However, Lowson and Ollerhead base this conclusion on the assumption that all loading harmonics are of equal amplitude, when in fact they are normally dropping off with increasing frequency. Therefore, a simple study has been performed to determine if such a large number of loading harmonics is really needed. Using the λ^{-2} decay rate, noise has been calculated for a large number of individual loading harmonics, and the contributions added together, starting with the steady loading, to determine the point where individual loading harmonics are no longer significant. Results are shown in Figures 2.6 and 2.7 for fifth and tenth noise harmonics respectively. In Figure 2.6, the curve showing the incremental effects would be symmetrical about $\lambda = 15$ with significant values from $\lambda = 4$ to $\lambda = 24$ if all loading harmonics were of the same magnitude, but because of the decay, all the loading harmonics beyond $\lambda = 9$ contribute less than 1/2 dB to the total. An automatic cutoff has been included in the program to limit the number of loading harmonics, based on what has been empirically found to be necessary for the highest noise harmonic of interest. Cutoff points are shown in Figures 2.6 and 2.7 for the cases shown.

2.5. CONCLUSIONS

This work has shown that Lowson and Ollerhead's calculation procedures are basically sound, and that only a few minor corrections are necessary to their assumptions to obtain good correlation between calculated and measured data. Another calculation procedure has been produced which gives good correlation with test data for a wide range of thrusts, RPMs, and rotor diameters. However, there is still a great deal of work yet to be done in understanding and predicting helicopter rotor rotational noise. Good correlation has been shown here only for test stand data, simulating a hovering single rotor helicopter. Other types of aircraft in other types of situations would presumably have other types of blade loading harmonic distributions. Work recently done under an Army program (Reference 3), for instance, has indicated that a $\lambda^{-1.4}$ decay rate is probably more accurate than the λ^{-2} decay rate for the case of an overlapped tandem rotor. In addition, the decay rate is very likely less for high speed conditions than for

2.5 CONCLUSIONS (Continued)

hover conditions. Certainly, when a rotor at very high speeds encounters drag divergence and produces a "Mach bang", the loading harmonic structure is radically different from hover conditions. On the other hand, if absolutely quiescent conditions could be achieved, (perhaps for an aircraft hovering on a windless day, out of ground effect) the loading harmonic decay rate might be greater than λ^{-2} . These questions cannot be answered without more test data, either in the form of noise measurements, blade loading measurements, or, preferably, both. Finally, some work should be done to help explain the great scatter of test data which has been observed. It has been suggested above that the scatter is associated with wind and other random phenomena, but considerable scatter exists between points even after the data has been averaged for 30 seconds or more.

TABLE 2-1

EFFECT OF SPANWISE LOADING APPROXIMATIONS ON NOISE

Loading Curves of Fig. 2.3

Noise Harmonic	Curve A	Curve B	Curve C	Curve D
1	102.1dB	101.7dB	102.5dB	102.6dB
2	96.6	95.7	96.9	97.1
3	90.8	89.4	91.1	91.8
4	85.1	83.2	85.4	85.5
5	79.4	77.2	79.7	79.8
6	73.8	71.3	74.2	74.2
8	62.8	59.6	63.2	63.2
10	53.0	49.5	53.4	53.4

TABLE 2-II

EFFECT OF AIRLOAD HARMONIC PHASING ON ROTOR NOISE

1000 lb. Peak Lift at Tip

Noise Harmonic	Airload Harmonic	1	2	3	4	9
1		± 1.0	± 0.1	± 0.1	± 0.1	
2		± 1.1	± 0.2	± 0	± 0	
3		± 1.0	± 0.2	± 0.1	± 0	
4		± 1.2	± 0.2	± 0	± 0.1	
5		± 1.2	± 0.2	± 0.1	± 0.1	
6		± 1.3	± 0.3	± 0.1	± 0.1	± 0.1
7				± 0.2		± 0.1
8		± 1.4	± 0.3	± 0.2	± 0.1	± 0.1
9						± 0.1
10		± 1.4	± 0.4		± 0.5	± 0.2

NOTE:

Numbers shown as \pm dB are the range of variation obtained by varying noise and airload harmonic phasing by 15° increments.

TABLE 2-III

EFFECT OF RELATIVE PHASING OF LOADING HARMONICS

Noise Harmonic	Loading Harmonics			
	Steady & 1	3 & 4	6 & 7	8 & 9
1	±7.4 dB	±5.2 dB	±2.4 dB	
2	±7.2	±9.9	±3.2	±10.6 dB
3	±7.1	±7.6	±5.7	
4	±7.1	±5.9	±5.3	±5.1
5	±7.1	±5.2	±15.4	±3.4
6	±7.1	±4.9	±9.0	±7.3
7	±7.1	±4.7	±7.3	±9.5
8	±7.1	±4.5	±6.4	±8.1
9	-	-	±5.7	±7.2
10	±7.2	±4.6	±5.6	±6.9

NOTE:

Numbers shown as ±dB are the range of variation obtained by varying relative phasing between adjacent, equal amplitude loading harmonics by 15° increments.

TABLE 2-IV

EFFECT OF BLADE LOADING APPROXIMATIONS
ON SOUND PRESSURE LEVEL

Noise Har- monic	6 Radial Stations Precise Loading* Curve A	6 Radial Stations Simplified Loading* Curve C	Percent Radius			
			.90	.85	.80	.75
			Concentrated Loadings			
1	113.1 dB	110.7 dB	112.5 dB	111.7 dB	111.0 dB	110.2 dB
2	108.9	106.3	109.4	107.7	106.1	104.4
3	104.0	101.5	105.1	102.8	100.8	98.8
4	99.2	97.2	100.9	98.3	96.5	94.6
5	94.8	93.5	97.4	94.8	93.5	91.6
6	91.1	90.4	94.7	92.1	91.2	89.1
7	88.1	88.0	92.6	89.9	89.2	86.9
8	85.5	85.7	90.7	87.7	87.4	84.4

* Reference Figure 2.3

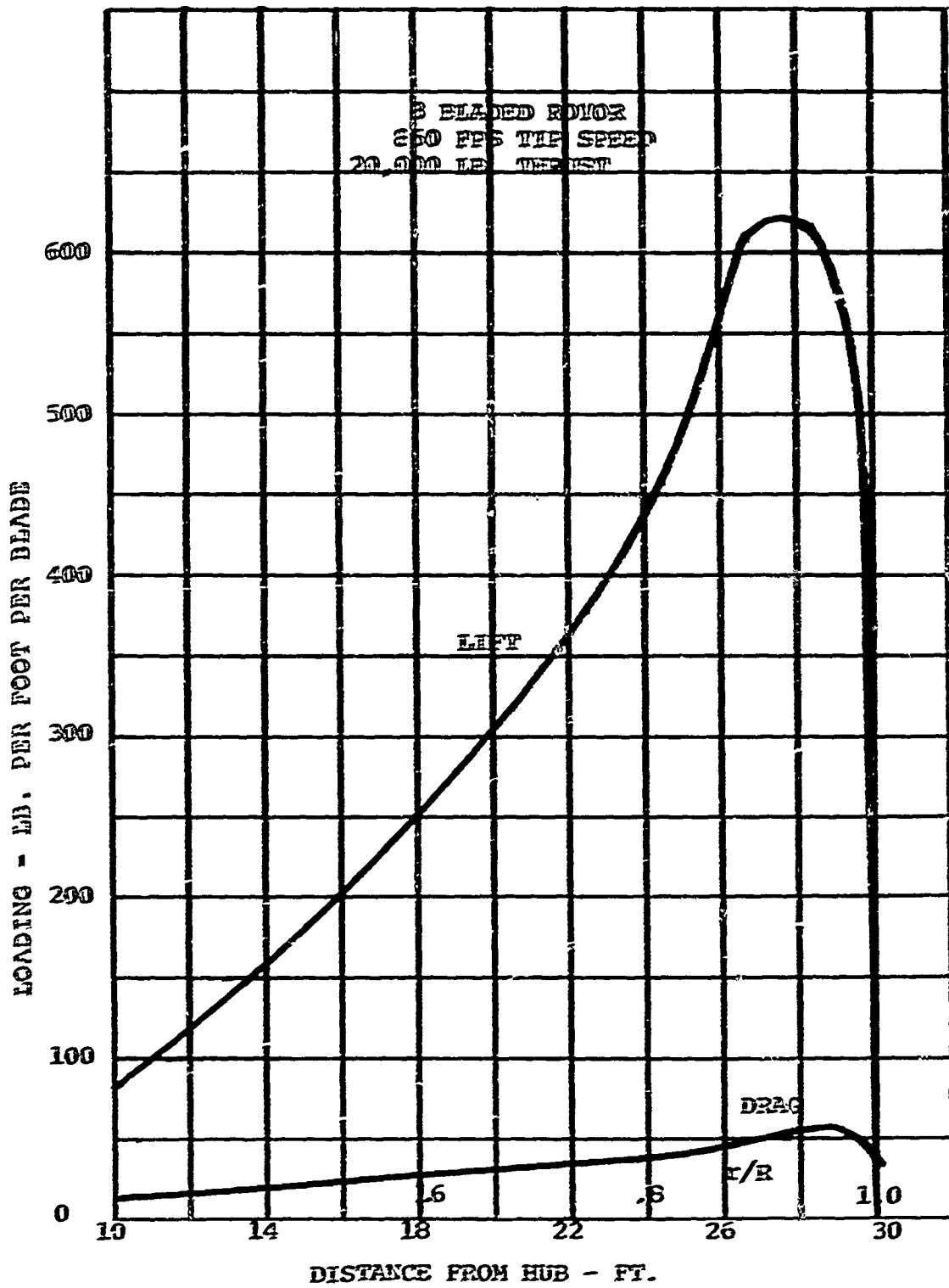


FIGURE 2.1 RADIAL DISTRIBUTION OF BLADE LOADINGS

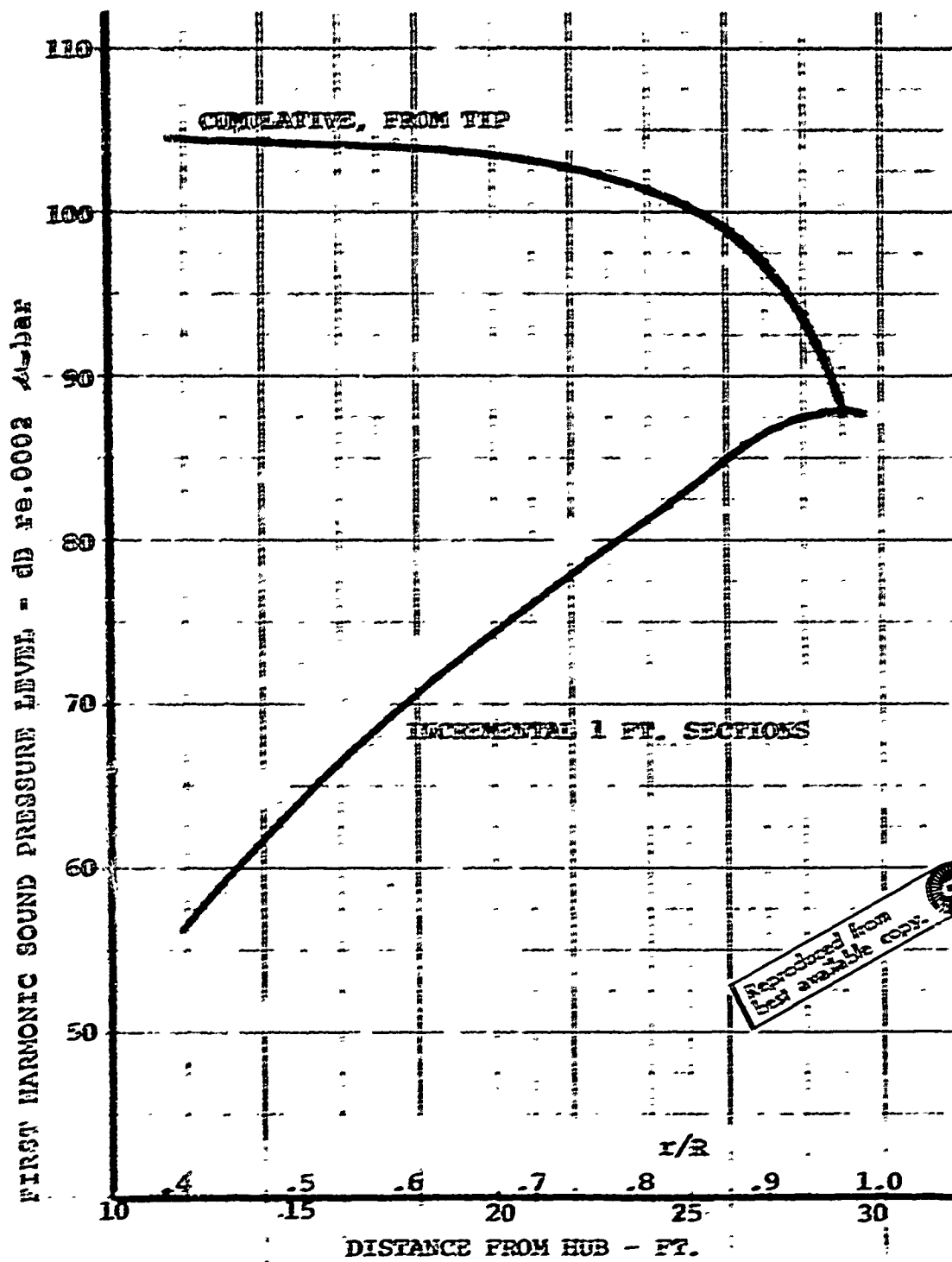


FIG. 2.2 INFLUENCE OF EACH RADIAL STATION ON TOTAL NOISE

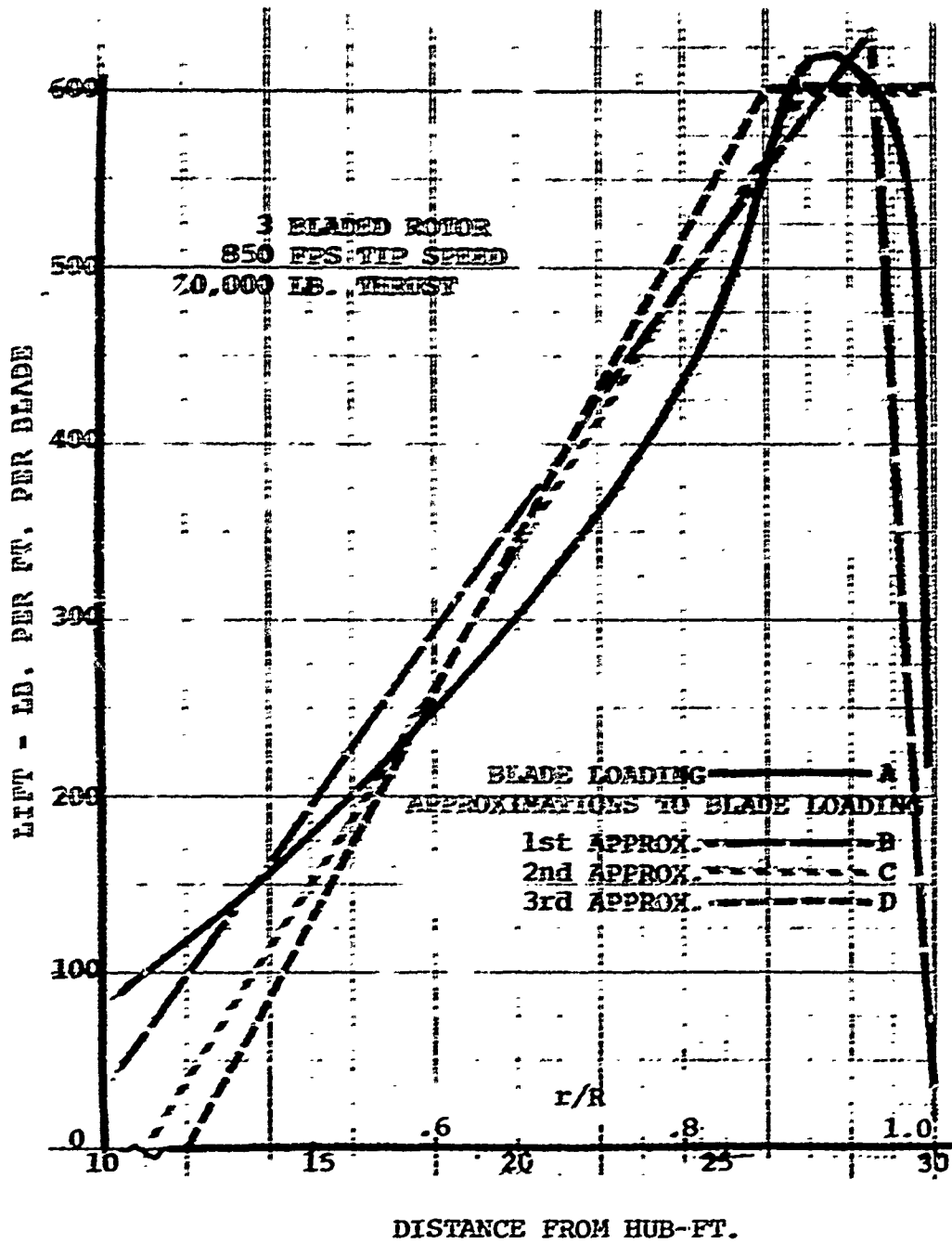


FIGURE 2.3 LOADING APPROXIMATIONS

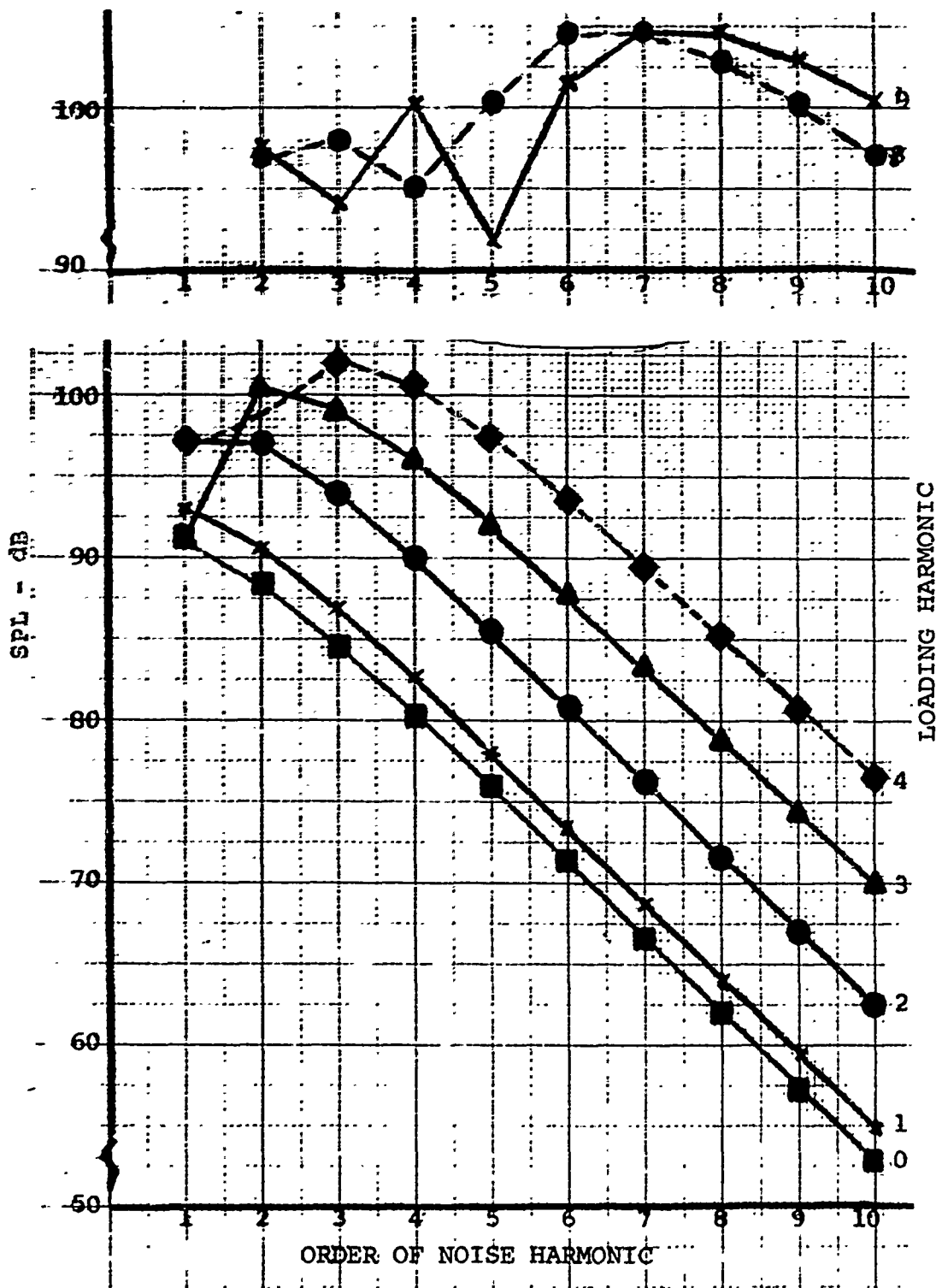


FIGURE 2.4 EFFECTS OF LOADING HARMONICS ON NOISE

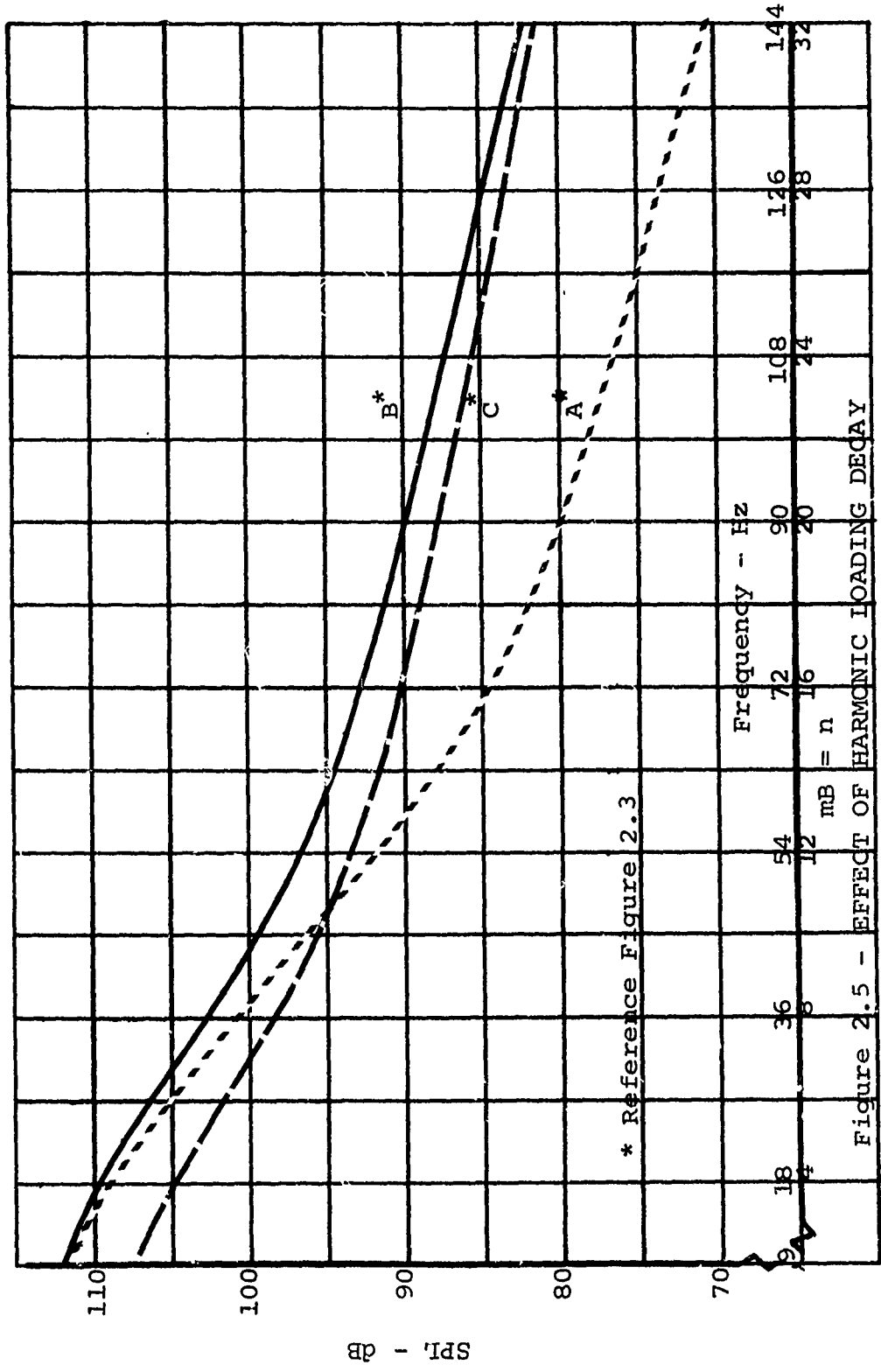


Figure 2.5 - EFFECT OF HARMONIC LOADING DECAY

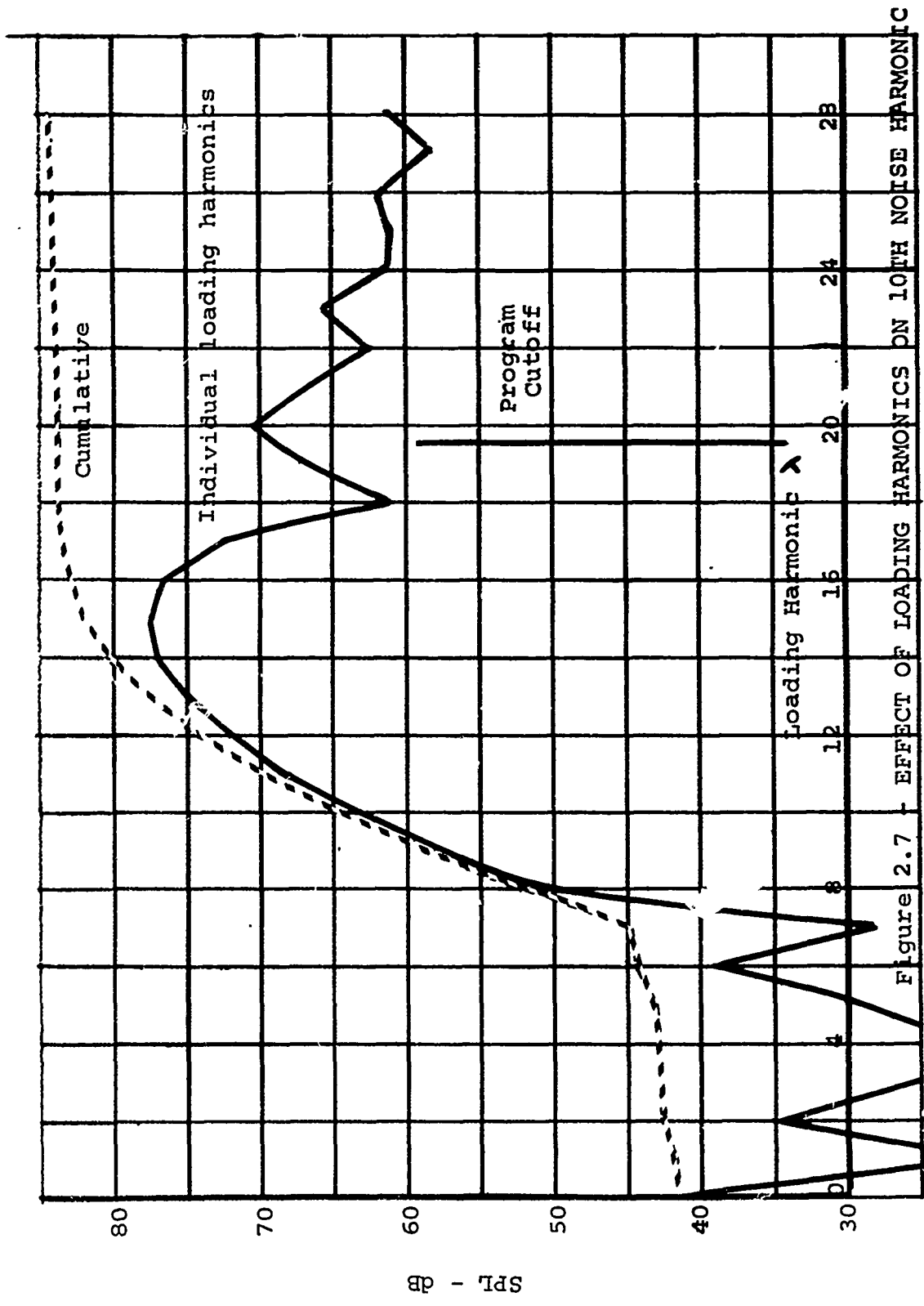


Figure 2.7 - EFFECT OF LOADING HARMONICS ON 10TH NOISE HARMONIC

SPL - dB

3.0 COMPARISON OF FULL SCALE AND MODEL ACOUSTICAL DATA

3.1 ROTATIONAL NOISE

3.1.1 Theoretical Development

In considering scaling parameters to be used in the acoustic measurement of helicopter rotor systems, the different equations and boundary conditions may be used for the fractional analysis suggested by Kline in Reference 4. Although the governing equation approach is advisable, rotor noise scaling involves a number of problems which makes the nondimensionalizing of the solution more attractive. The principal one is to incorporate the transfer of axes from the source to the observer.

The rotor noise equations of Lawson, Reference 2, have been recast into the following form: instantaneous sound pressure $P(t)$ due to the far field and near field terms is:

$$P(t) = \left[\frac{\bar{F}}{4\pi(1-M_r)^2 r^2 a_0} \left\{ \frac{\partial \bar{F}}{\partial t} + \frac{\bar{F}}{1-M_r} \frac{\partial M_r}{\partial t} \right\} + \frac{1}{4\pi(1-M_r)^2 r^2} \left\{ \frac{\bar{F} \cdot \bar{F}}{r} \frac{(1-M^2)}{(1-M_r)} - \bar{F} \cdot \bar{M} \right\} \right] \quad (1)$$

The square brackets are incidental to the scaling problem in that they indicate that the included quantities are evaluated at the time the noise is generated whereas the sound pressure $P(t)$ is that noise detected at a later time, by the observers located at a position \bar{r} relative to the source. The other terms in the equation are defined as follows:

a_0 = speed of sound,

\bar{M} = Mach number (vector),

\bar{F} = aerodynamic force on the blade (vector)

$r = |\bar{r}|$

3.1.1 Theoretical Development (Continued)

$$M = |\bar{M}|$$

$$M_r = \frac{\bar{M} \cdot \bar{r}}{r} \quad \text{magnitude of the Mach number in the direction of the vector } \bar{r}$$

The characteristic time is the blade passage period,

$$t' = \frac{t}{2\pi/b\omega}, \quad (2)$$

and is the fundamental measure for both the waveform and harmonic analysis of the sound pressure. All prime quantities are non-dimensionalized.

The characteristic dimension used is the diameter D ,

$$r' = \frac{r}{D}, \quad (3)$$

$$\bar{r}' = \frac{\bar{r}}{D}. \quad (4)$$

The acoustic pressure will be nondimensionalized using the free stream dynamic pressure $\frac{1}{2} \rho V^2$.

$$p' = \frac{p}{\frac{1}{2} \rho V^2}; \quad (5)$$

and the aerodynamic load by some aerodynamic coefficient C_f ,

$$\bar{F}' = \frac{\bar{F}}{\frac{1}{2} \rho V^2 C_f C \Delta l}, \quad (6)$$

where:

C = chord,

Δl = element of span,

3.1.1 Theoretical Development (Continued)

Equation 1 is changed by the inclusion of equation 2 through 6 as,

$$\frac{1}{2} \rho V^2 P'(t) = \left[\frac{D \bar{F}'}{4\pi (1-M_r)^2 D^2 r'^2 a_0} \cdot \left\{ \frac{\frac{1}{2} \rho V^2 C_f C_{\Delta L}}{2\pi / b \omega} \frac{\partial \bar{F}'}{\partial t'} \right. \right. \\ \left. \left. + \frac{\frac{1}{2} \rho V^2 C_f \Delta L \bar{F}'}{2\pi / b \omega (1-M_r)} \frac{\partial M_r}{\partial t'} \right\} + \frac{1}{4\pi (1-M_r)^2 D^2 r'^2} \left\{ \frac{1}{2} \rho V^2 C_f C_{\Delta L} \frac{\bar{F} \cdot \bar{F}'}{r'} \right. \right. \\ \left. \left. - \frac{1-M^2}{1-M_r} - \frac{1}{2} \rho V^2 C_f C_{\Delta L} \bar{F} \cdot \bar{M} \right\} \right],$$

or,

$$P'(t) = \frac{1}{4\pi} \left[\frac{b C}{\pi D} \frac{\Delta L}{D} C_f \frac{D \omega}{2 a_0} \bar{F}' \cdot \left\{ \frac{\partial \bar{F}'}{\partial t'} + \frac{\bar{F}'}{1-M_r} \frac{\partial M_r}{\partial t'} \right\} \right. \\ \left. + \frac{C_f}{(1-M_r) r'^2} \frac{C}{D} \frac{\Delta L}{D} \left\{ \frac{\bar{F}' \cdot \bar{F}'}{r'} \frac{1-M^2}{1-M_r} - \bar{F}' \cdot \bar{M} \right\} \right]$$

Now it is understood that the variables are all nondimensionalized and for convenience the primes will be dropped.

$$P(t) = \frac{1}{4\pi} \left[\sigma M_{r,tip} C_f \frac{\Delta L}{D} \bar{F} \cdot \left\{ \frac{\partial \bar{F}}{\partial t} + \frac{\bar{F}}{1-M_r} \frac{\partial M_r}{\partial t} \right\} \right. \\ \left. + \frac{C_f}{(1-M_r) r^2} \frac{C}{D} \frac{\Delta L}{D} \left\{ \frac{\bar{F} \cdot \bar{F}}{r} \frac{1-M^2}{1-M_r} - \bar{F} \cdot \bar{M} \right\} \right] \quad (7)$$

The nondimensional parameters on the RH side of the above equation require the following model scaling parameters:

- 1) Geometric similarity of the rotor: $b, \frac{C}{D}, \frac{\Delta L}{D}$
- 2) Scaling of the observer location: \bar{r}, r
- 3) Mach number simulation of the rotor: \bar{M}, M, M_r, M_{tip}
- 4) Similarity in C_f which implies scaling Mach number d , and Reynolds number. The scaling of the angle of

3.1.1 Theoretical Development (Continued)

4) Continued

attack implies kinematic similarity, i.e., similar velocity triangles. As is the case in all model rotor testing, Reynolds number matching is the most difficult and is usually not attained.

The sound pressure parameter on the left hand side needs further exploration since for hover noise measurements, the absence of free stream, dynamic pressure will result in anomalies of the sound pressure and the aerodynamic force. Hence, the velocity V should include the rotational speed ωR .

$$V = U_{\infty} + \omega R$$

U_{∞} = free stream velocity

The Doppler shift will not directly affect the sound pressure; however, it will affect the harmonic analysis since the Doppler shift is given by $\frac{U_{\infty}}{\lambda}$ or $\frac{U_{\infty}}{c}$.

Since Mach number and advance ratios are matched as a necessity for kinematic similarity, the freestream velocity number will be matched. Hence, the Doppler shift will be correctly scaled with respect to frequency.

3.1.2 Comparison of Measured and Predicted Data

Verification of the suggested scaling parameters for the hover condition was investigated by comparison of data taken on the full scale CH-47 rotor, reported in Reference 1 and data which was taken on a 1/11 scale model of the same rotor. During the model testing, which was conducted by Boeing/Vertol as part of a blade development program, one microphone position exactly scaled the one diameter microphone position of the Reference 1 full scale data as shown in Figure 3.1. Blade planform, airfoil, and twist were modeled as closely as possible.

Of that model and full scale data which was available, five sets were found which were suitably matched for valid comparison. These data were analyzed, using digital averaging techniques, and the resulting frequency spectra are presented in Figure 3.2 through Figure 3.6. Figure 3.7 through 3.9 compare each modeled and full scale measured harmonic. Also shown are the corresponding analytical predictions using the

3.1.2 Comparison of Measured and Predicted Data (Continued)

Lowson method with modified loading law developed under this program and discussed in Section 2. In evaluating this data an experimental accuracy of ± 1 dB should have been considered for the model data and ± 3 dB for the full scale data. This is based on an instrumentation and analysis accuracy of 1 dB for both systems and a possible ± 2 dB ground reflection effect on the full scale data (see Reference 1, Figure 22). The location of the microphone in the wind tunnel was sufficiently close to the blade tip that it appeared that wind tunnel wall effects could be neglected.

In general the agreement between model and full scale measured data is of such a high degree that it appears reasonable to conclude that by matching M_t and C_t/σ in hover, the absolute values of near field harmonic data of a full scale rotor and a high quality model will duplicate each other with respect to trend and absolute value. That this should be so is analytically verified by the close match between predicted and measured data for corresponding conditions.

3.2 BROADBAND NOISE

Broadband noise (sometimes referred to as vortex noise) is defined, for purposes of this program, as the sound pressure spectrum over the frequency range in which harmonically spaced discrete frequencies are not evident.

In measuring broadband noise it is important to recognize that a clear representation of broadband noise requires averaging techniques in addition to frequency analysis. Narrow band spectra are required at least for initial data screening in order to separate the rotational or harmonically related components of the rotor noise from the purely broadband part of the noise.

Figure 3.10 shows a typical spectrum acquired near the Boeing/Vertol engineering whirl tower. This spectrum from 0 to 2000 Hz was analyzed using a 1.6 Hz bandwidth filter and averaging over 30 seconds of data. The advantage of averaging spectra can be seen in the comparison with Figure 3.11 which shows the same data point unaveraged. The averaged record gives a statistically significant level which can be measured whereas the unaveraged record obviously is too small a sample to exhibit a consistent level.

3.2 BROADBAND NOISE (Continued)

Another feature of narrow band analysis of broadband noise is that the relative level between broadband and harmonic signals is inversely proportional to the bandwidth of the analysis equipment. If the analyzer is set up to produce levels according to the RMS value of the pressure (i.e., $SPL=20 \log P_{rms}/P_{ref}$) the levels of any pure tones, harmonics included, will be independent of the analyzer bandwidth. The RMS value of the broadband noise will be proportional to the square root of the energy passed by the filter. This, in turn, is proportional to the bandwidth of the filter. Thus the level of the broadband noise will drop at $-10 \log \Delta f$ where Δf is the bandwidth of the filter.

A more correct method of displaying broadband noise is to use power spectral density. Power Spectral Density (PSD) expresses the level in units of (power/1 Hz), the amount of acoustic power transmitted through a one Hz wide filter. (See Reference 6, p. 15 and p. 364.) However, in these terms, the level of a sine wave (a pure tone or a harmonic) is dependent upon the filter bandwidth, increasing as $10 \log \Delta f$.

Thus, care must always be exercised when analyzing a signal containing both pure tones and broadband noise. If a PSD is used, the broadband level remains constant with bandwidth and the harmonics increase with decreasing bandwidth by $10 \log \Delta f$. If a sound pressure level (RMS pressure) spectrum is used, the harmonics remain constant and the broadband level decreases with decreasing bandwidth by $10 \log \Delta f$.

In comparing broadband levels, Figures 3.2 - 3.6, it is therefore necessary to apply a correction of 10 dB to allow for the fact that the full scale data bandwidth is .1 that of the model.

In order to convert these broadband levels to an equivalent overall sound pressure level, it is also necessary to sum over the frequency range in question. Thus for the full scale data analyzed over a range of 500 Hz with a 1 Hz bandwidth filter the overall sound pressure level is the peak of the broadband plus 27 dB ($10 \log \frac{500}{1}$). A similar value ($10 \log \frac{5000}{10}$) is added to the model data. Figure 3.12 shows the comparison of full scale and model broadband noise and indicates that, in general the model data is low with respect to the full scale data.

3.2 BROADBAND NOISE (Continued)

The origins of broadband noise generation are not as well defined as rotational noise and no rigorous prediction methods are currently available. At least three sources are generally considered as probable major contributors. They are turbulence in the wake, random airloads on the blade, and vortex shedding. Although the latter is a discrete frequency at any single point along the blade, it varies radially along the blade, and results in what would be described as non-harmonic noise when the data is measured in the non-rotating far field. Paterson, et al (Reference 5) have shown that the conditions for noise due to vortex shedding appear to be a function of Reynolds number and angle of attack as shown in Figure 3.13. Also shown are the ranges covered by the test data which indicate that no pure tone region would be encountered on the model but that the portion of the full scale blade inboard of about 20% r/R would be expected to generate this type of noise. Therefore scaling of even the proper mechanism of noise generation is Reynolds number dependent.

Once the vortex or turbulence noise has been generated, its propagation and decay are dependent on the molecular structure, and hence kinematic viscosity, of the medium, but blade Reynolds number is no longer a consideration. This implies that scaling of Reynolds number by operating in gasses other than air will not serve for fixed system noise measurement and that the characteristic dimension (chord) and tip speed may be the more valid scaling parameters. It therefore appears that further refinement and understanding of what generation mechanisms are responsible for the so-called broadband noise generated by a rotor are needed before the important scaling parameters can be separated out.

TABLE 3-I

SYMBOLS FOR FIGURES 3.7 - 3.9

SET	V_T (FPS)	C_T/σ	MEASURED	SYMBOLS PREDICTED
1	600	.0730	●	○
2	700	.0789	▲	△
3	750	.0850	■	□
4	800	.0819	◆	◇
5	850	.0797	♣	♠

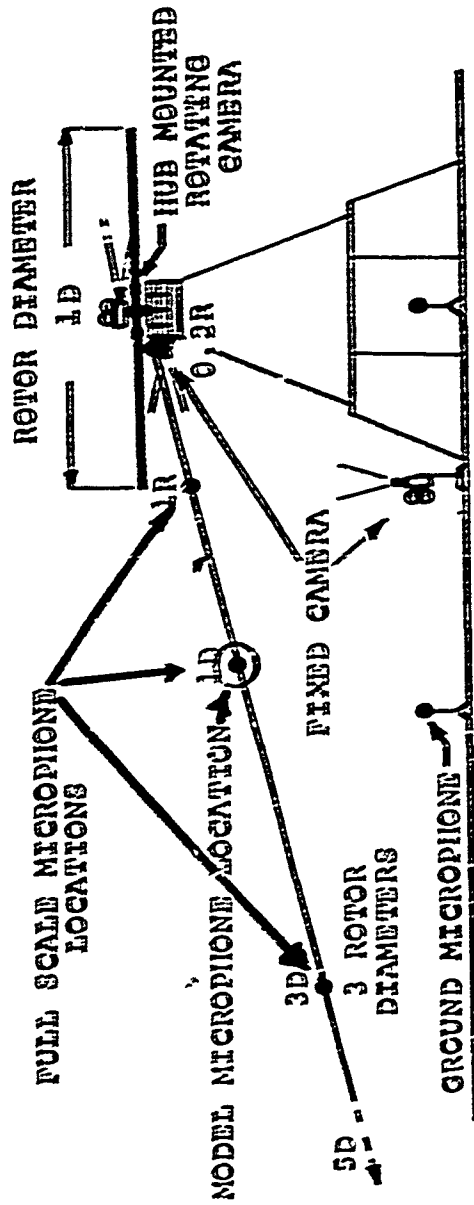
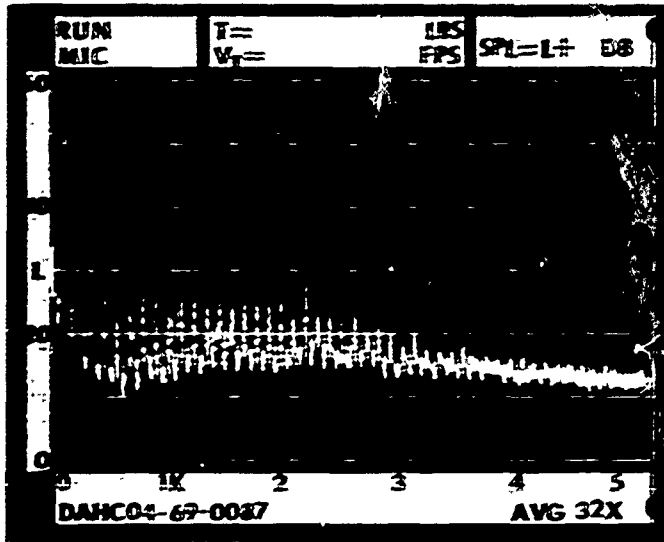


FIGURE 3.1 - FULL SCALE WHIRL TOWER TEST SETUP SHOWING CORRESPONDING MODEL MICROPHONE LOCATION

SOUND PRESSURE LEVEL - dB

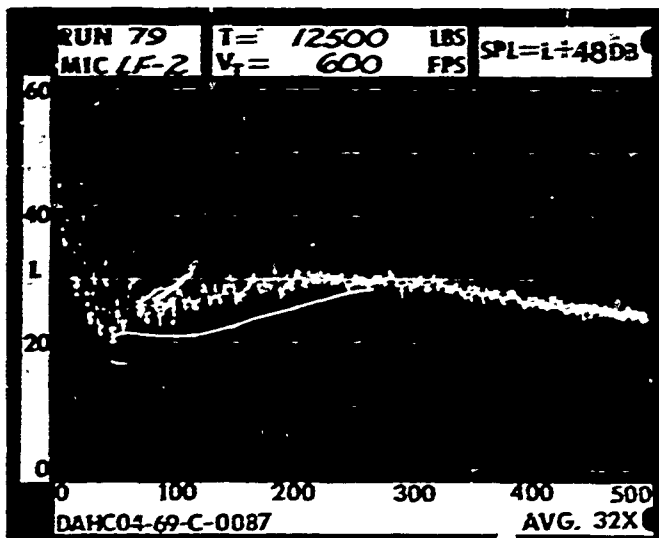


FREQUENCY - KEZ

MODEL

RPM = 2067
T = 107 lbs

$V_T = 602$ ft/sec
 $C_T/\sigma = .0785$



FREQUENCY - Hz

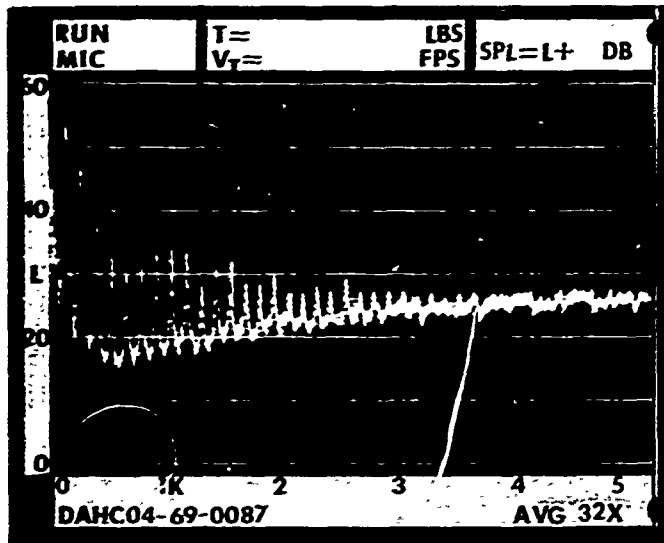
FULL SCALE

RPM = 191
T = 12,500 lbs

$V_T = 600$ ft/sec
 $C_T/\sigma = .0730$

Figure 3.2
COMPARISON OF MODEL & FULL SCALE NOISE DATA

SOUND PRESSURE LEVEL - dB

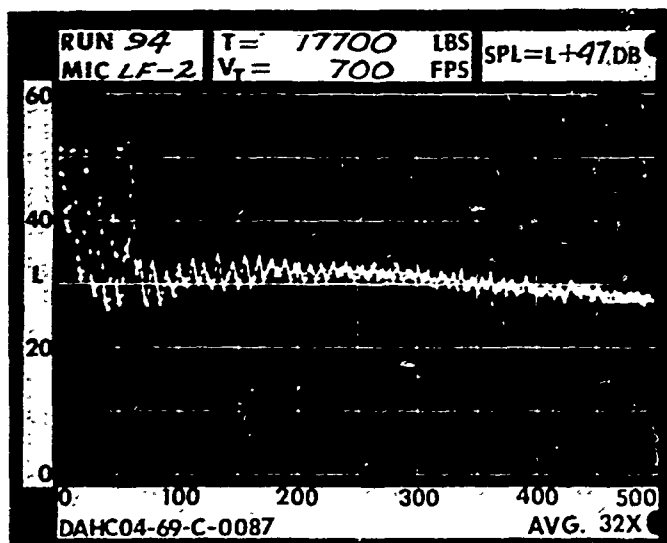


MODEL

RPM = 2415
T = 151 lbs

V_{T1} = 704
 C_{T1}/σ = .0815

FREQUENCY - KHz



FULL SCALE

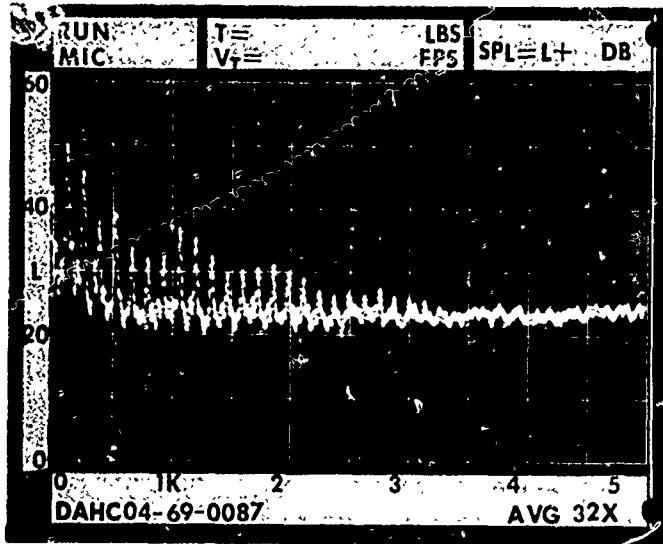
RPM = 233
T = 17,700 lbs

V_T = 703 ft/sec
 C_T/σ = .0789

FREQUENCY - Hz

Figure 3.3
COMPARISON OF MODEL & FULL SCALE NOISE DATA

SOUND PRESSURE LEVEL - dB

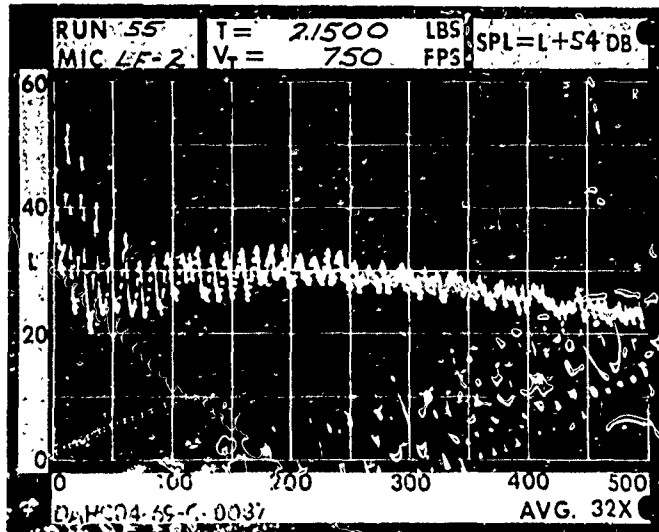


MODEL

RPM = 2591
T = 176 lb

$V_T = 755$
 $C_T/\sigma = .0828$

FREQUENCY - KHz



FULL SCALE

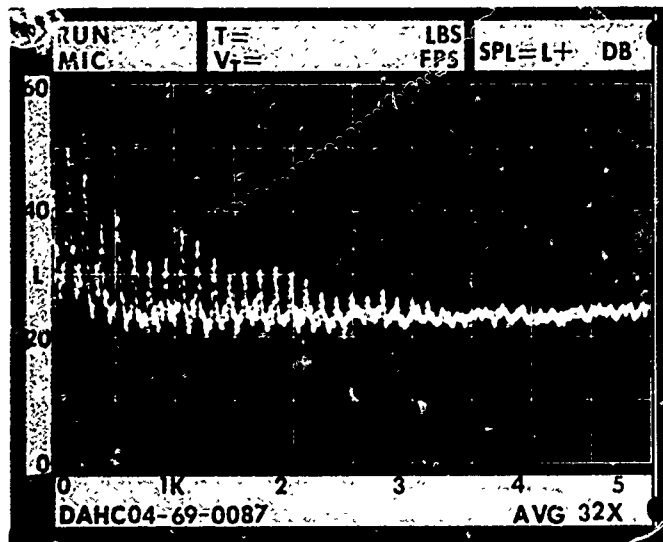
RPM = 239
T = 21,500 lbs.

$V_T = 753 \text{ ft/sec}$
 $C_T/\sigma = .0850$

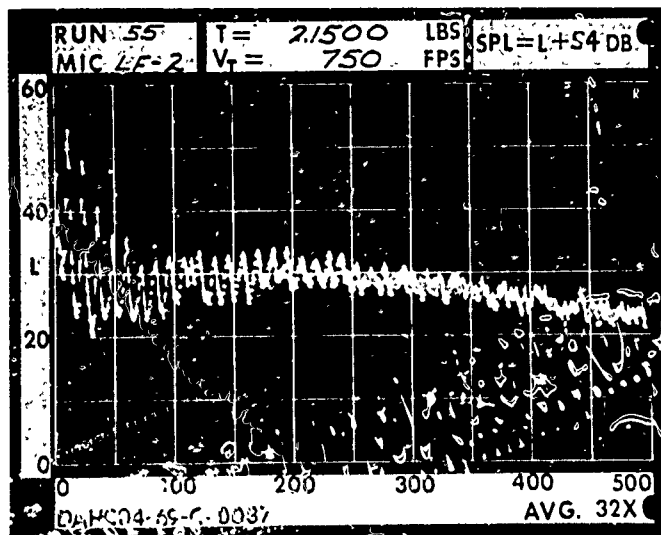
FREQUENCY - Hz

Figure 3.4
COMPARISON OF MODEL & FULL SCALE NOISE DATA

SOUND PRESSURE LEVEL - dB



FREQUENCY - KHz



FREQUENCY - Hz

MODEL

RPM = 2591
T = 176 lb

$V_T = 755$
 $C_T/\sigma = .0828$

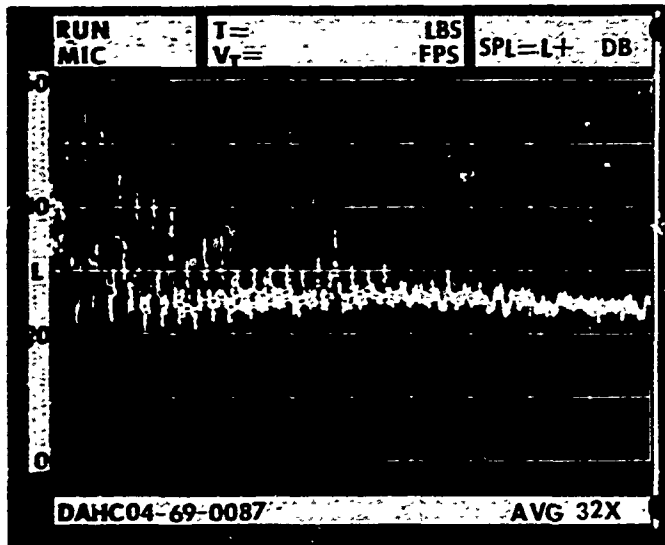
FULL SCALE

RPM = 239
T = 21,500 lbs.

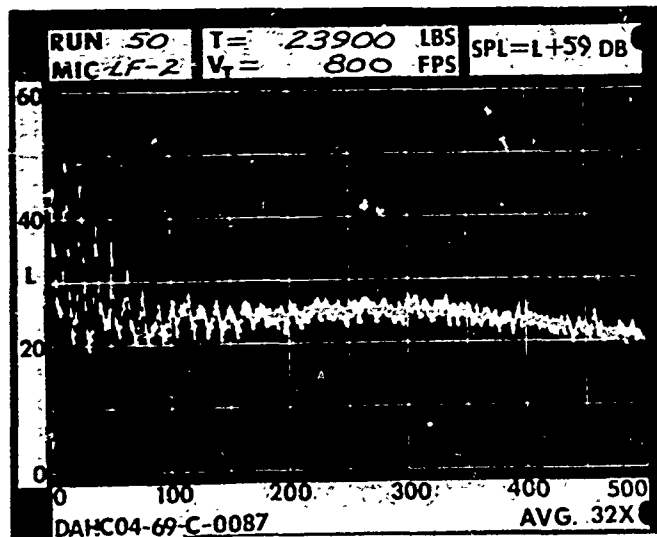
$V_T = 753$ ft/sec
 $C_T/\sigma = .0850$

Figure 3.4
COMPARISON OF MODEL & FULL SCALE NOISE DATA

SOUND PRESSURE LEVEL - dB



FREQUENCY - KHz



FREQUENCY - Hz

MODEL

RPM = 2742
T = 196 lbs.

V_T = 799 ft/sec.
C_T/σ = .0825

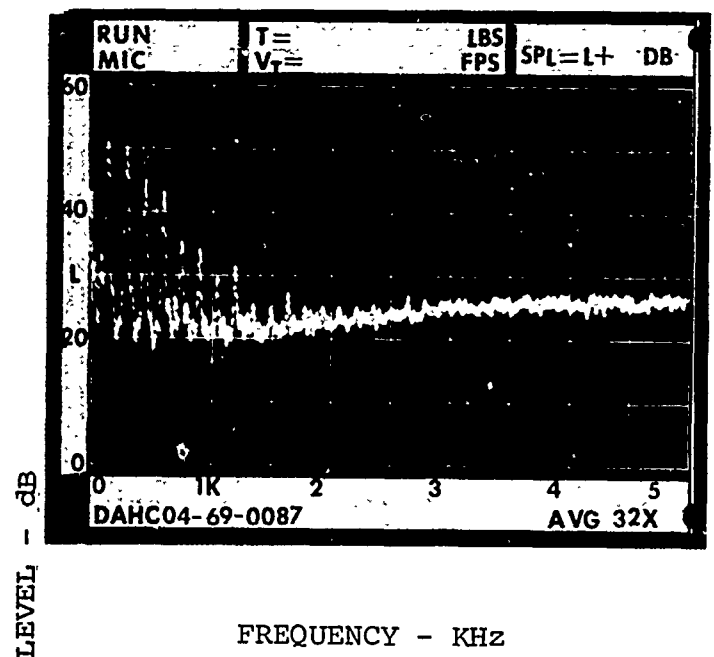
FULL SCALE

RPM = 255
T = 23,900 lbs.

V_T = 797 ft/sec
C_T/σ = .0819

Figure 3.5
COMPARISON OF MODEL & FULL SCALE NOISE DATA

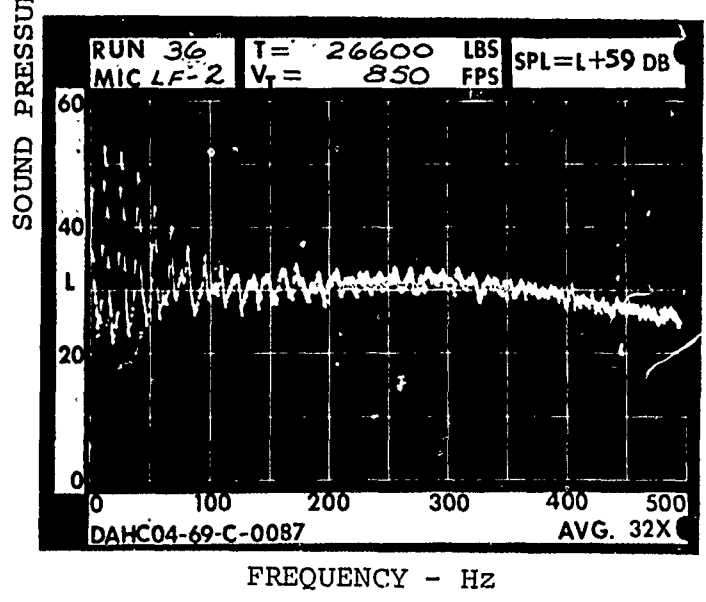
Reproduced from
best available copy.



MODEL

RPM = 2912
T = 210 lbs.

V_T = 848 ft/sec
C_T/σ = .0784



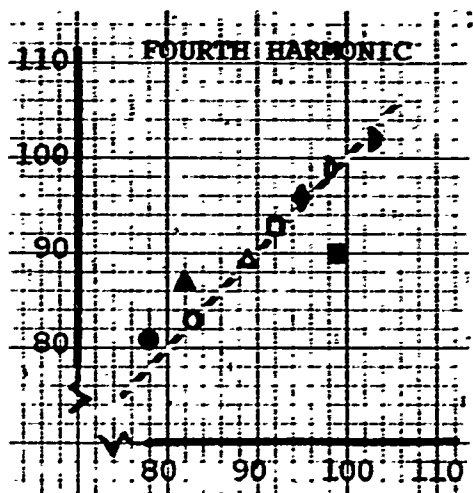
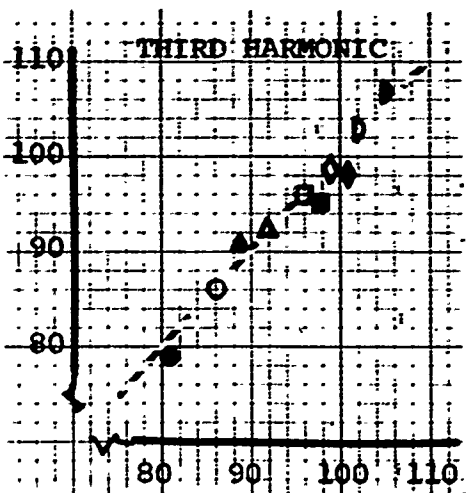
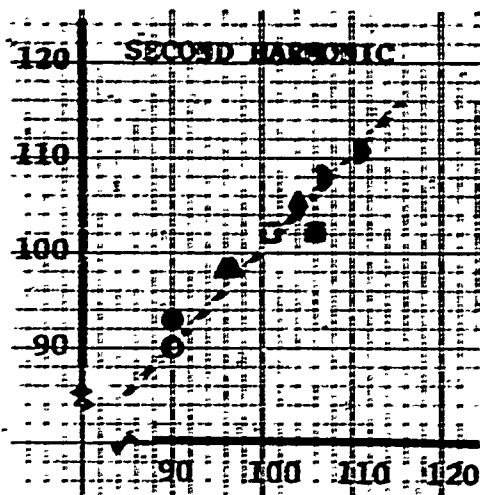
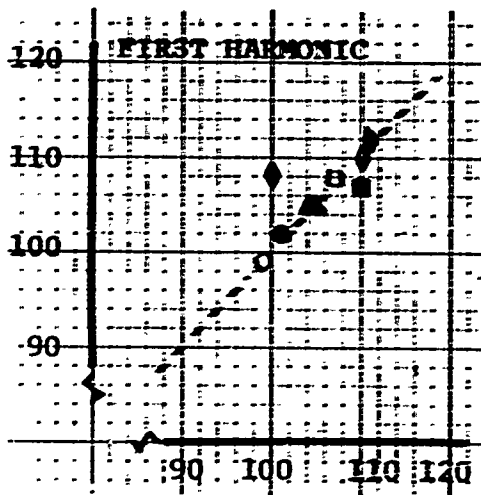
FULL SCALE

RPM = 271
T = 26,600 lbs.

V_T = 850 ft/sec
C_T/σ = .0797

Figure 3.6
COMPARISON OF MODEL & FULL SCALE NOISE DATA

FULL SCALE SPL - dB

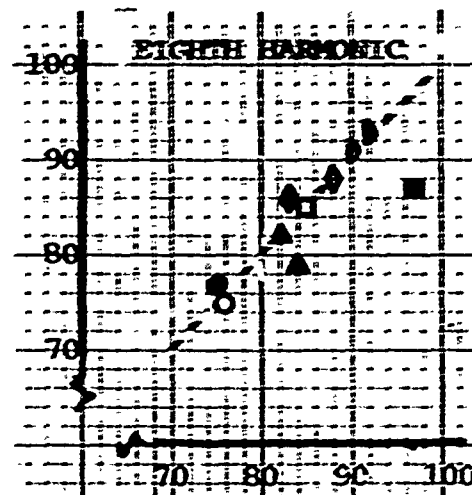
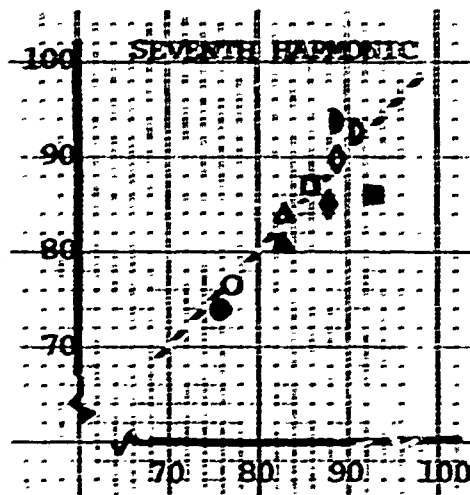
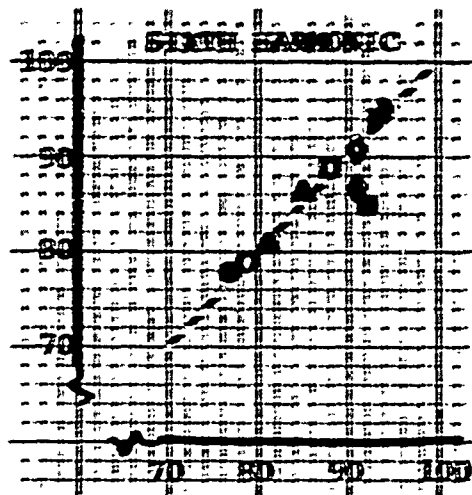
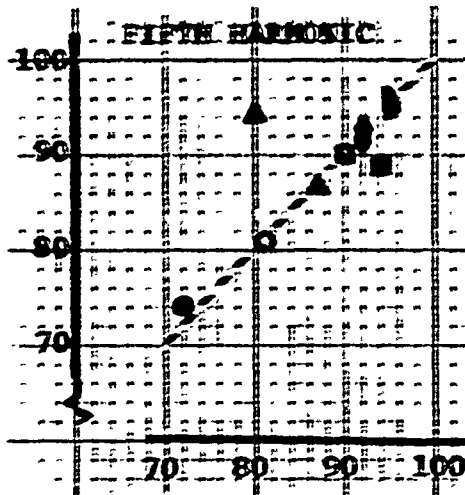


MODEL SPL - dB

(FOR SYMBOLS - SEE TABLE 3-1)

Figure 3.7
COMPARISON OF FULL SCALE & MODEL ROTATIONAL NOISE

FULL SCALE SPL - dB

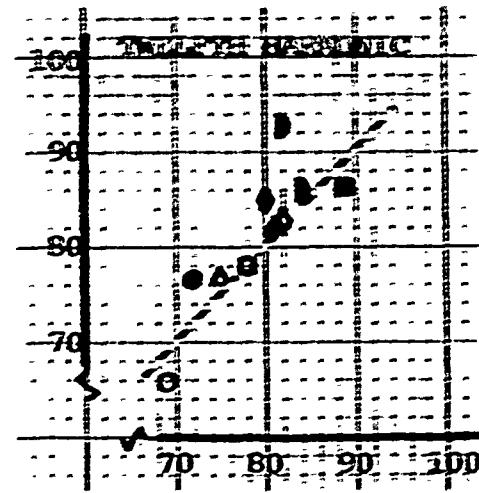
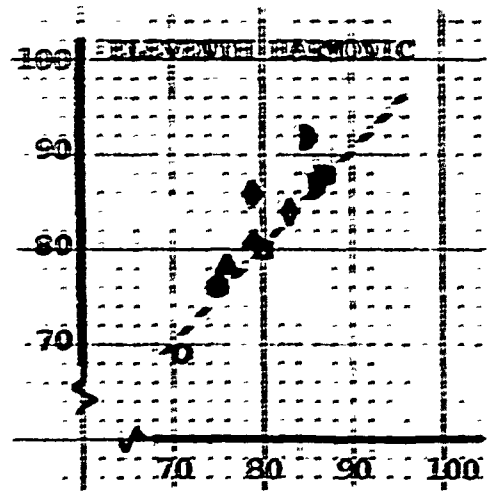
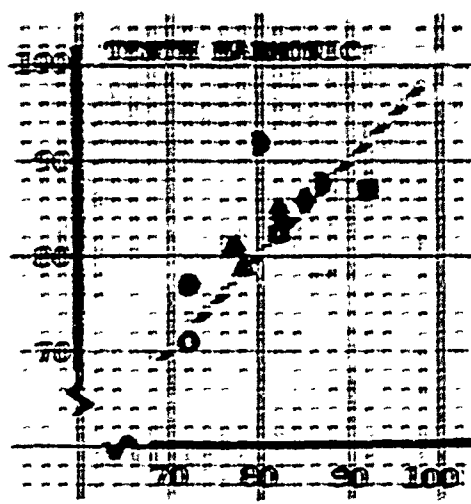
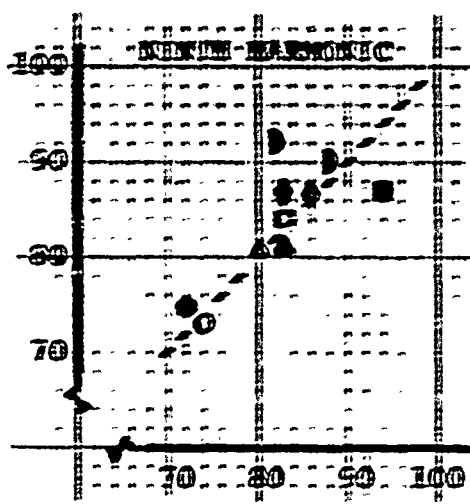


MODEL SPL - dB

(FOR SYMBOLS - SEE TABLE 3-1)

Figure 3.8
COMPARISON OF FULL SCALE & MODEL ROTATIONAL NOISE

FULL SCALE SPL - dB



MODEL SPL - dB

(FOR SYMBOLS - SEE TABLE 3-I)

Figure 3.9
COMPARISON OF FULL SCALE & MODEL ROTATIONAL NOISE

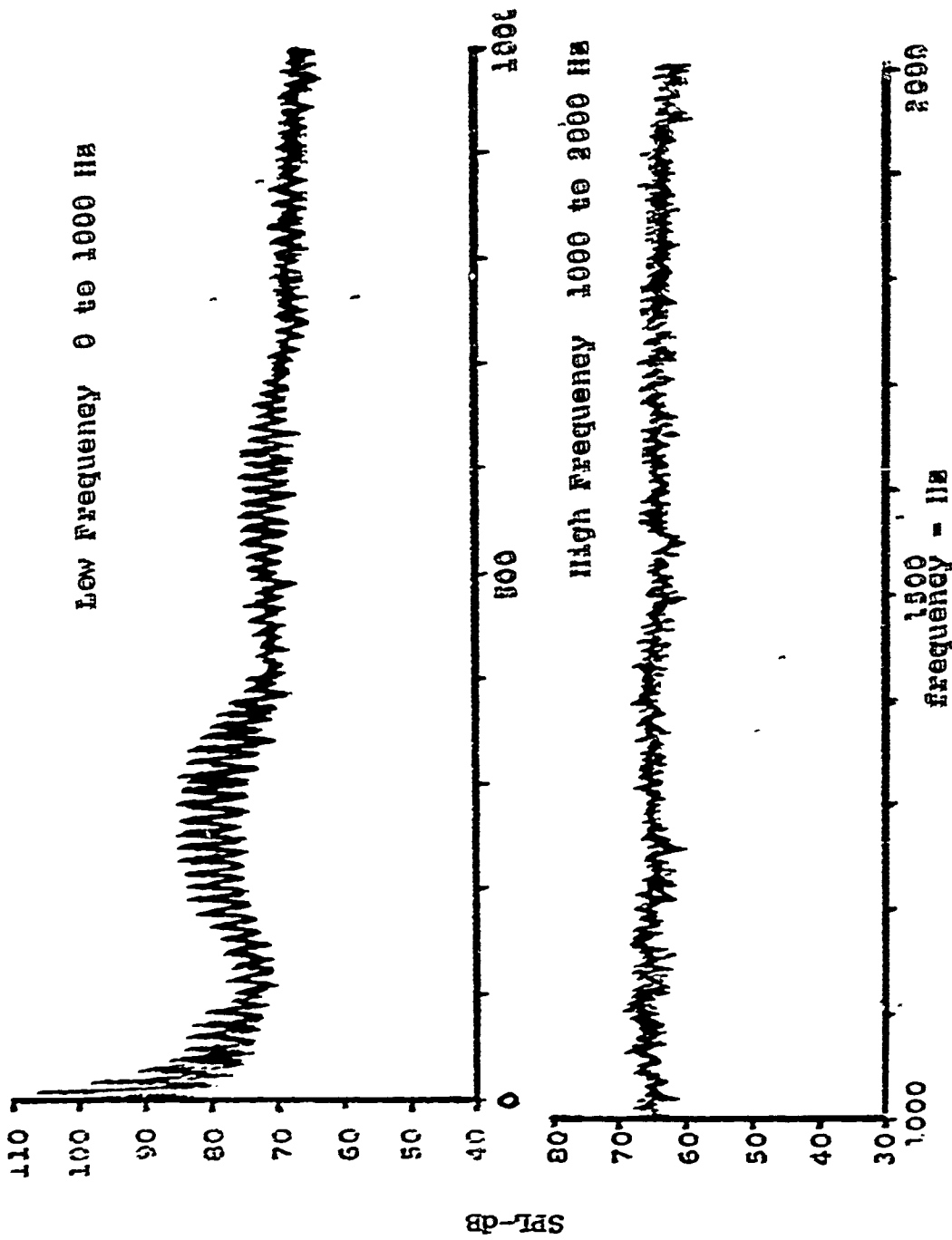
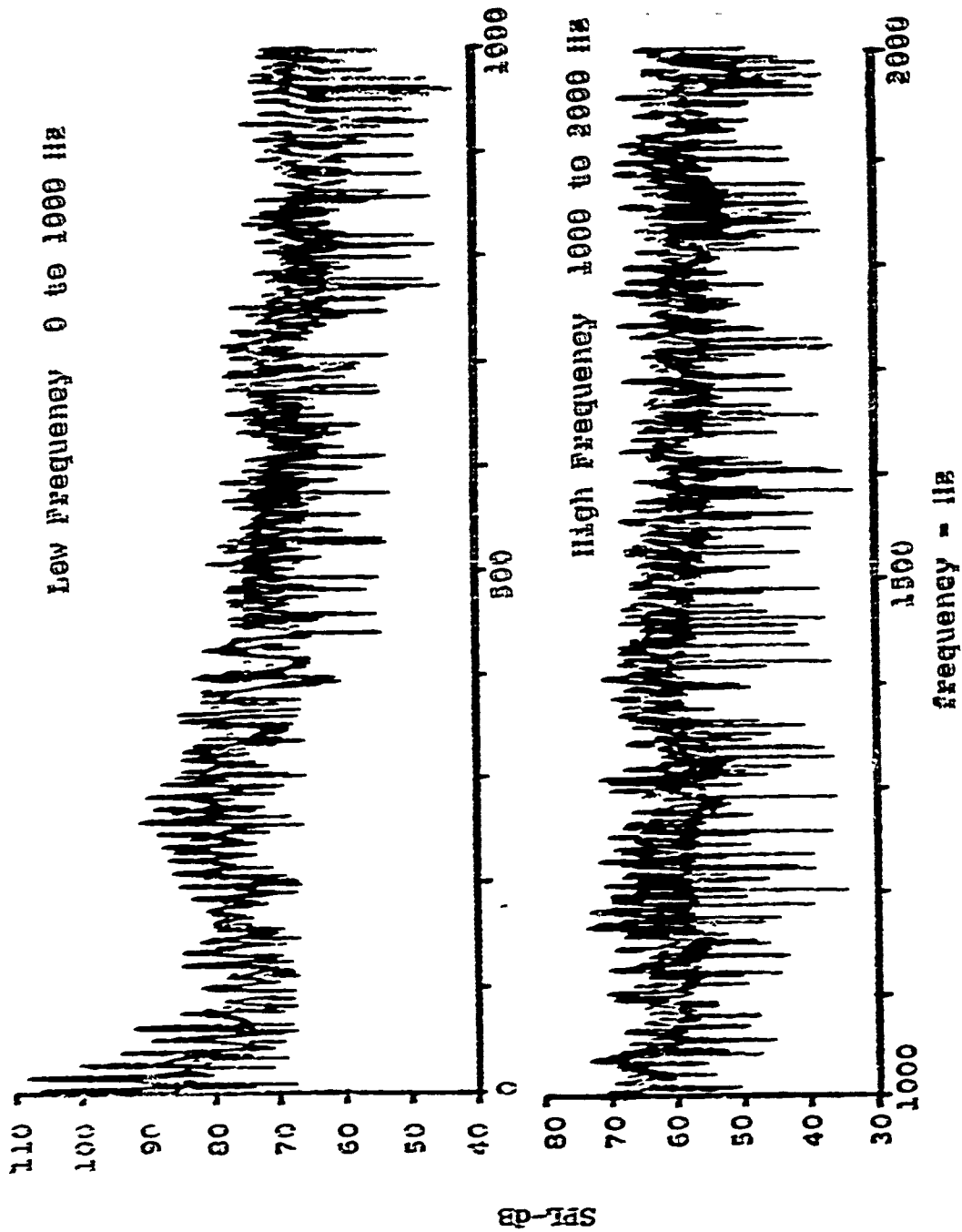


Figure 3.10 - AVERAGED SPECTRUM OF WIRE TOWER ROTOR NOISE



Reproduced from
Best available copy.

Figure 3.11 - UNAVERAGED SPECTRUM OF WIRE TOWER ROTOR NOISE

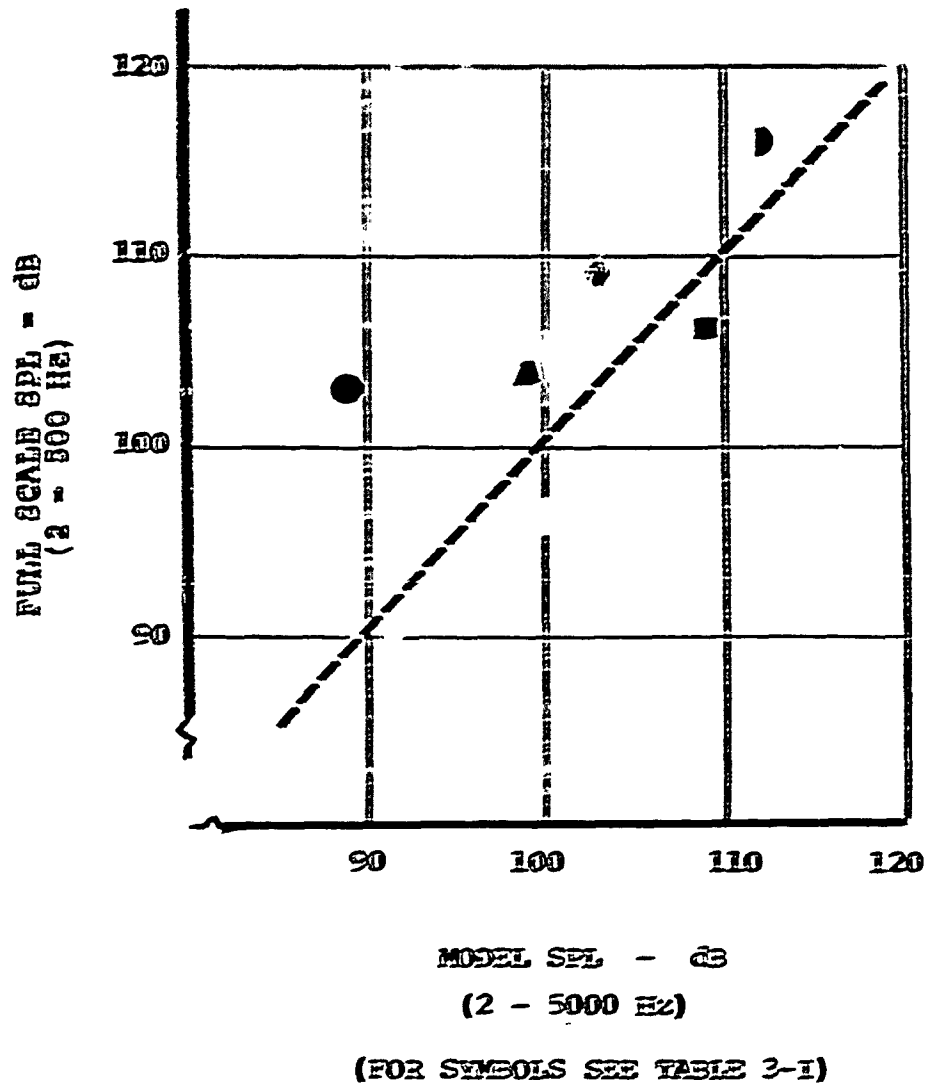
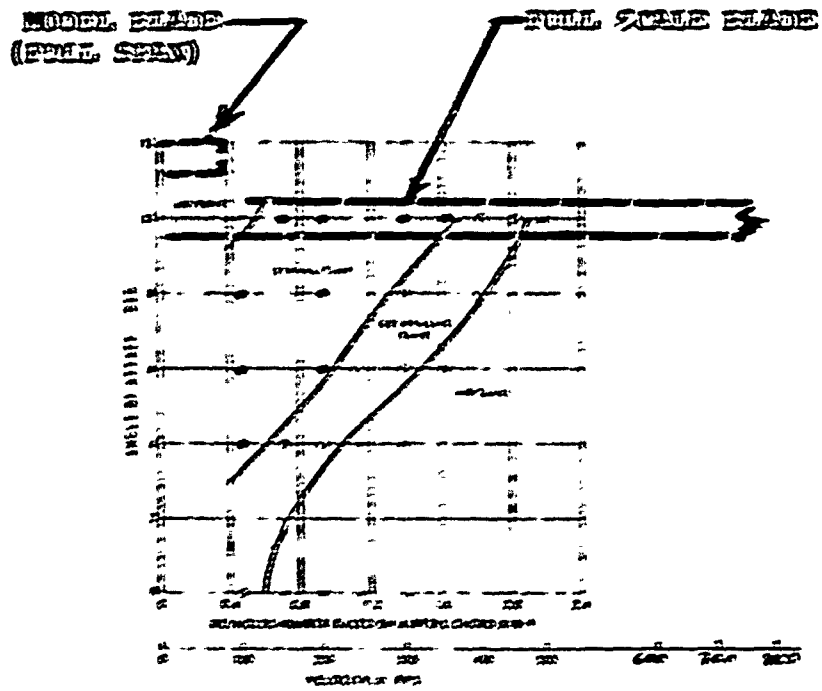


Figure 3.12
COMPARISON OF FULL SCALE & MODEL BROADBAND NOISE



(FIGURE WITHOUT MODEL AND FULL SCALE
REGIONS FROM REF. 5)

Figure 3.13
REGIONS OF PURE TONE GENERATION

4.0 EFFECT OF ROTOR DESIGN

4.1 INTRODUCTION

Researchers in rotary wing acoustics are continually confronted with the task of reducing noise levels as rotor performance levels are continually increased. Along with these improvements in rotor performance, often by modification to blade airfoil and planform geometry there is generally an increase in noise, but little has been published in the way of a systematic study of the role which airfoil and planform geometry can have in establishing rotor noise levels. The availability of data on rotors of the same diameter and blade number, but of different airfoil section and of different planform geometry made it attractive to compare the noise of these blade designs more systematically than has been accomplished in the past. These design variables will be described for each rotor under consideration and it will be seen that the rotors display some interesting similarities as well as differences.

4.1.1 Description of the Rotors

Noise levels of the rotor configurations illustrated in Figure 4.1 were recorded during past test programs conducted on the Boeing-Vertol Engineering Whirl Tower facility described in Reference 1, the initial phase of this study. The blade used as the baseline for this comparison study is employed on the CH-47C and is rectangular in planform (Figure 4.1a) and has a Vertol 23010-1.58 section, constant along the radius. A second configuration, also rectangular in planform has an NACA 0012 airfoil and is the blade used on the CH-47A aircraft (Figure 4.1a). A third configuration, experimental, is tapered in planform along the outboard 30% of span, but maintains a constant 0012 section along the blade (Figure 4.1b). A fourth configuration known as the Advanced Geometry Blade (AGB) is also an experimental configuration and is varied in planform as shown (Figure 4.1c) but in addition has an airfoil section which varies from 12% thick at $r/R = 0.325$ to 6% thick at the tip. The effect of these two variables, planform configuration and airfoil section, are inseparable in the noise data of the Advanced Geometry Blades, but the configuration provides an interesting comparison with the standard reference blade.

The theory used for predicting the effects of planform and airfoil was developed by Lawson and Ollerhead (Reference 2) and modified as described in Section 2 of this report. As noted by the authors of the Reference 2 study and discussed in Section 2 of this report, the ability of the method to

4.1.1 Description of the Rotors (Continued)

predict the noise of a rotor with any accuracy is dependent on the airload used as input to accurately derive higher loading harmonics. For this reason, the airloads used in the subject study imposed a limit on the noise prediction harmonics. The initial noise harmonics (1-5) have been shown to be very similar for rotors of the same blade number and operating conditions and thus noise level predictions for secondary configuration changes of planform and airfoil being investigated in this study are identical.

4.2 EFFECT OF AIRFOIL SECTION

Comparison of the symmetrical and cambered airfoils on the basis of equal thrust and tip speed has been made and is illustrated in Figures 4.2 through 4.4. It should be pointed out that the low harmonics of blade passage display a reasonable agreement for both blades and at nearly all operating conditions, thus illustrating that blade design does not substantially influence this region of the noise spectra. Some general trends are displayed by the higher harmonic portion of the spectra. For example, at low tip speeds and regardless of the thrust, sound pressure levels for the symmetrical airfoil are consistently higher than that of the cambered airfoil. At $V_t = 750$ ft/sec. no consistent trend is displayed and at $V_t = 850$ ft/sec., the symmetrical airfoil displays lower noise levels in the higher harmonics than the cambered airfoil.

4.3 EFFECT OF PLANFORM

A limited amount of data is available to investigate the effect of planform on noise. A comparison of the noise of the rectangular blade with symmetrical airfoil is made with a set of blades which had been tapered in planform in Figures 4.5 and 4.6. Comparison data exists for tip speeds of ~ 650 and ~ 725 ft/sec. only. Here again there appears to be little or no effect on lower rotational harmonics. At the lower tip speed, however, the tapered blade produces higher broadband noise levels at the highest thrust shown, while at 750 ft/sec. both blades display very similar noise spectra. This again confirms the conclusion that blade design has a secondary effect on the noise of a rotor system.

4.4 EFFECT OF COMBINED PLANFORM AND AIRFOIL EFFECTS

Data from 3 bladed rotors with both a planform and airfoil modification (AGB) relative to the 23010 rectangular blade is illustrated in Figs. 4.7-4.9. Although the $C_{T/\sigma}$

4.4 EFFECT OF COMBINED PLANFORM AND AIRFOIL EFFECTS (Continued)

for the AGB is about 25% higher at any given condition, the airloading distribution for these two blades is very similar as shown in Figure 4.10 and therefore a large difference in noise level would not be expected. A consistent trend between the two blades is not displayed, although the AGB configuration does exhibit considerably lower levels than the 23010 at thrust of 9000 lb. and $V_t = 750$ ft/sec. Since this trend is not continued for this tip speed at higher thrusts, no general conclusion can be drawn, except that the statistical variation which can be expected in higher harmonic data is greater than the magnitude of change due to the types of blade variations which were investigated.

4.5 COMPARISON OF WAVEFORMS

Waveforms were normalized to approximately the same amplitude for comparison purposes. The standard CH-47C rotor is compared with the AGB rotor in Figure 4.11. A comparison of waveforms such as this reveals information about the time dependence of rotor noise not available from an averaged spectra plot such as previously illustrated. The waveforms for each rotor configuration generally display a similarity in rise times but show a trend, as a whole, toward symmetry of the AGB waveform about the peak pressure that is not generally present for the rectangular blade. Time histories for this latter configuration have an initial symmetry about the peak, but then decay much less rapidly indicating a trend toward higher harmonic content as revealed by the high frequencies imposed on the waveform of the rectangular blade.

Some of the data in the comparisons in this section can be grouped to illustrate that while the lowest harmonics are extremely stable the higher harmonics of a given blade planform or airfoil may display a trend with tip speed or thrust when compared with the reference blade, and there are trends associated with tip speed or thrust for any specific blade in the study. But, just as important in making a comparison of this nature, is that trends in rotor noise data must be viewed in the light that measurement programs on whirl towers frequently result in scatter in data which may be as much as 6 dB for repeated points. Figure 4.12 shows, for example, the scatter of 6 repeated test points and reveals that a trend or effect displayed by a change in blade design can be at least partially contained in the scatter of repeated data. It has already been noted, in Section 2, that small changes in the phase of rotor airloads can result in substantial changes to the noise of the rotor.

4.5 COMPARISON OF WAVEFORMS (Continued)

On the other hand, only small changes in noise level in the low harmonics are expected with large blade design changes, since airload predictions do not distinguish between design variations of the magnitude being evaluated. This is particularly true for the low harmonics of rotational noise, where the data substantiates only small magnitude variations in the first five noise harmonics. It is only in the higher harmonics of rotational noise and in the region where broadband noise governs that identifiable and repeatable effects are displayed. Since this is where the largest change in noise is displayed, it is where future research should be concentrated.

Ambient wind, both in magnitude and direction, plays a substantial role in the wake geometry of a given rotor and therefore of the noise which that rotor radiates. It must not be concluded, however, that improvements to the geometry of a rotor blade should not be studied in order to achieve the ultimate magnitude of noise reduction that can be realized by proper design. But the total effect of rotor blade design variations on radiated far field noise is an order of magnitude below the potential which can be realized from rotor tip speed alone. Perhaps the optimum rotor should be defined in terms of a blade geometry which permits the rotor to be operated at tip speeds which achieve good performance while maintaining acceptable noise levels to the observer in the near and far fields.

4.6 EFFECT OF NUMBER OF BLADES ON ROTATIONAL NOISE

Given the pressure time history of a one bladed rotor, $P_1(t)$ with period τ and frequency $\omega_1 = 2\pi/\tau$, the pressure time history of a B bladed rotor, $P_B(t)$, can be found by adding the one bladed waveform to itself but shifted by the blade passage period, τ/B .

$$P_B(t) = \sum_{k=1}^B P\left(t + \frac{k\tau}{B}\right). \quad (-1-)$$

The Fourier Analysis of this gives components A_m (which are complex numbers):

$$A_m = \frac{B}{\tau} \int_0^{\tau/B} P_B(t) e^{im\omega_0 t} dt \quad (-2-)$$

$$\text{where } \omega_0 = \frac{2\pi B}{\tau}$$

4.6 EFFECT OF NUMBER OF BLADES ON ROTATIONAL NOISE
(Continued)

Substituting from equation (-1-) gives:

$$A_m = \frac{B}{\tau} \int_0^{\tau/B} \sum_{k=1}^B P\left(t + \frac{k\tau}{B}\right) e^{im\omega_0 t} dt$$

or, interchanging the integral and the summation because they are over different parameters, k and t ,

$$A_m = \frac{B}{\tau} \sum_{k=1}^B \int_0^{\tau/B} P\left(t + \frac{k\tau}{B}\right) e^{im\omega_0 t} dt \quad (-3-)$$

The Fourier analysis of the one bladed waveform produces harmonics of ω , given by:

$$C_n = \frac{1}{\tau} \int_0^{\tau} P(t) e^{i\omega_n t} dt \quad (-4-)$$

or by dividing up the limits of integration into B segments each τ/B long we can write

$$C_n = \frac{1}{\tau} \sum_{j=1}^B \int_{(j-1)\tau/B}^{j\tau/B} P(t) e^{i\omega_n t} dt \quad (-5-)$$

Changing variable from t to $t + j\tau/B$ gives:

$$C_n = \frac{1}{\tau} \sum_{j=1}^B \int_0^{\tau/B} P\left(t + \frac{j\tau}{B}\right) e^{i\omega_n(t+j\tau/B)} dt \quad (-6-)$$

4.6 EFFECT OF NUMBER OF BLADES ON ROTATIONAL NOISE
(Continued)

A comparison of equations(3)and(6)shows that when $k = j$ and

$$e^{im\omega_B t} = e^{i\omega_n(t+j\tau/B)} \quad \text{for all } t, \quad (-7-)$$

then $A_m = B \cdot C_n$.

Equation (-7-) is true when the exponents differ by 2π or some integral multiple of 2π , $2\pi(Z)$: $Z = 0, \pm 1, \pm 2, \dots$

$$m\omega_B t = \omega_n(t + j\tau/B) + 2\pi Z$$

$$m\omega_B t = \omega_n t + \frac{\omega_n \tau}{B} n_j + 2\pi Z$$

In order for this to be true for all time:

$$m\omega_B t = \omega_n t \quad \text{or} \quad \frac{\omega_B}{\omega_n} = \frac{n}{m} \quad (-8-)$$

and

$$\frac{\omega_n \tau n_j}{B} + 2\pi Z = 0.$$

Recalling that $\frac{\tau}{B} = \frac{2\pi}{\omega_B}$, then

$$-2\pi Z = \frac{2\pi \omega_n n_j}{\omega_B} \quad \text{giving} \quad -Z = \frac{\omega_n n_j}{\omega_B}$$

and substituting from (-8-) gives

$$-Z = \frac{m n_j}{n} = m_j \quad (-9-)$$

which must always be true because the product of two integers m and j must be an integer, $-Z$.

4.6 EFFECT OF NUMBER OF BLADES ON ROTATIONAL NOISE
(Continued)

Recalling that $\omega_r = 2\pi/\tau$ and $\omega_b = 2\pi B/\tau$, we find that (From Eq.(8)) this condition reduces to:

$$\frac{h}{m} = B.$$

Thus, it has been shown that the m^{th} harmonic of a B bladed rotor is B times the $mB^{\text{th}} = n^{\text{th}}$ harmonic of a one bladed rotor with the same loading per blade:

$$A_m = BC_n.$$

This leads to the conclusion that for a given thrust, tip speed and diameter, the envelope of the Sound Pressure Level-Frequency spectrum is independent of the number of blades in the rotor system but the frequencies at which rotational harmonics occur are not. This is illustrated in Figure 4.13 for a rotor of the size tested in the Reference 1 program at a thrust of 10,000 pounds. Note, for example that the 6th harmonic of a two bladed rotor, the 4th harmonic of a three bladed rotor, and the 3rd harmonic of a 4 bladed rotor all have the same sound pressure level since they all fall at the same frequency.

The thrust of a hovering rotor is:

$$T = t_c \sigma \pi R^2 \rho V_t^2 \quad (\text{Reference 7})$$

- where T = Thrust
 t_c = Thrust coefficient
 σ = Rotor solidity
R = Blade radius
 ρ = Density of air
 V_t = Tip speed

Since $\sigma \pi R^2$ is the total blade area this may be rewritten:

$$T = t_c n A_b \rho V_t^2$$

where: A_b = The area of one blade

n = Number of blades

An example of this can be seen in that the thrust of a CH-47 rotor using three (3) 23010 blades at a tip speed of 750 FPS is very closely matched at a tip speed of 650 FPS by a four (4) bladed rotor of the same airfoil or by the three bladed, Boeing/Vertol Advanced Geometry Blade rotor of varying optimized airfoil and planform. If the blade aerodynamic design is fixed the role of number of blades is either to relocate the harmonic frequencies, at constant tip speed, or to permit a reduction in tip speed. In evaluating the merits of these approaches it becomes important to carefully specify the definition of rotational noise. Figure 4.14 presents the calculated values of the first nine harmonics of a three bladed rotor at a tip speed of 750 FPS. The corresponding Overall Sound Pressure Level is 100 dB. This spectrum however has high amplitude low frequency components to which the human ear is relatively insensitive. If one applies the conventional "C" weighting network which is generally used to specify acoustical overall sound pressure levels, the first several harmonics are substantially degraded (as shown in Figure 4.14) and the resultant Overall Sound Pressure Level is reduced to 93 dB.

Other frequency weighting systems, such as dBA, PNdB, etc., may also be considerably affected by relatively small shifts in the frequency of the lower harmonics as controlled by number of blades.

Despite these "number games" which must be played very carefully, the most powerful effect on the noise generated by a rotor of a given thrust remains tip speed. Figure 4.15 illustrates this effect and by returning to the example of equal thrust for a 3 bladed rotor at 750 FPS or a 4 bladed rotor at 650 FPS it can be seen that the latter will reduce the noise by 6 dB.

The problem in resorting to tip speed reduction however lies in the fact that for a fixed radius lower tip speed means lower rotor speed and hence higher torque, which in turn requires larger components in the drive system. These

4.6

EFFECT OF NUMBER OF BLADES ON ROTATIONAL NOISE
(Continued)

combined with the added blade and hub weights can impose severe weight penalties on the helicopter. An example of the weight increase of a CH-47 helicopter which accompanies a 750 FPS to 650 FPS (3 to 4 blade) change is:

Drive System	+ 455 lbs.
Blades	+ 600 lbs.
Hub	+ 470 lbs.
<u>Flight Controls</u>	+ 90 lbs.
Total weight increase	+ 1615 lbs.

Since the aircraft gross weight increases approximately two pounds for every pound of weight empty, the gross weight increase to maintain performance is 3230 pounds or an increase of approximately 10%. This in turn will raise the rotational noise by about .8 dB thereby decreasing the net improvement.

	CE-47A	CE-47C	TAPERED	ADVANCED GEOMETRY BLADE (AGB)
Number of Blades	3	3	3	3
Airfoil	0012	23010-1.58	0012	Varies (see sketch)
Radius	29.5 ft.	30 ft.	29.5	30 ft.
Chord	23"	25.25"	Varies(c)	Varies (c)
Twist	9.0°	9.147°	9°	6°
Outout	5.7 ft.	5.8 ft.	5.7 ft.	5.0 ft.

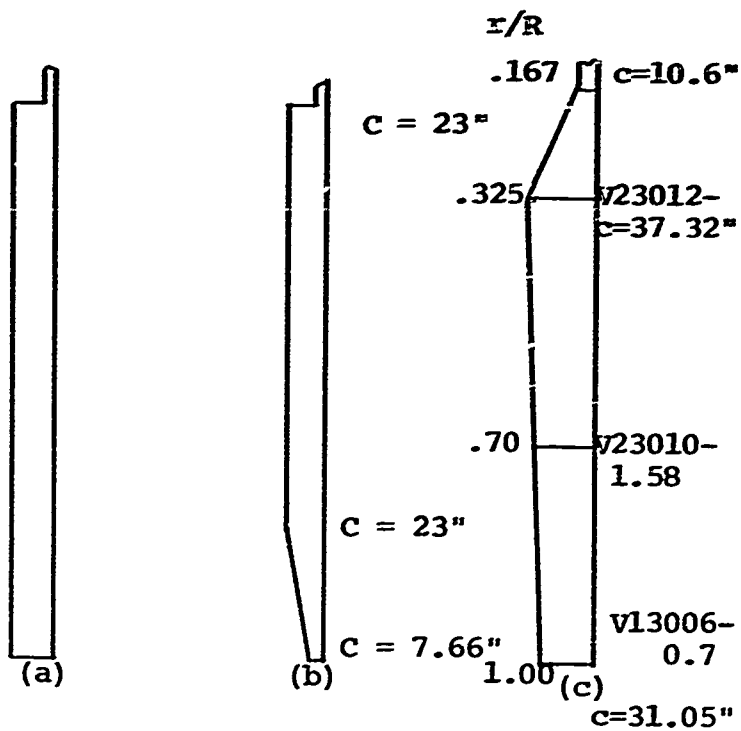
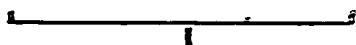


Figure 4.1 - BLADE DESIGNS

AIRFOIL { ——— 23010 Rect.
 { - - - 0012 Rect.

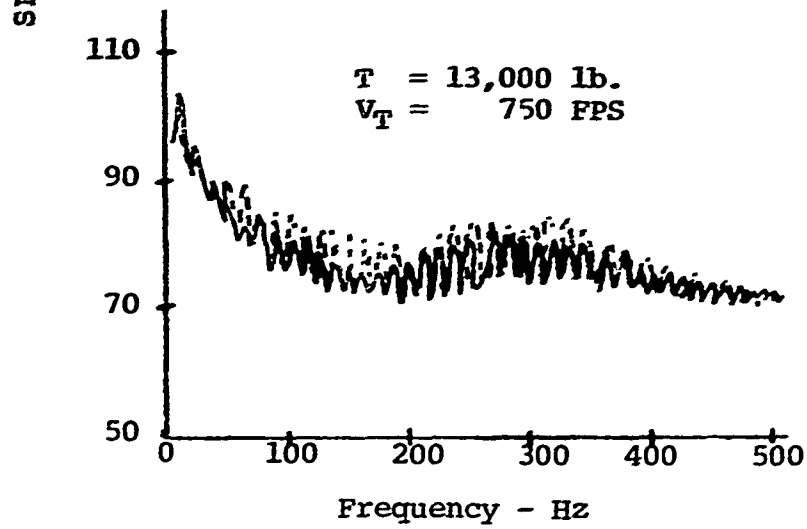
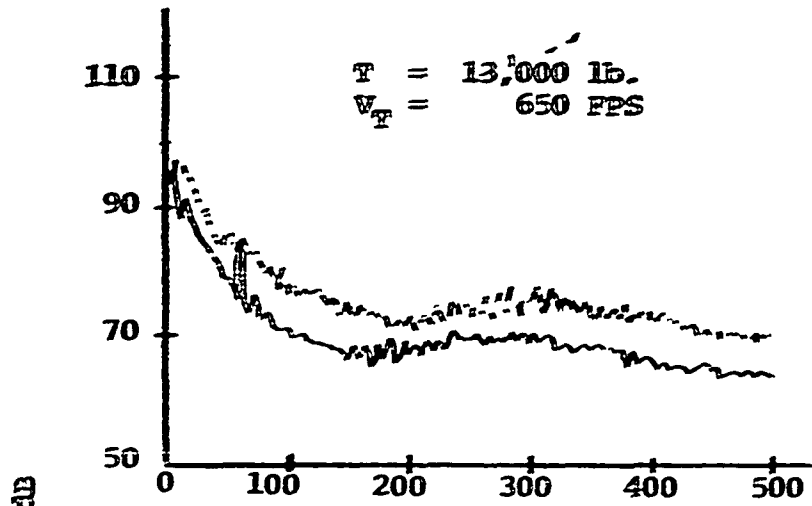


Figure 4.2 - EFFECT OF AIRFOIL SECTION

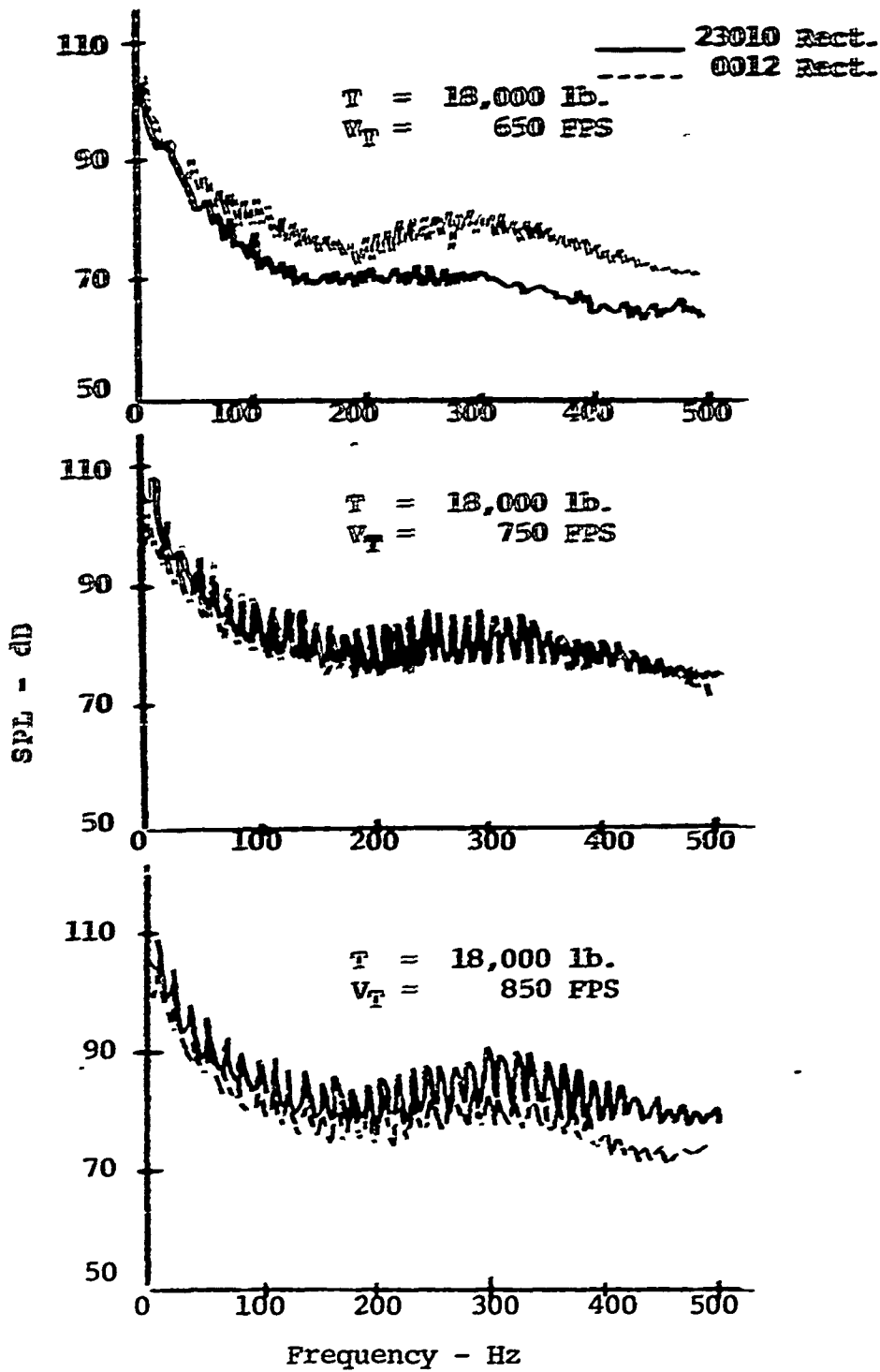


Figure 4.3 - EFFECT OF AIRFOIL SECTION

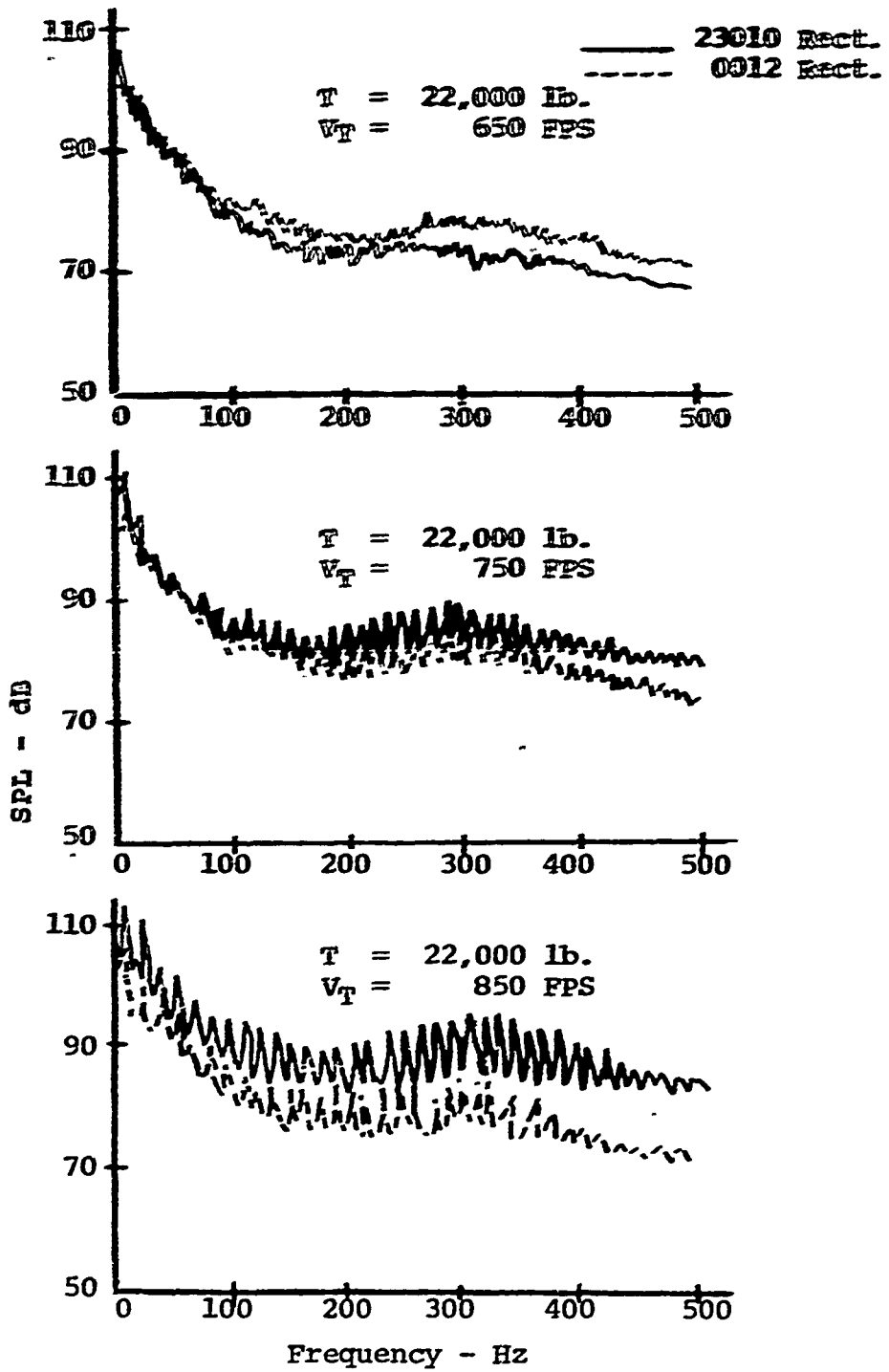


Figure 4.4 - EFFECT OF AIRFOIL SECTION

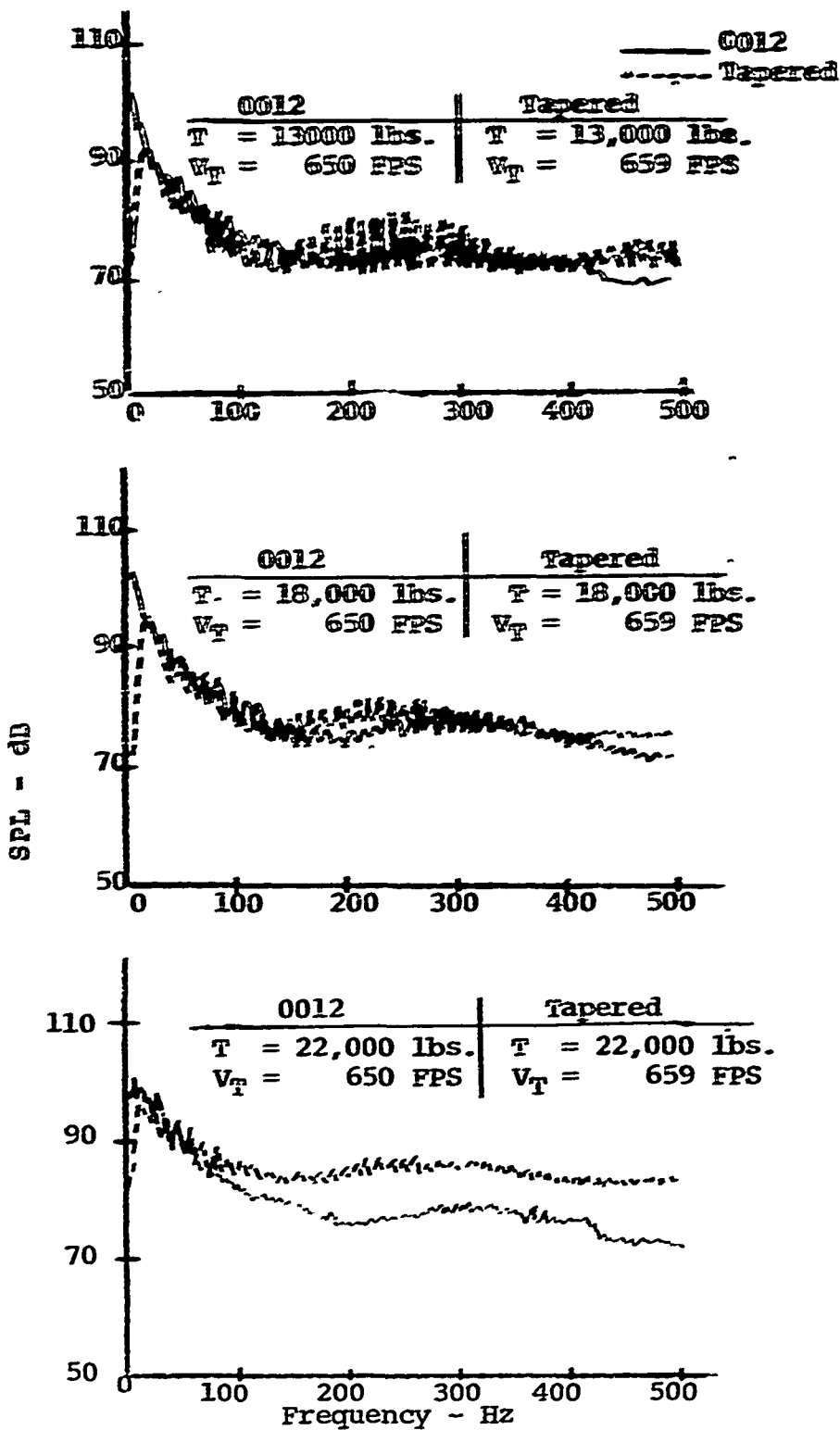


Figure 4.5 - EFFECT OF PLANFORM

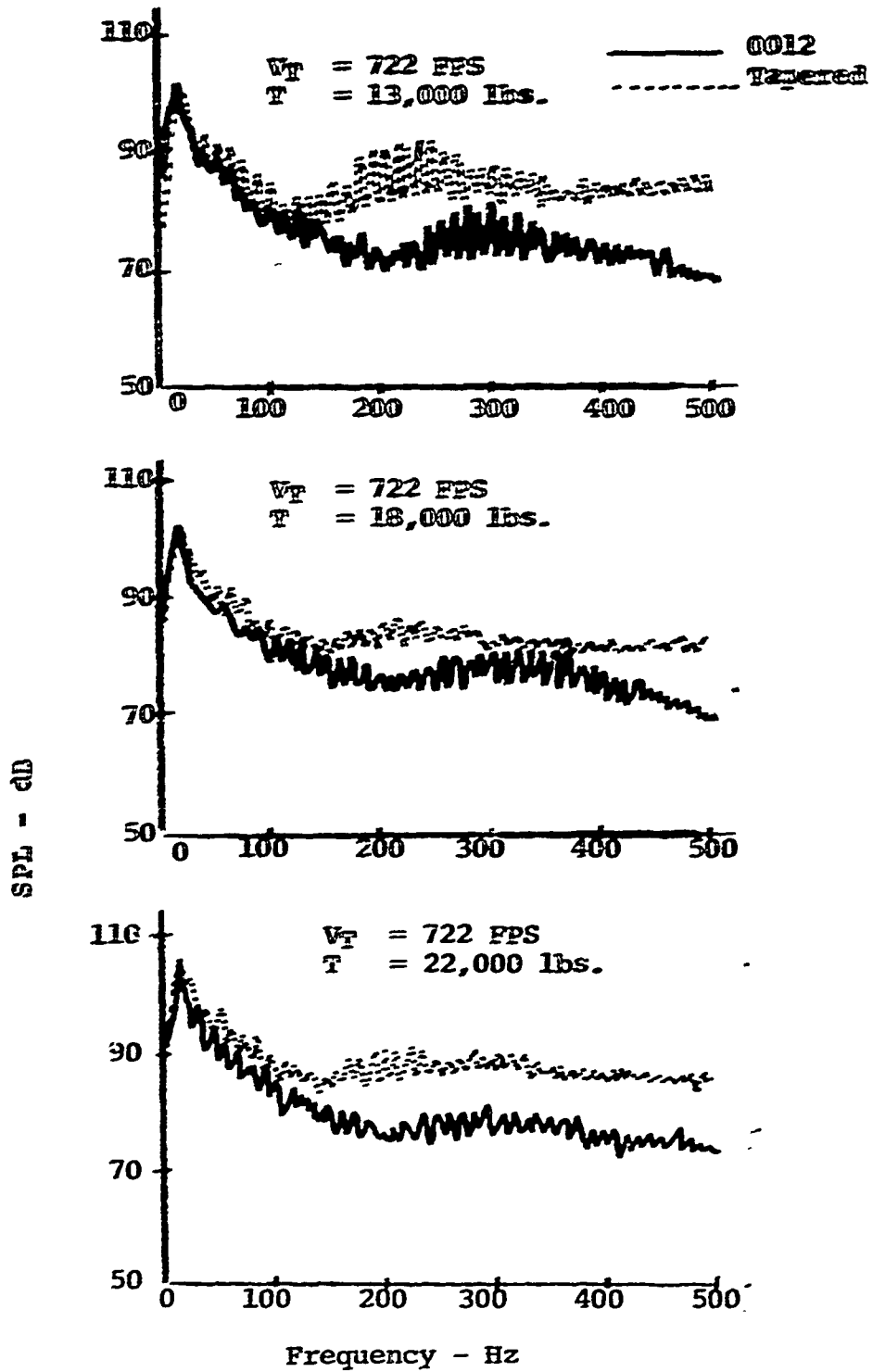
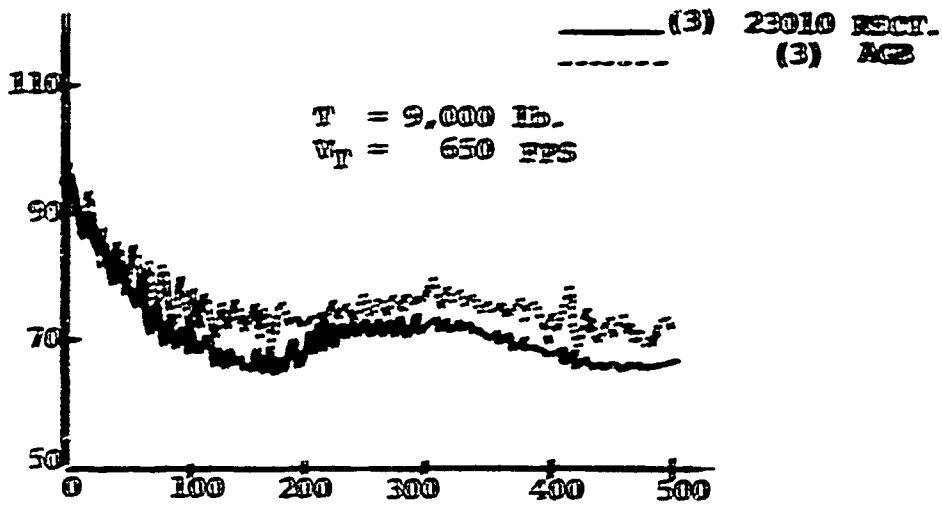


Figure 4.6 - EFFECT OF PLANFORM



SPL - dB

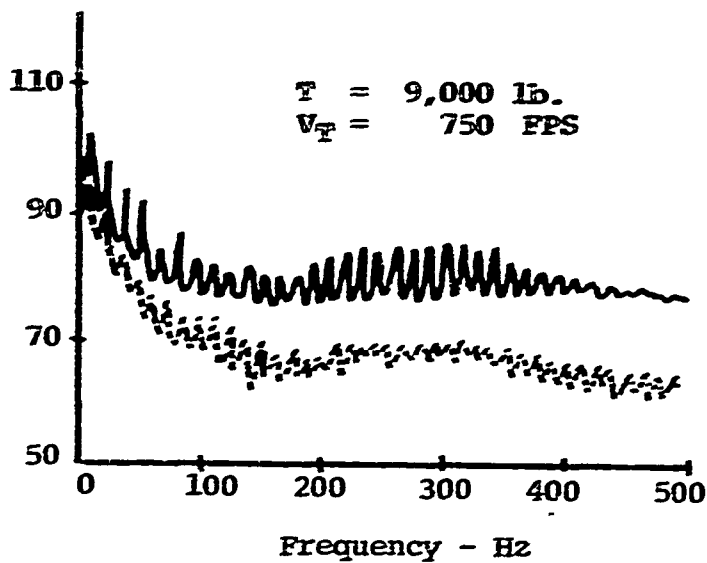


Figure 4.7 - EFFECT OF COMBINED PLANFORM AND AIRFOIL

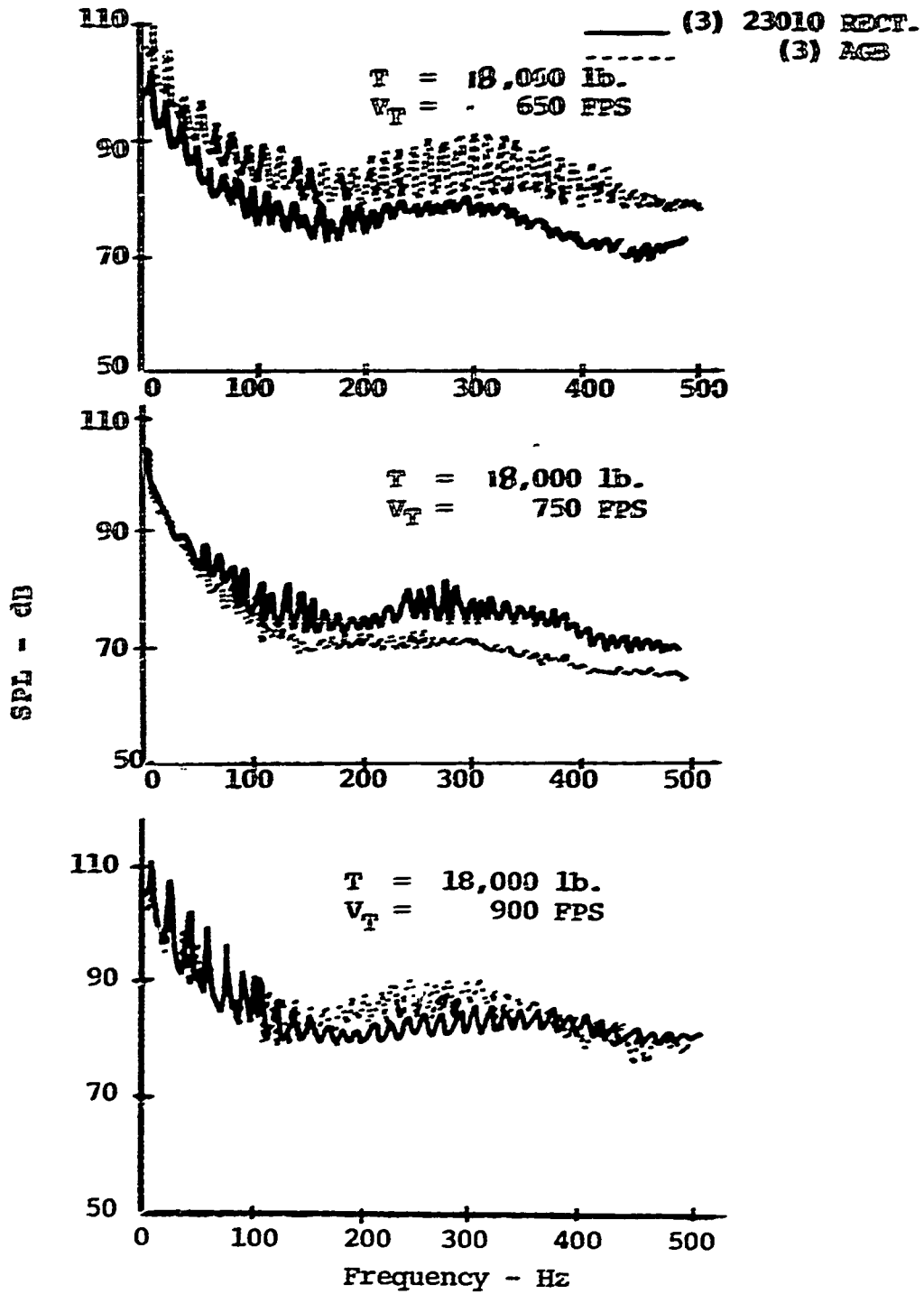


Figure 4.8 - EFFECT OF COMBINED PLANFORM AND AIRFOIL

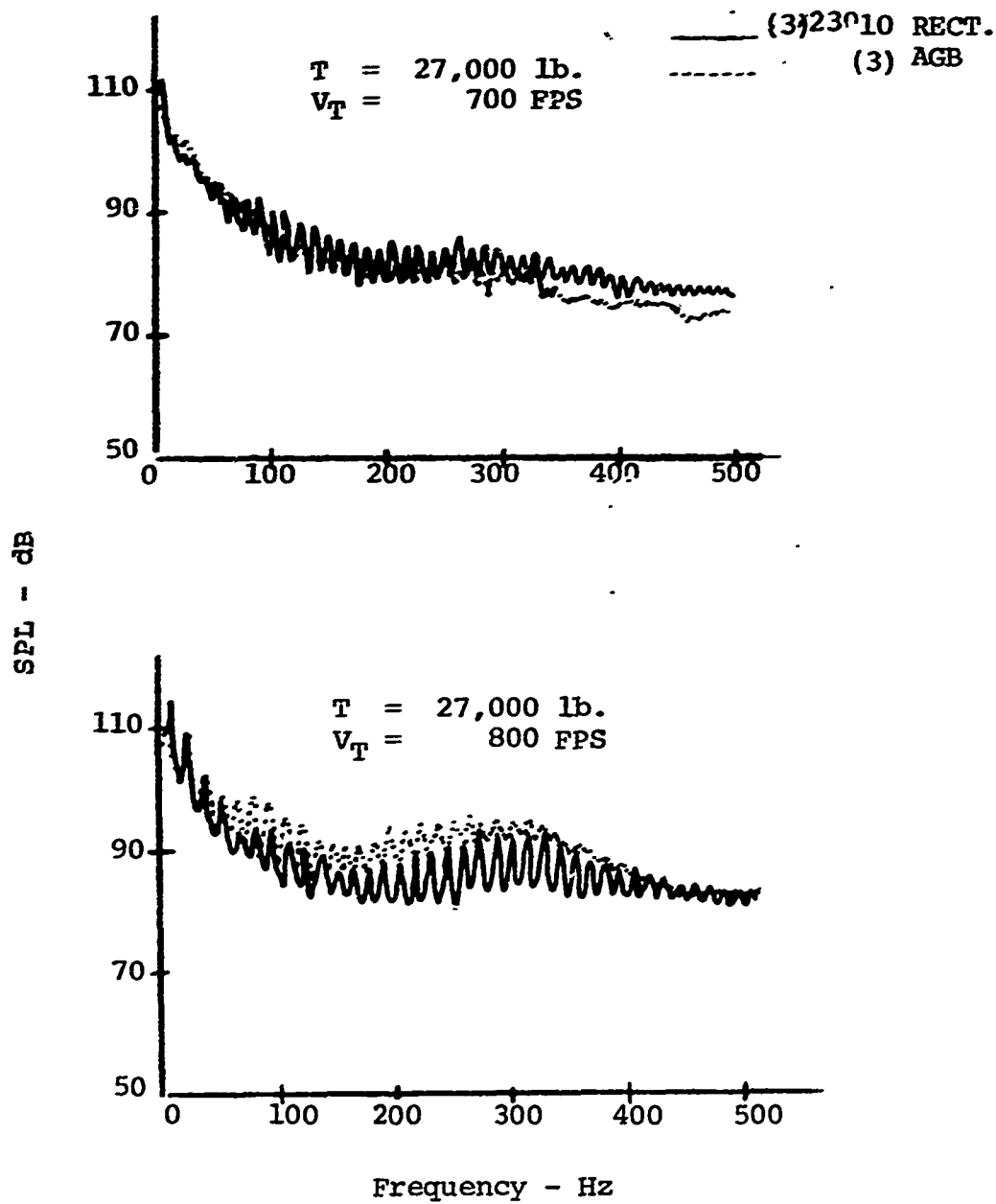


Figure 4.9 - EFFECT OF COMBINED PLANFORM AND AIRFOIL

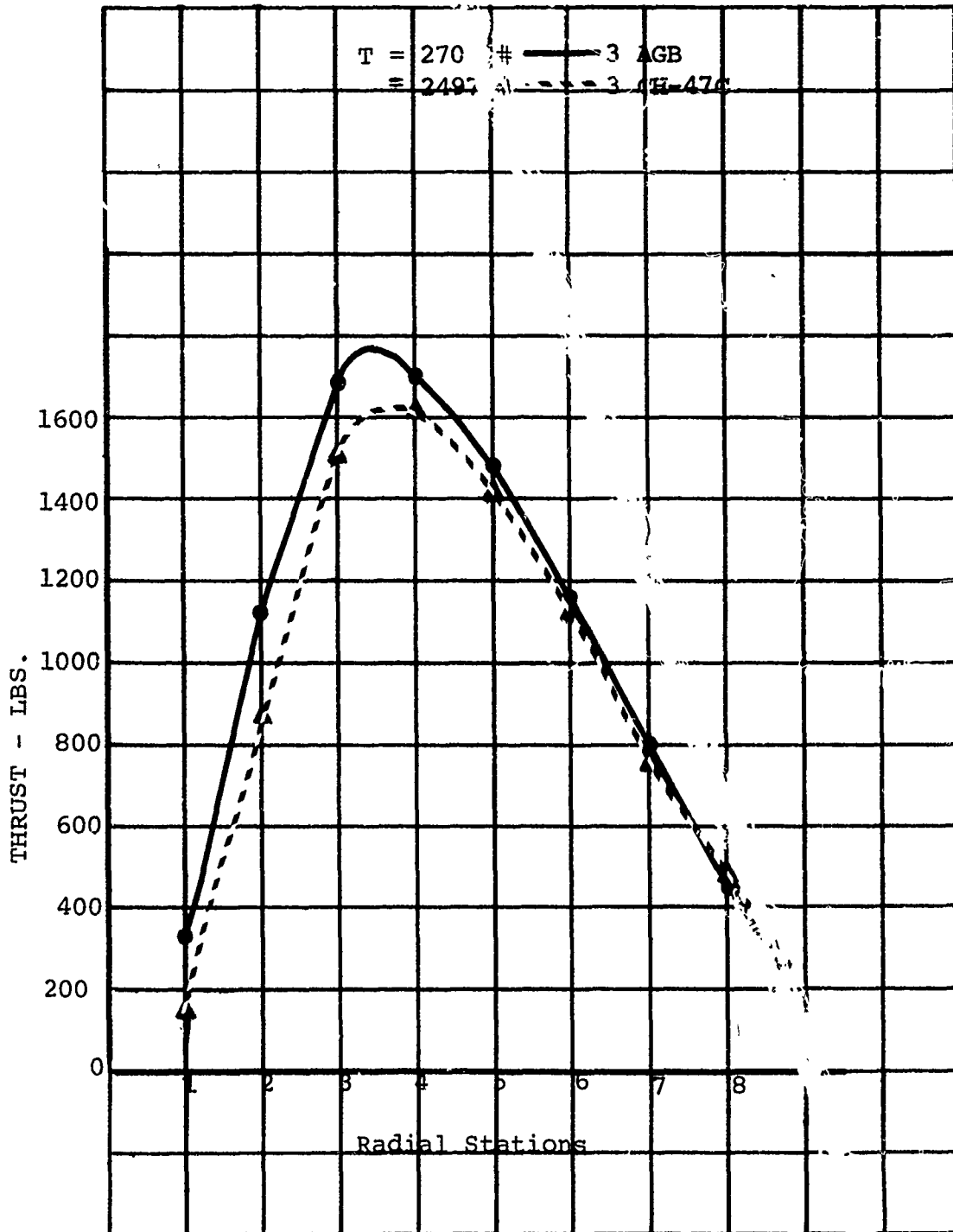
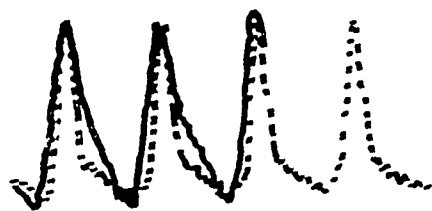
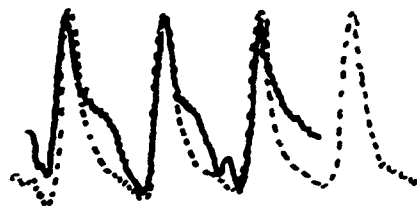


Figure 4.10- THRUST DISTRIBUTION 26,000#

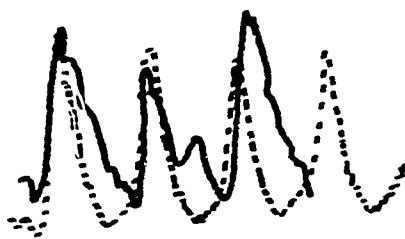
—— 23010 (3)
 AGB (3)



	23010	AGB
T	9700#	11313#
V _T	753 FPS	751 FPS



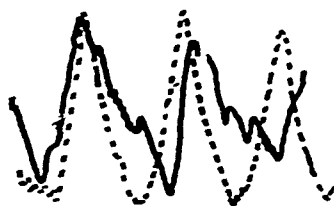
	23010	AGB
T	18985#	20726#
V _T	750 FPS	754 FPS



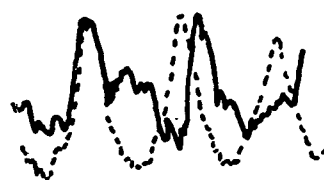
	23010	AGB
T	25960#	29264#
V _T	750 FPS	26960 FPS



	23010	AGB
T	26709#	27855#
V _T	650 FPS	660 FPS



	23010	AGB
T	17445#	17659#
V _T	650 FPS	660 FPS



	23010	AGB
T	8595#	9629#
V _T	650 FPS	657 FPS

Figure 4.11
 COMPARISON OF ROTOR NOISE WAVEFORMS FOR HOVERING AIRCRAFT

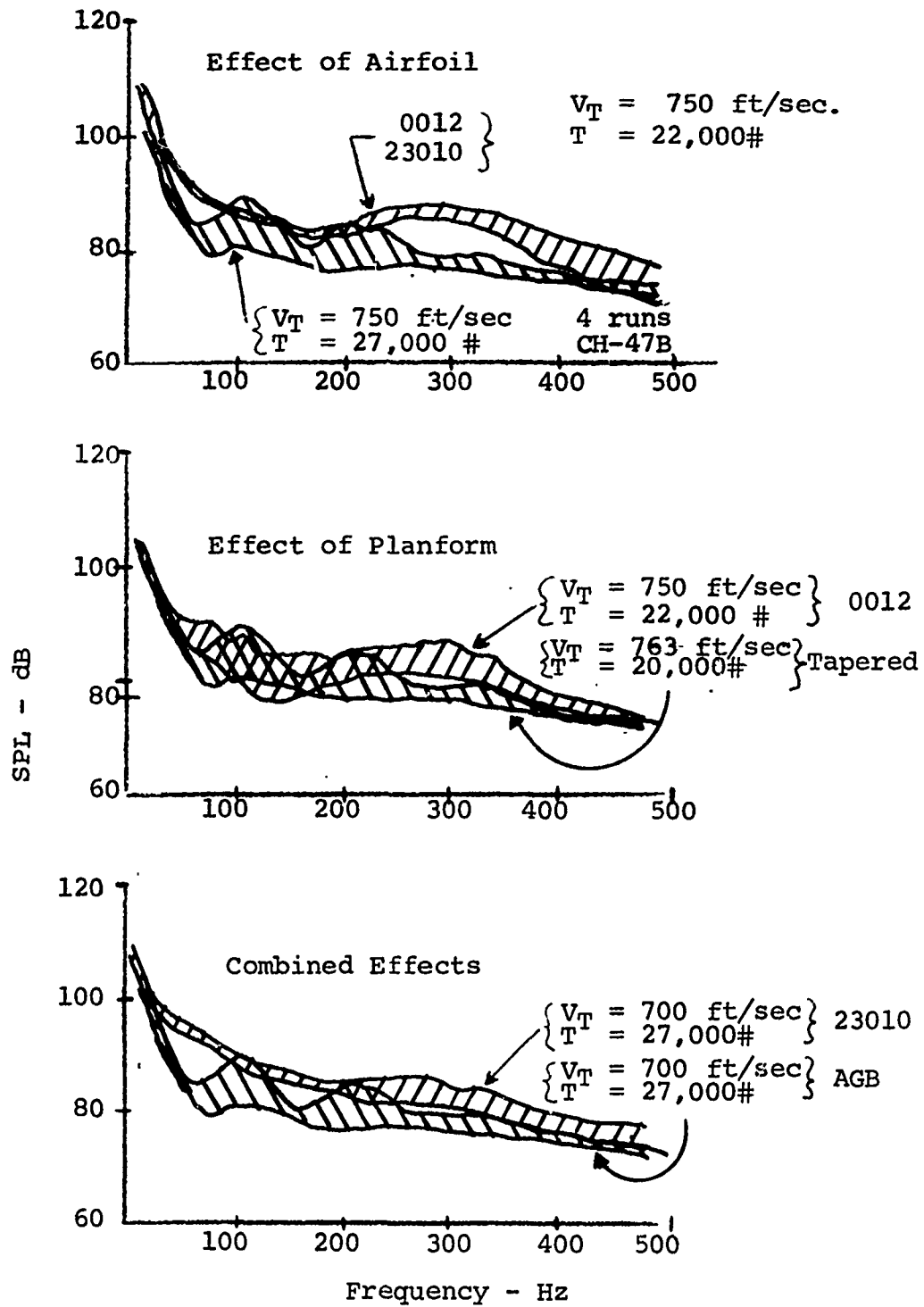


Figure 4.12 - COMPARISON OF VARIOUS EFFECTS

Notation Bn

B = Number of Blades
n = Harmonic Number

NOTE: Prediction shown is for 10,000# thrust.
Other thrust values will be parallel
and shifted by 6 dB/Doubling of thrust..

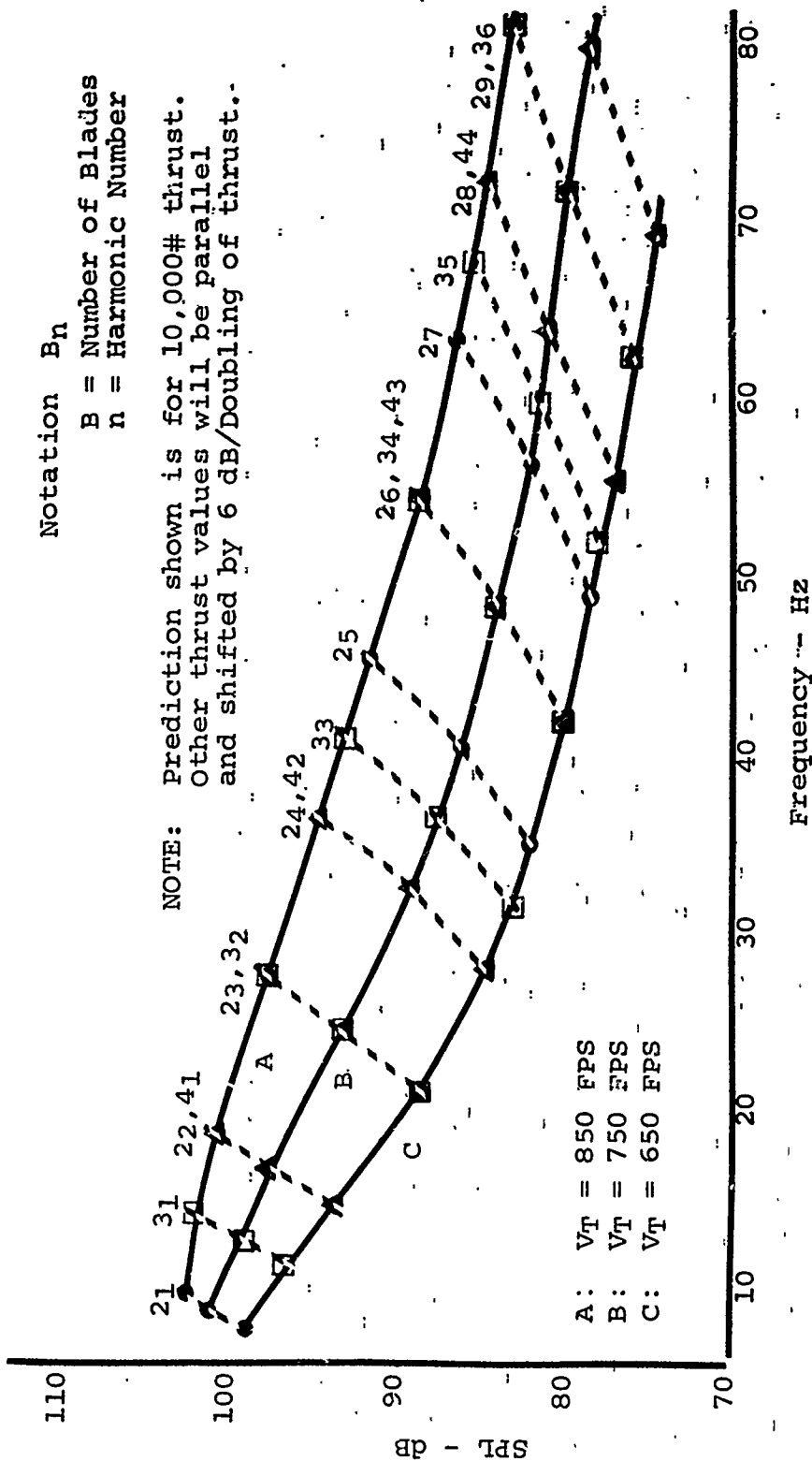


Figure 4.13 -- PREDICTED EFFECT OF TIP SPEED AND NUMBER OF BLADES

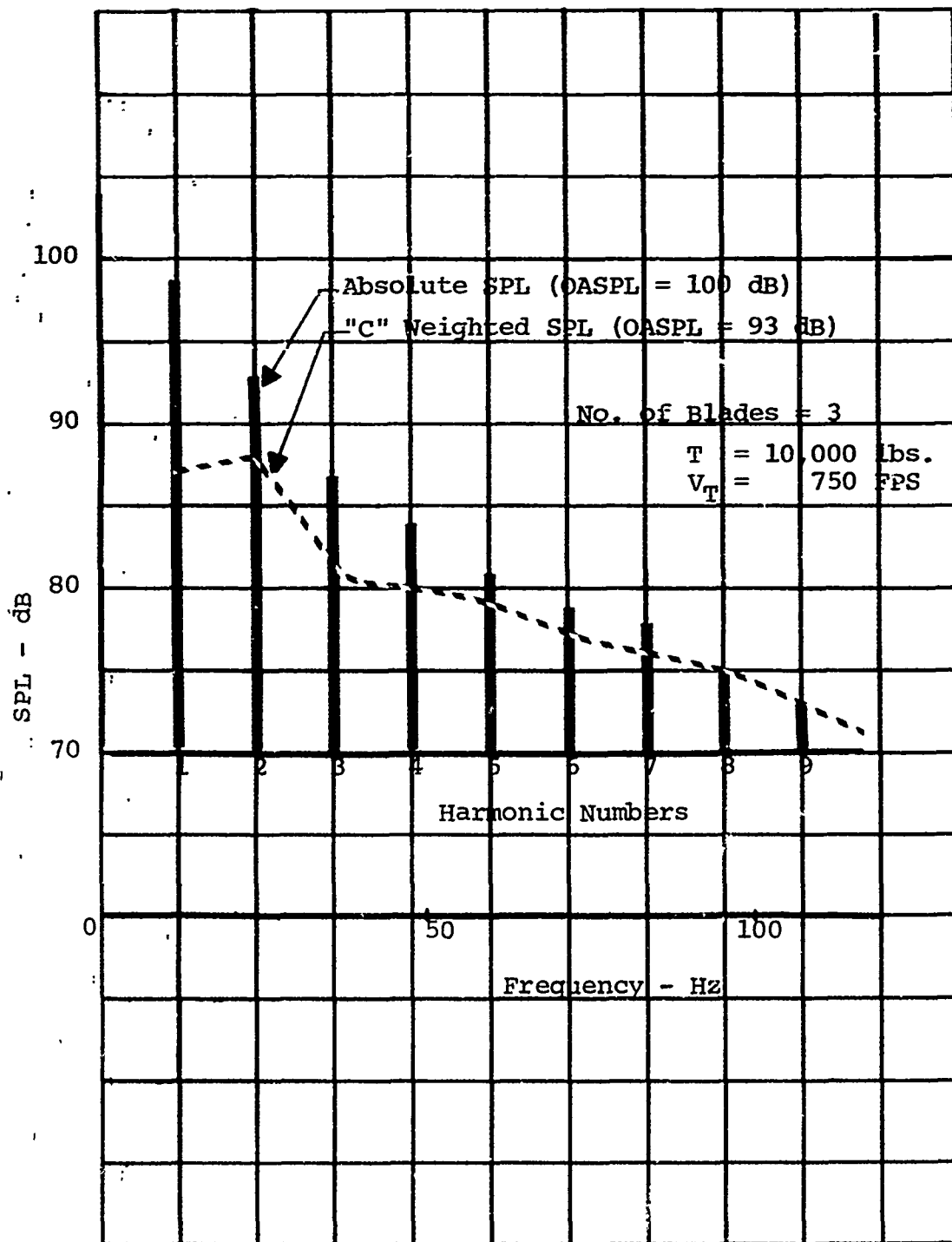


Figure 4.14 - COMPARISON OF ABSOLUTE & "C" WEIGHTED SPL

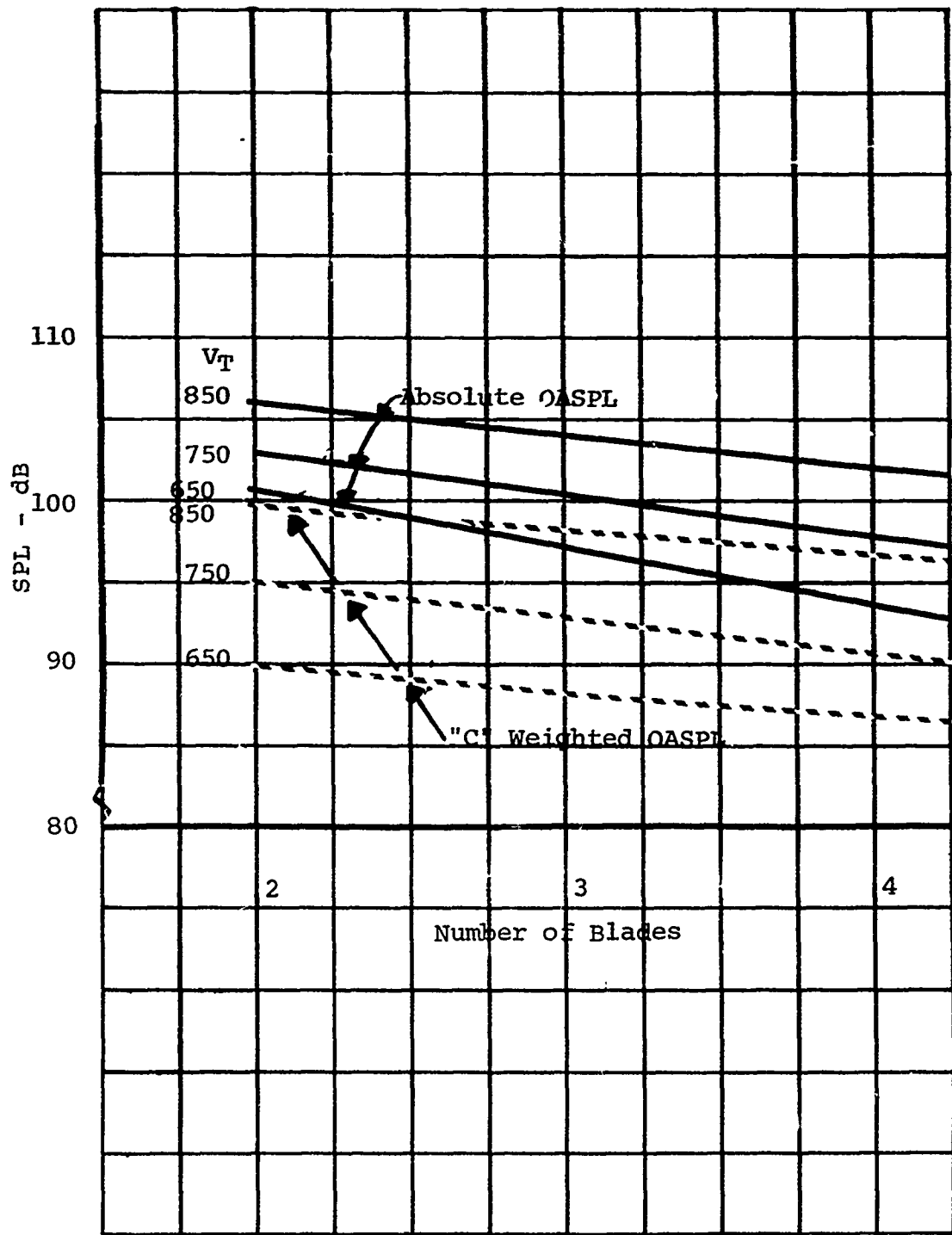


Figure 4.15 - EFFECT OF NUMBER OF BLADES

5.0 HOVERING SINGLE ROTOR IMPULSIVE NOISE

5.1 SUMMARY

A series of whirl tower test programs were completed in 1968 and 1969, studying the acoustical properties of a variety of hovering rotors over a wide range of test conditions. During these test programs, subjective ratings of the impulsive nature of the rotor noise were recorded by a ground observer located 100 ft. from the rotor. Correlation of these subjective ratings, local flow conditions, vortex position studies, and two-dimensional airfoil characteristics have led to a postulated mechanism of single rotor impulsive noise as described below and illustrated on Figure 5.1.

During tests of two, three and four-bladed rotors, flow visualization studies of vortex position were made using smoke trailed from a blade tip. Details of the three bladed study were presented in Reference 1. For each of the test conditions recorded, the vortex was found to intersect or closely approach the following blade. Based on this photographic data, the blade radial location of vortex intersection or near intersection was obtained. The local life coefficient and Mach number were then calculated at this intersection point for the test conditions.

Subjective ratings of each of the test conditions for two, three and four-bladed rotors identified banging and non-banging points and established a common boundary between banging and non-banging conditions.

A study of two-dimensional C_l versus Mach number data for the Vertol 23010-1.58 airfoil used in these tests indicates that the lift divergence boundary ($dC_l/dM = 0$) agrees well with the subjectively rated hover banging boundary. Examination of upper surface pressure distributions for this airfoil reveal that below the lift divergence boundary, the flow is essentially shock-free and above the lift divergence boundary shock waves exist on the surface of the airfoil.

The mechanism of hovering single rotor impulsive noise is, therefore, postulated to depend on the interaction of a blade tip vortex with a following blade, producing short time duration changes in the local flow conditions and either shock wave formation or motion of an existing shock wave. The pressure pulse created by these localized changes in flow conditions has been termed "hover bang".

5.1 SUMMARY (Continued)

In the discussion that follows, subjectively rated test data and two-dimensional airfoil data are presented in more detail for a two, three and four-bladed CH-47C rotor as well as advanced geometry and swept tip blades to verify this approach to the hover banging boundary. An analytical method for predicting sound pressure level is presented which describes the mechanism of single rotor impulsive noise. Using this method, calculation of sound pressure levels for conditions subjectively rated as banging and non-banging have been made and compared with test recorded levels.

5.2 CRITERIA FOR HOVERING SINGLE ROTOR IMPULSIVE NOISE GENERATION

From the vortex visualization studies of Reference 1, blade intersections with the vortex from the preceding blade were found to occur or nearly occur for all of the recorded test conditions. The radial locations of these intersections for the two, three and four-bladed rotors were found to be approximately .90R, .93R and .96R, respectively. Using these intersection points, values of local lift and Mach number were calculated for test points of each of the three rotor configurations. This data has been presented in Figure 5.2 along with the subjective ratings of each of these test conditions. Solid symbols were rated as banging points and open symbols as non-banging. In this figure, a boundary is defined outside of which no single rotor impulsive noise has been observed, for these rotors and within which the data do not group by blade number.

The two, three and four-bladed rotor tests all utilized CH-47B/C blades which use the V23010-1.58 airfoil. C_l at constant angle of attack vs Mach number data for this airfoil are plotted in Figure 5.3 and the locus of points at which the lift coefficient significantly deviates ($\frac{dC_l}{dM} = 0$) from the Karman-Tsien growth rate with Mach number is shown. Figure 5.4 compares this lift divergence boundary with the "no impulsive noise" boundary of Figure 5.2 and demonstrates that the two boundaries are very similar. This implies that hovering single rotor impulsive noise can be controlled by utilizing airfoils with increased Mach number for lift divergence on rotor blades at spanwise stations subject to vortex intersections. Figure 5.5 shows the lift divergence boundaries for several airfoils and indicates that airfoils such as the V13006-.7 can substantially improve the allowable rotor "no impulsive noise"

5.2 CRITERIA FOR HOVERING SINGLE ROTOR IMPULSIVE NOISE GENERATION (Continued)

operating boundary. A rotor with this airfoil, the AGB rotor, has been tested by Boeing-Vertol. Results from the whirl tower tests are shown in Figure 5.6. The rotor was tested at tip speeds and thrust levels at which the CH-47B/C rotor produced impulsive noise; no impulsive noise was noted subjectively or in the waveforms of the AGB testing. RPM restrictions on the rotor prevented testing at conditions above the lift divergence boundary for the V13006-.7 airfoil; however, the testing does clearly demonstrate that blade loading and tip speed alone are insufficient criteria for defining hovering single rotor impulsive noise avoidance boundaries as the AGB spanloadings and tip speeds did achieve levels identical to those at which the CH-47B/C rotors produce impulsive noise (Figure 5.7). Similarly, test of a "swept" tip rotor produced no impulsive noise at conditions identical to the spanloadings and tip speeds at which the CH-47B/C isolated rotor produces impulsive noise (Figures 5.8 and 5.9). Figure 5.9 illustrates that the lift divergence boundary applies to this swept tip data if the local sweep angle at the most probable radial station for blade vortex intersection is used to define an effective local Mach number.

Based on the above evidence and results of model rotor testing, the criteria for single rotor hover impulsive noise to occur has been postulated as:

1. The vortex from a preceding blade must pass near the blade producing the noise and must also change its position relative to that blade.
2. A shock wave must exist (or nearly exist) on the surface of the blade where the vortex passes.

Thus, the mechanism of hovering single rotor impulsive noise is postulated to depend on the interaction of a blade tip vortex with a following blade resulting in short time duration change in local flow conditions and either shock wave formation or motion of an existing shock wave. The pressure pulse created by these localized changes in flow conditions has been termed "hover bang".

A study of tip vortex motions and blade-vortex interactions as related to the mechanism of "hover bang" is given in the following paragraphs.

5.3 MECHANISM OF VORTEX INTERACTION

The vortex shed from the tip of a hovering rotor is embedded in the flow field which is moving axially downward with an accompanying small radial motion. This axial motion has been measured by Landgrebe and reported in Reference 8. The downward drift of the tip vortex is shown in this reference to be very slow until the passage of the following blade. Figure 5.10 illustrates that the following blade causes an increase in the drift rate after its passage. Therefore, the nominal position of the tip vortex is closer to the following blade than calculated by a uniform drift assumption.

The empirical equation given in Reference 8 for the position of the tip vortex before interaction with the following blade is:

$$\bar{z}(\psi) = .25 (C_T/c + .001 \theta_{\text{DEG}}) \psi \quad (1)$$
$$0 \leq \psi \leq 2\pi/b$$

where $\bar{z} = z/R$ N.D.

$\theta =$ Twist in degrees

$\psi =$ Azimuth position behind the blade shedding of the vortex

An expression for the radial position of the vortex at the following blade has been given by Landgrebe in Reference 8 as a function of rotor thrust coefficient. However, a study of the data presented in his reference indicates that for the time period of one blade passage and for the range of thrust coefficients presented, the radial vortex position is relatively insensitive to changes in rotor thrust coefficient. Based on Boeing-Vertol test data, the vortex radial positions at the following blade have, therefore, been assumed to be .90R, .93R and .96R for the two, three and four-bladed rotors, respectively.

The position of the tip vortex is further altered by the presence of ground wind. From potential flow theory, lift is generated when a uniform flow field is imposed perpendicular to a vortex filament. The tip vortex rotates in the direction from the blade lower surface to the upper surface at the tip of the blade. Hence, the vortex motion is up at the upwind azimuth location and down at the downwind location. At the 90° and 270° azimuth, the orientation of the vortex filament is parallel to the

5.3 MECHANISM OF VORTEX INTERACTION (Continued)

velocity and no lift is generated. Relative to the following blade, the tip vortex is at its lowest position at $\psi = 0^\circ$ and at its highest position at $\psi = 130^\circ$.

The measurements that were made for Figure 5.11, show this nearly sinusoidal oscillation of the tip vortex. The amplitude of the "apparent" oscillation of the vortex relative to the following blade was obtained from the data of Reference 8 as:

$$A = 522.4 (C_T / \sigma)^{.9349} (\beta)^{.13577} (V_g / V_n)^{1.0422} \quad (2)$$

where A = amplitude in inches

$$\beta = 1 - M_{TIP}^2$$

V_g = ground wind velocity

V_n = average induced velocity

Hence the vortex position may be given by:

$$h - Z + A \cos \psi \quad (3)$$

A further consideration relating to the effects of blade vortex interaction is that the velocity field induced by the vortex is not established instantaneously. The vortex core is established during the initial roll-up over the blade tip. Additional vorticity is fed into it from the trailed wake from the outer portion of the blade. However, the vortex induced velocity field is established by viscosity over a finite time. When considering the problem of blade vortex interactions, this time element relates to the blade passage frequency. For a representative case of a three-bladed rotor at 240 RPM, the time for one blade passage is 1/12 second.

The diffusion of vorticity is given in Reference 9 as:

$$V = \frac{\Gamma}{2\pi r} e^{-r^2/4\nu t} \quad (4)$$

r = radius of vortex

Γ = strength of tip vortex

ν = kinematic coefficient of viscosity

5.3 MECHANISM OF VORTEX INTERACTION (Continued)

Considering that the viscosity for turbulent flow may be greater than the kinematic viscosity, and the representative time for one blade passage, the exponential term is sufficiently small so that the flow field due to the tip vortex is not established by the time the following blade encounters the vortex. Therefore, the vortex induced velocity at the following blade results primarily from the vortex core.

A literature search has been conducted to determine a representative core size. However, the available data does not give a definitive value. Johnson, Reference 12, and Widnall, Reference 13, used core radii on the order of 18% to 20% of the blade chord. On the other hand, the data of Dosanjth, et al, Reference 14, and McCormick, Reference 15, result in core radii of 8% of the chord. The more recent data of Rorke, et al, Reference 16, gives a core radius to blade chord ratio of .05. Measurements by Chigier and Consiglia, Reference 17, give core radius equal to .09 chord. The measurement of vortex velocity necessary to establish the core radius is sensitive to the oscillation of the vortex especially when probing the region where the velocity reaches its maximum value. Other data indicate that the vortex core size measured from wings may differ substantially from core size of vortices generated by rotor blades.

Because of this variation in the published core size data, the numerical calculations have been carried out for three core sizes, $\frac{r_{\text{core}}}{\text{chord}}$ equal to .20, .143 and .08. When the vortex is very close to the blade, Johnson, Reference 12, showed that following modifications are required:

$$\Gamma_{\text{EQ}} = [1.35 + 0.65 (\sqrt{2}h/r_c)] \Gamma_{\infty} (1 - h^2/r_c^2) \quad (5)$$

$$h_{\text{EQ}} = (r_c^2 - h^2)^{1/2} \quad (6)$$

$$V_{\text{MAX}} = \frac{\Gamma_{\text{EQ}}}{4\pi h_{\text{EQ}}} \quad (7)$$

r_c = core radius of vortex

The velocity change at the blade is calculated assuming that the tip vortex is an infinite line vortex of finite core size located at a distance h below the blade as given in the expression above. The vertical component of the velocity results in a change of both the total velocity perpendicular to the blade and an angle of attack change. The first results in a change in Mach number and a significant chordwise shift in the shockwave when the blade segment is at or near the critical Mach number. The data of Reference 10 indicate that only slight changes in shockwave position occur due to changes in the angle of attack.

To properly evaluate the influence of these localized changes in flow conditions created by the proximity of a tip vortex, airfoil chordwise pressure distributions were required for a range of Mach numbers and angles of attack. Since experimental pressure data for the Boeing-Vertol airfoil section BV23010-1.58 was not available for the wide range of Mach numbers and angles required, theoretical pressure distributions were obtained from the Boeing computer program TSONIC for the mixed subsonic-supersonic flow. The composite plots of upper surface pressure distribution obtained from the program indicate the magnitude of the loading changes associated with the shock motion, Figures 5.12 to 5.15. The change in normal force coefficient, ΔC_N , between two Mach numbers is equivalent to the difference in area under the respective Mach number curves. Figure 5.16 presents the changes in normal force coefficients computed from the data of Figures 5.12 through 5.15. The reference C_N value at each angle of attack was obtained from the pressure distribution which indicated no shock formation. With the finite number of data obtained from TSONIC, the reference C_N value for each angle of attack could not be pinpointed accurately. The change in C_N with Mach number is, therefore, assumed linear and is based on the higher Mach number curves where the shock wave is well established.

The analytical expression for the vortex position as a function of blade azimuth and, thereby, time can be combined with the theoretical velocity induced by a vortex core, to produce a variation in velocity locally on the blade as a function of time. This change in velocity and, thereby, Mach number with time produces a change in pressure or normal force as indicated in Figure 5.16. The resulting short time duration pressure pulse has been identified in test recorded waveforms of hover banging data.

5.3 MECHANISM OF VORTEX INTERACTION (Continued)

5.3.1 Sound Pressure Level

The sound pressure corresponding to the change in lift was obtained from the acoustic theory presented in Section 3 earlier in this report.

$$P(t) = \left[\frac{\bar{r}}{4\pi(1-M_r)^2 r^2 a_0} \left\{ \frac{\partial \bar{F}}{\partial t} + \frac{\bar{F}}{(1-M_r)} \frac{\partial M_r}{\partial t} \right\} + \frac{1}{4\pi(1-M_r)^2 r^2} \left\{ \frac{\bar{F} \cdot \bar{r}}{r} \frac{(1-M^2)}{(1-M_r)} - \bar{F} \cdot \bar{M} \right\} \right] \quad (8)$$

Only the first two terms on the right hand side, $\frac{\partial \bar{F}}{\partial t}$ and $\frac{\partial M_r}{\partial t}$, are due to changes resulting from the shock motion and contribute to the impulsive noise. The other two terms are rotational noise terms. The sound pressure in the above equation is that measured at the observer while the square bracket indicates that all of the terms are calculated at the point where the sound is generated. The vector \bar{r} is the distance from the source to the observation point and the term M_r is the component of the Mach number in the direction of \bar{F} .

5.3.2 Calculation of Sound Pressure Level

The analytical model for the single rotor hover impulsive noise postulated has been applied to two cases monitored during acoustics tests of a three-bladed CH-47 rotor conducted by Boeing-Vertol in 1968. The two data points selected are located on the noise criteria plot of Figure 5.17 as test points 43 and 14. Test point 43 was subjectively rated as a heavy banging point and is located close to the impulsive noise boundary. Test point 14 showed no indication of banging, however, it does have a reasonable blade loading as reflected in the lift coefficient.

For these two test conditions, calculations have been made of vortex position, induced velocity, and sound pressure level as outlined in previous paragraphs. Table 5-1 summarizes the blade characteristics, the test conditions along with the principal numerical results from the computations for three assumed core sizes (r_c/c). The strength of the tip vortex is relatively more significant for TP14 and the amplitude of the apparent oscillation is greater. However, the Mach number in the vortex interaction region is small and the increase in Mach number due to the vortex interaction does not result in an attached shock.

5.3 MECHANISM OF VORTEX INTERACTION (Continued)

5.3.2 Calculation of Sound Pressure Level (Continued)

The calculated sound pressure levels for both banging and non-banging test points are lower than the measured overall sound pressure level at these two conditions. This was expected since only the two terms relating to the shock motion in equation (8) were used in these computations. The significant result of the computation, however, is the agreement between the calculated and measured increment between banging and non-banging conditions, especially for the smaller core size assumptions.

Since the calculated values represent an impulsive type of loading this would evidence itself as a growth in many harmonics of the airload on the blade and hence of the acoustic radiation. The distribution of this energy and therefore the spectral distribution of the change in acoustical signature cannot be accounted for at the present time. The proposed mechanism of single rotor impulsive noise based on the interaction of a trailed vortex with the following blade and the resulting production or displacement of a shock wave, however, has led to a reasonable prediction of the peak to peak value pressure pulse associated with hover bang. A more rigorous methodology for computing this increment in sound pressure level would require improvements in the state-of-the-art of predicting vortex geometry and trajectory.

TABLE 5-1

CH-47C Rotor System
 Number of Blades = 3
 Radius = 30 ft.

Chord = 25.25 inches
 Solidity = .067
 Twist = -9.14 degrees

	Test Point 43 "Banging"		Test Point 14 "Non-Banging"
Thrust - lbs.	22007		20006
C_T	.00567		.00673
Tip Speed - FPS	754		660
Tip Mach Number	.682		.597
Ground Wind - KTS	10		10
Mean Position of Vortex Below Following Blade - Inches	14.2		17.5
Amplitude of Vortex "Oscillation" - Inches	23.7		34.7
Radial Position of Intersection - X/R	.93		.93
Local Mach Number*	.633		.55
Local Lift Coefficient	.567		.667
Local Angle of Attack*	4.5		5.7
		<u>Δ SPL</u>	
Calculated Sound Pressure			
Level SPL - db $l_c/c = .08$	97.9	11.1	86.2
$l_c/c = .143$	94.7	11.3	83.4
$l_c/c = .20$	89.2	6.5	82.7
Measured Overall SPL - db (Average) (Peak to Peak)	119	12	107

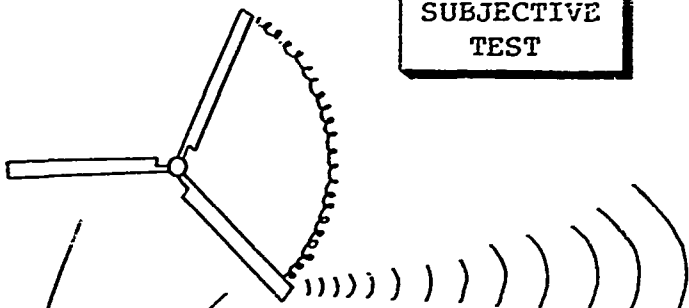
(*): The Mach number and angle of attack distribution along the blade were obtained from the Boeing-Vertol hover and axial flight analysis computer program, B-92.

SINGLE ROTOR HOVER IMPULSIVE NOISE CRITERIA

Subjective Evaluation

- Banging
- Nonbanging

SUBJECTIVE TEST



CALCULATE C_l and Mach No. at intersection

BOUNDARY based on subjective evaluation

FULL SCALE ROTOR TEST

LIFT COEFFICIENT AT INTERSECTION

NONBANGING

BANGING

SHOCK BOUNDARY or lift divergence boundary

MACH NUMBER AT INTERSECTION

2-D AIRFOIL CHARACTERISTICS

Pressure Distribution Upper Surface

$M = .7$ No shock
 $M = .75$ Shock

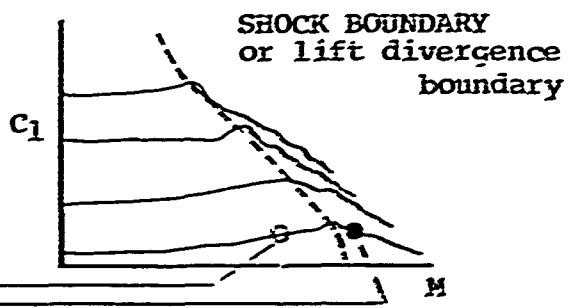
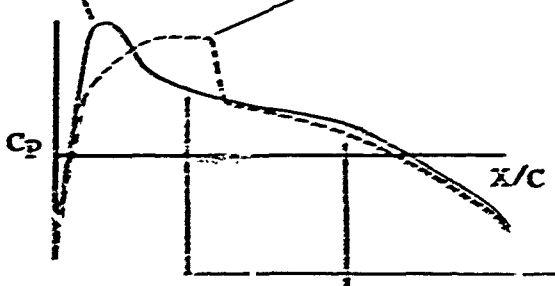


Figure 5.1

SINGLE ROTOR IMPULSIVE NOISE
REFERENCED TO LOCAL CONDITIONS AT
BLADE-VORTEX INTERSECTION POINTS

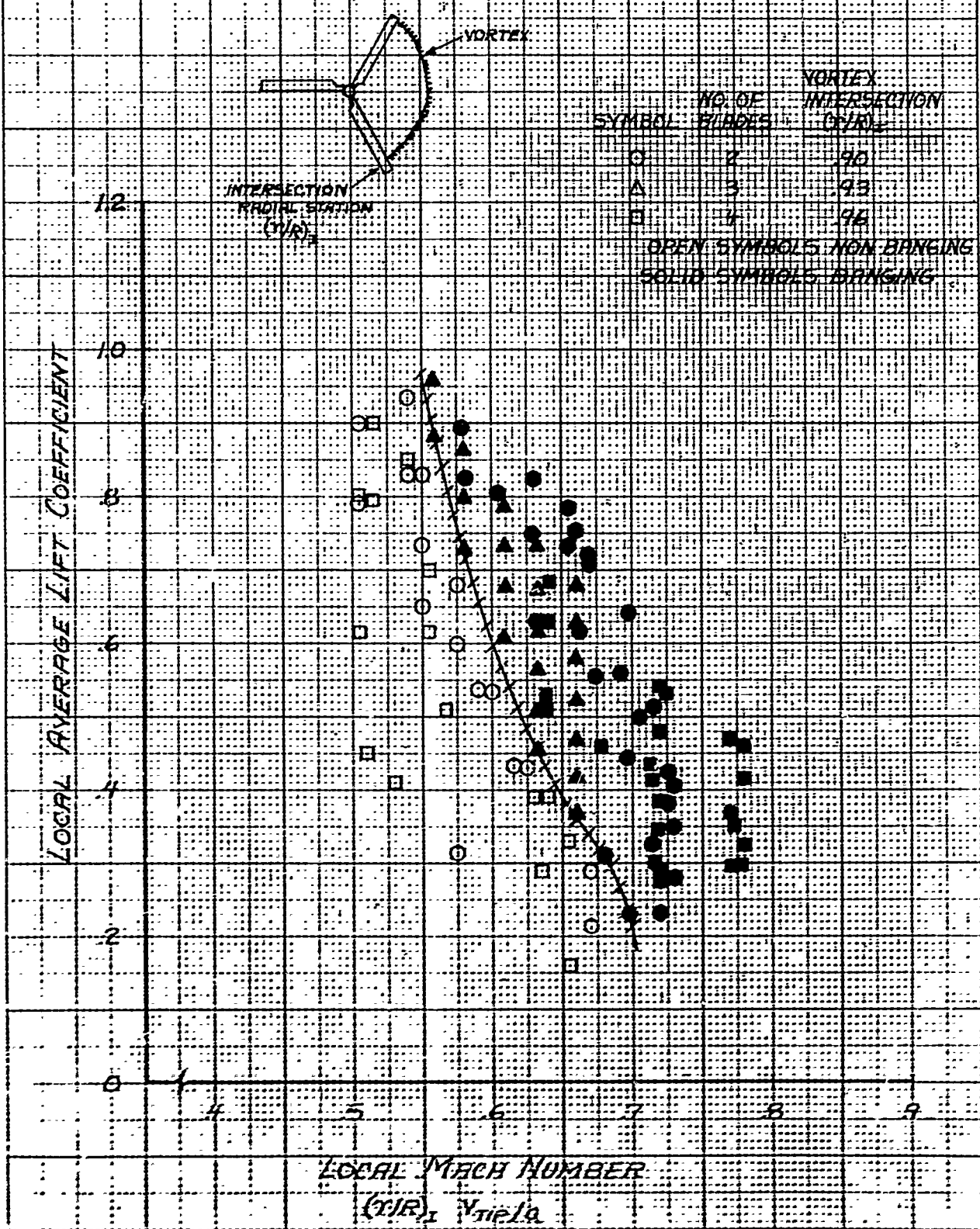


Figure 5.2

Boeing-Seattle 11-2172

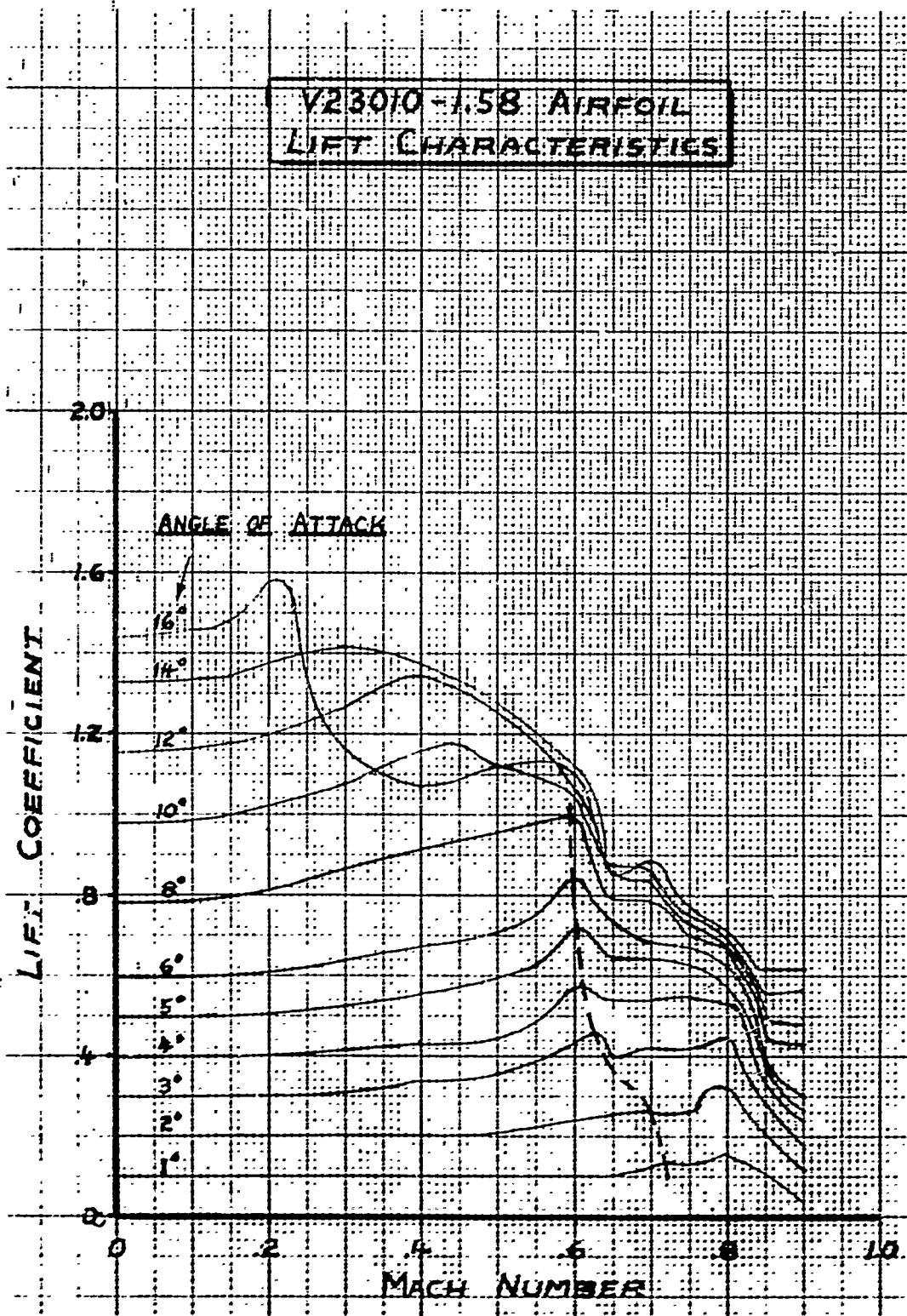


Figure 5.3

COMPARISON OF LIFT DIVERGENCE
AND NO IMPULSIVE NOISE BOUNDARIES

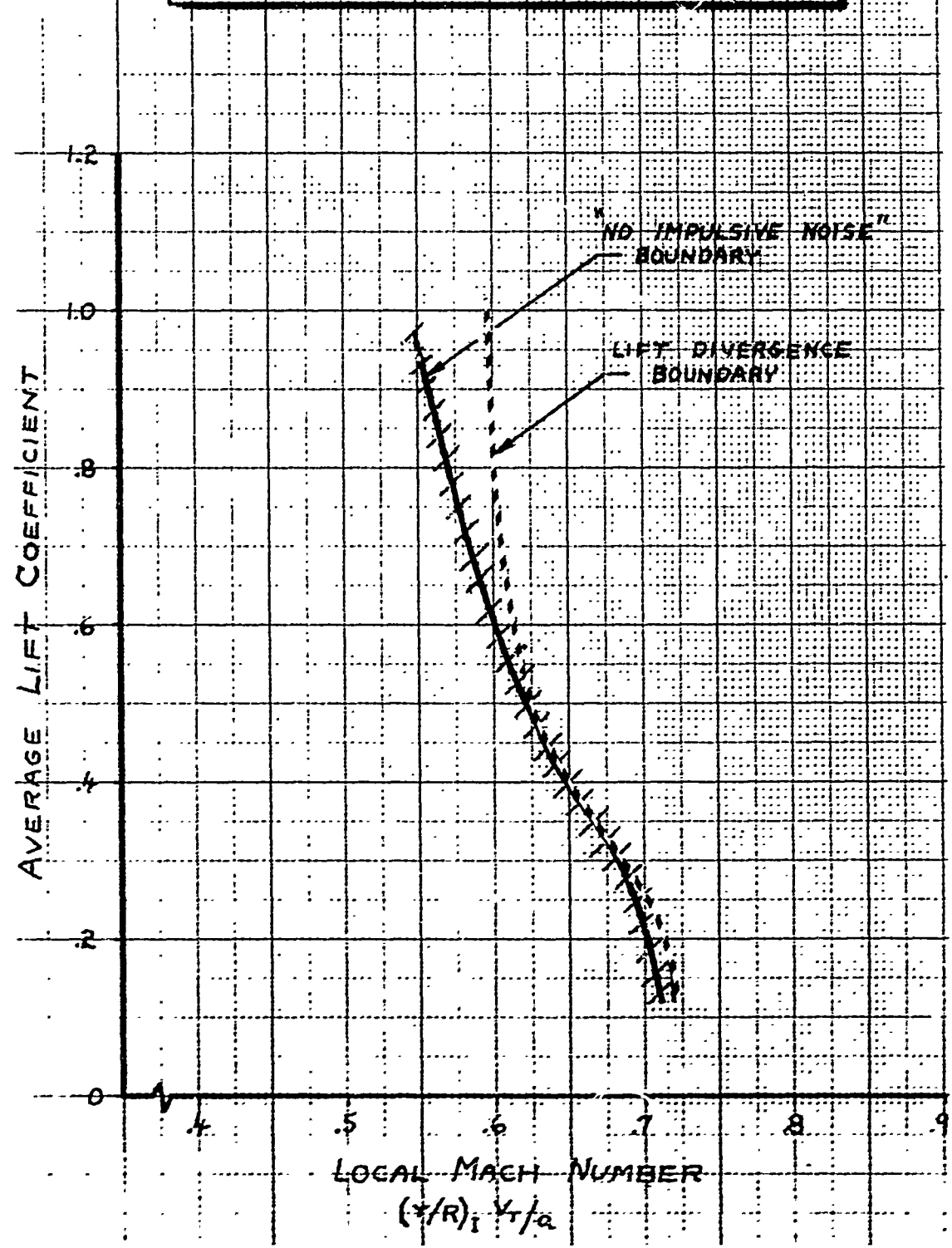


Figure 5.4

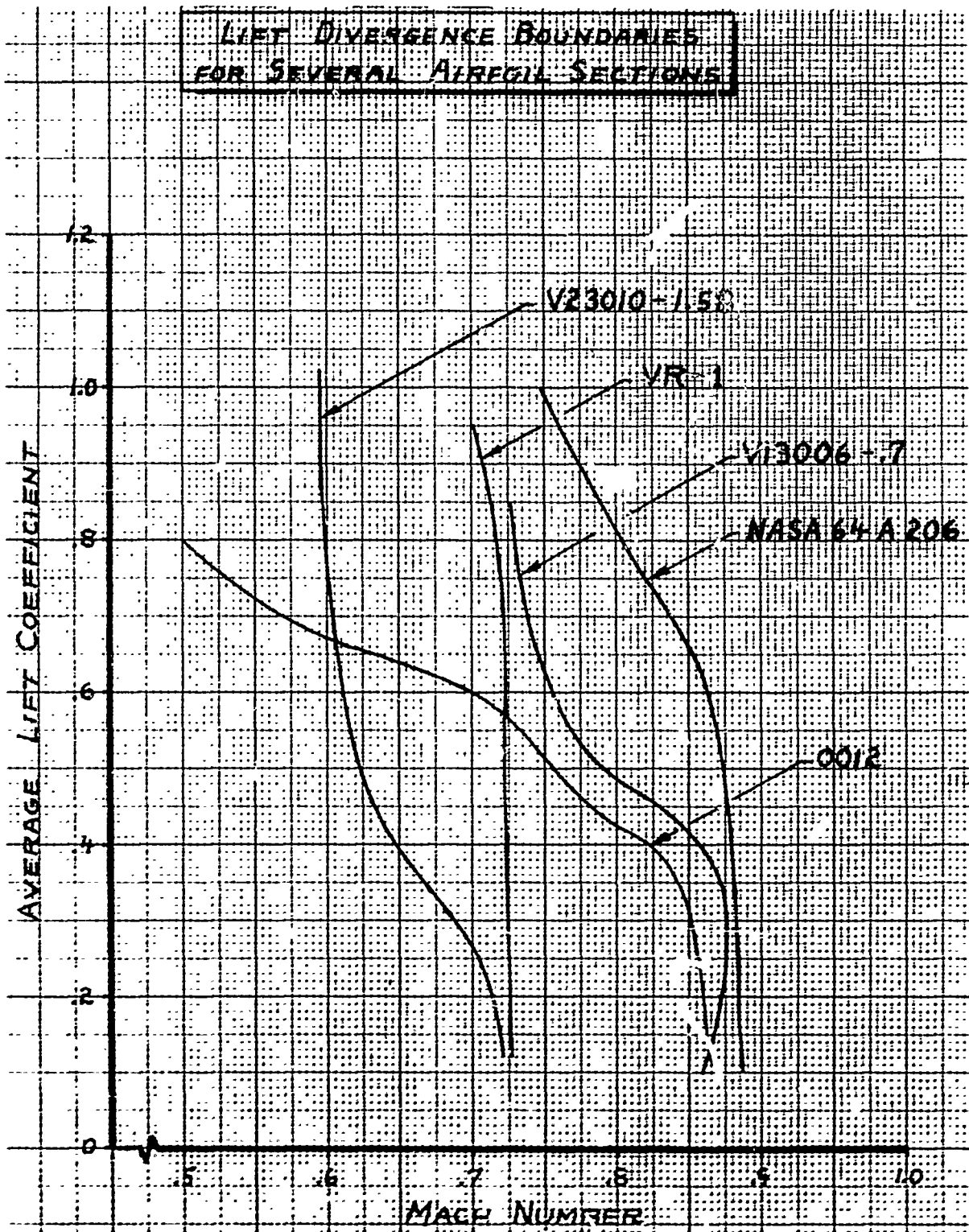


Figure 5.5

**WHIRL DIVER TEST OF
ADVANCED GEOMETRY BLADE ROTOR**

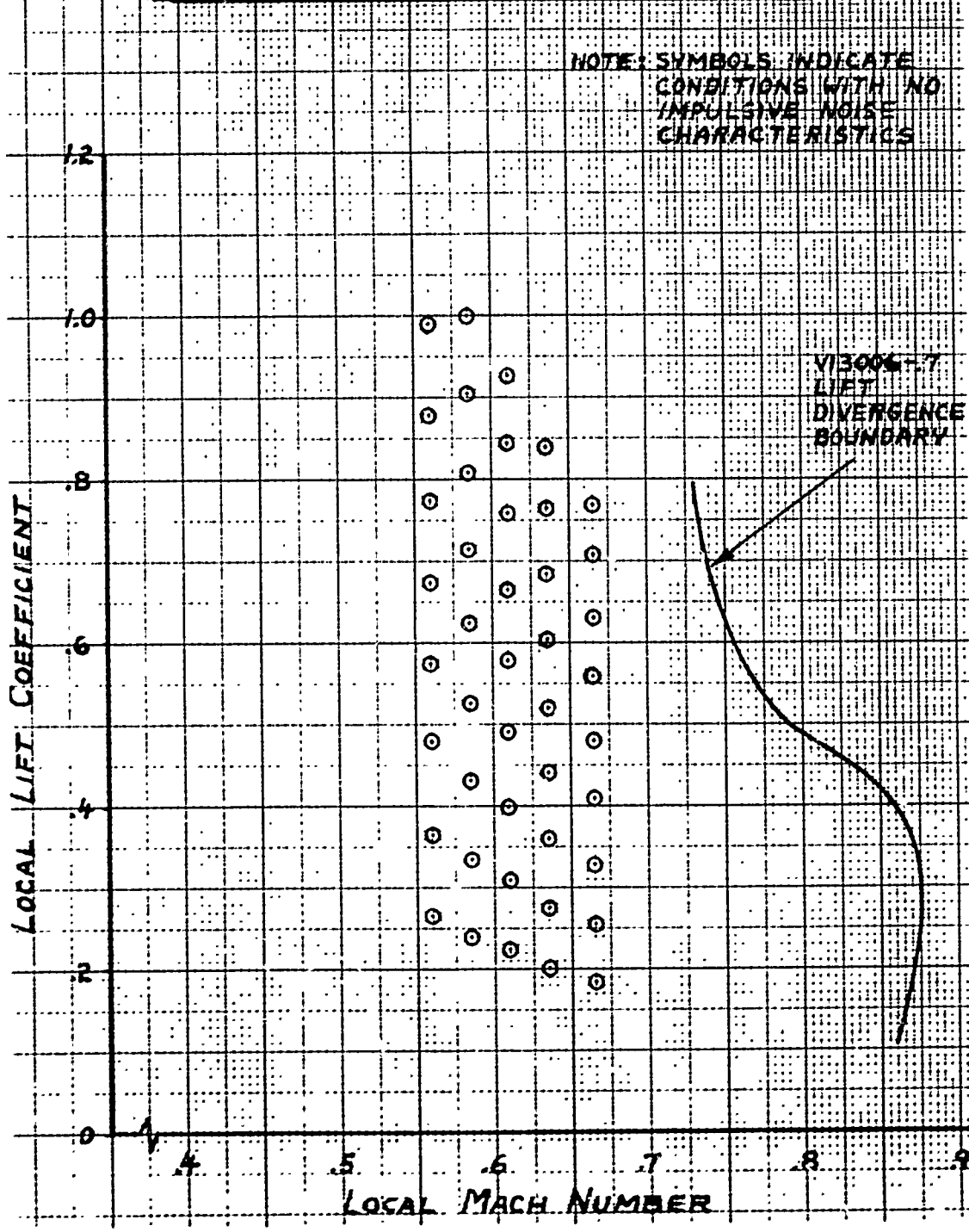


Figure 5.6

COMPARISON OF WHIRL TOWER
TEST CONDITIONS FOR
AGB AND CH-47 ROTORS

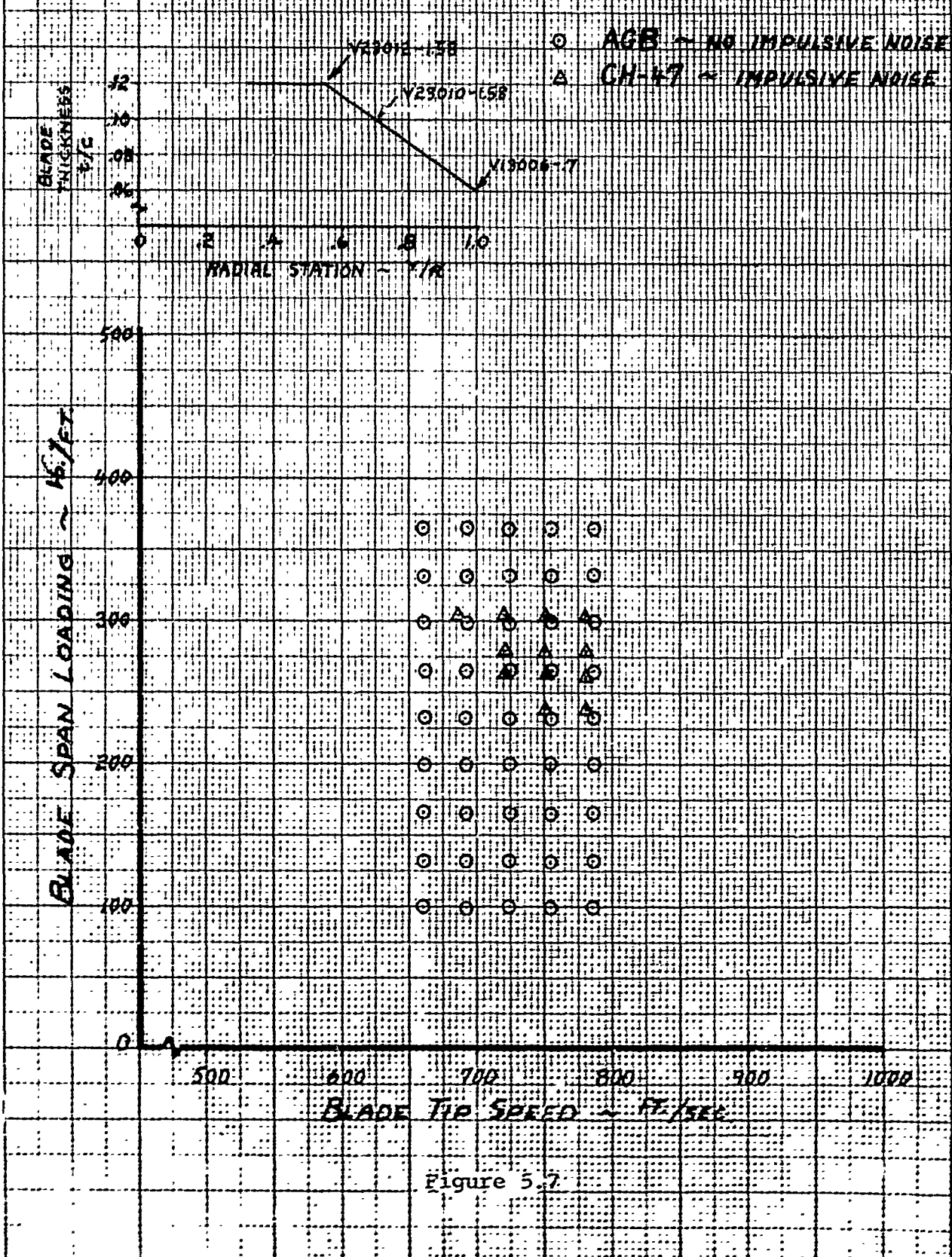


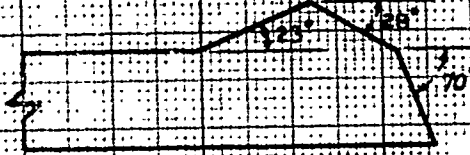
Figure 5.7

**THREE BLADED SWEEP-TIP
WHIRL TOWER TEST CONDITIONS**

NOTE: SYMBOLS INDICATE
CONDITIONS WITH NO
IMPULSIVE NOISE
CHARACTERISTICS

$\gamma/R = 90$

$\gamma/R = 92$



LOCAL AVERAGE LIFT COEFFICIENT

VE3010-1.58
LIFT
DIVERGENCE
BOUNDARY

0 .2 .4 .6 .8 1.0 1.2

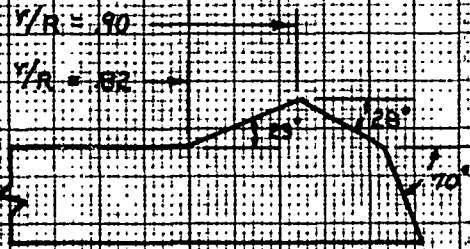
LOCAL MACH NUMBER

$(\gamma/R)_T V_T/a$

Figure 5.8

**THREE BLADED SWEEP-TIP
WHIRL TOWER TEST CONDITIONS**

NOTE: SYMBOLS INDICATE
CONDITIONS WITH NO
IMPULSIVE NOISE
CHARACTERISTICS



LOCAL AVERAGE LIFT COEFFICIENT

EFFECTIVE LOCAL MACH NUMBER

$$\left(\frac{Y}{R}\right) \sqrt{\cos \lambda} \cdot V/c$$

V23010-1.58
LIFT
DIVERGENCE
BOUNDARY

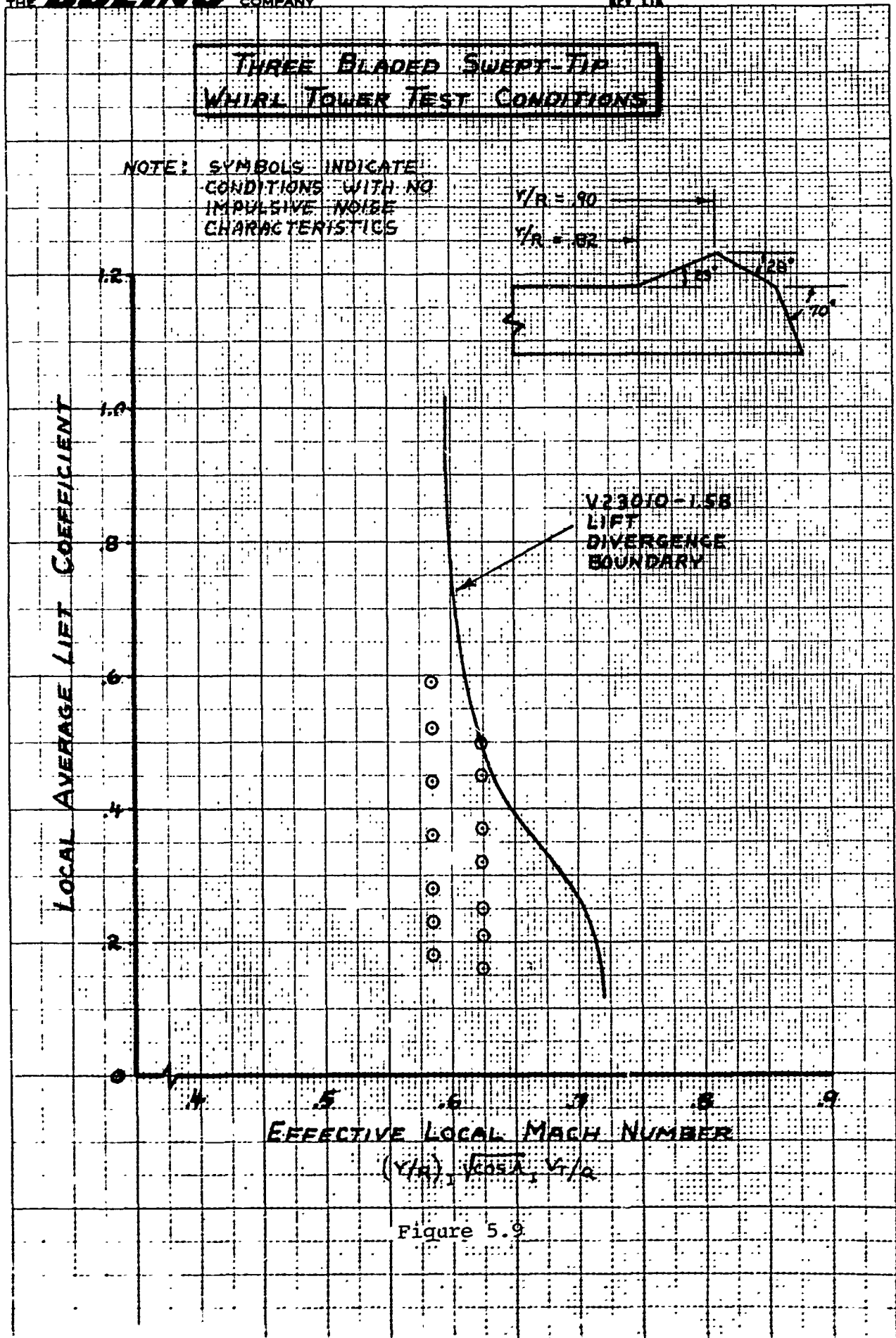


Figure 5.9

EFFECT OF FOLLOWING BLADE PASSAGE
ON VORTEX AXIAL POSITION

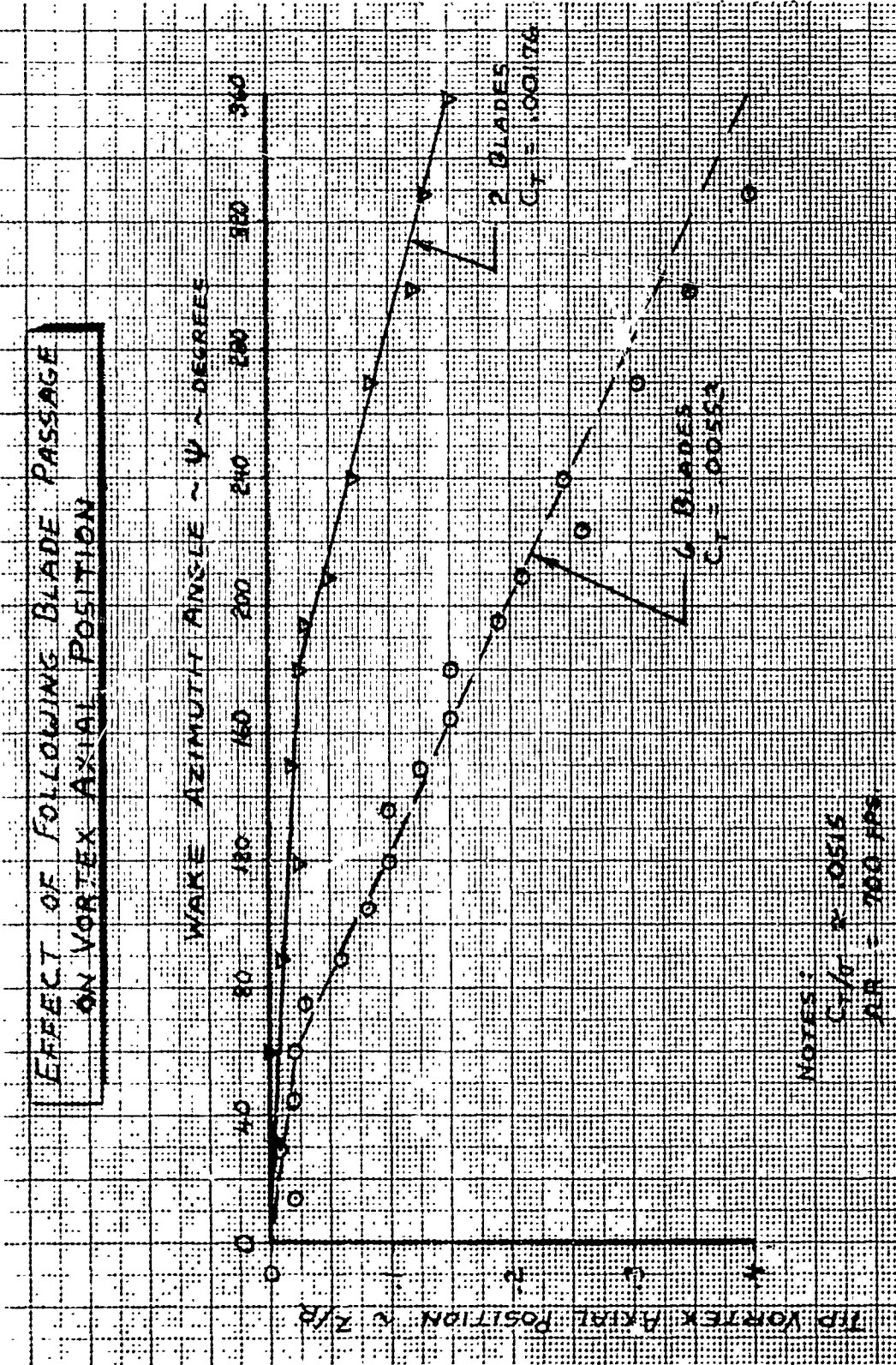


Figure 5.10

VERTICAL SEPARATION BETWEEN
TRAILED VORTEX AND FOLLOWING BLADE

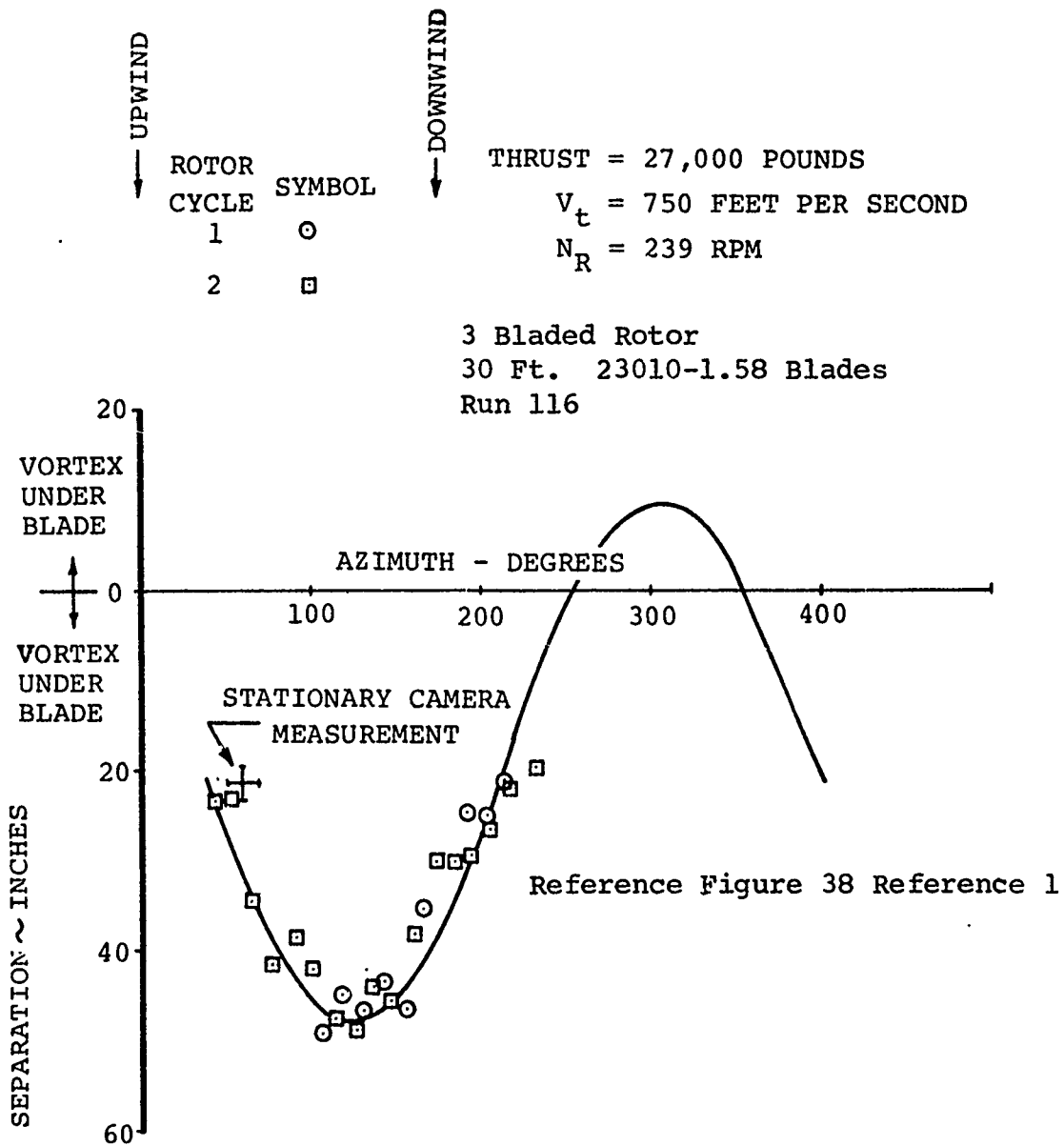


FIGURE 5.11

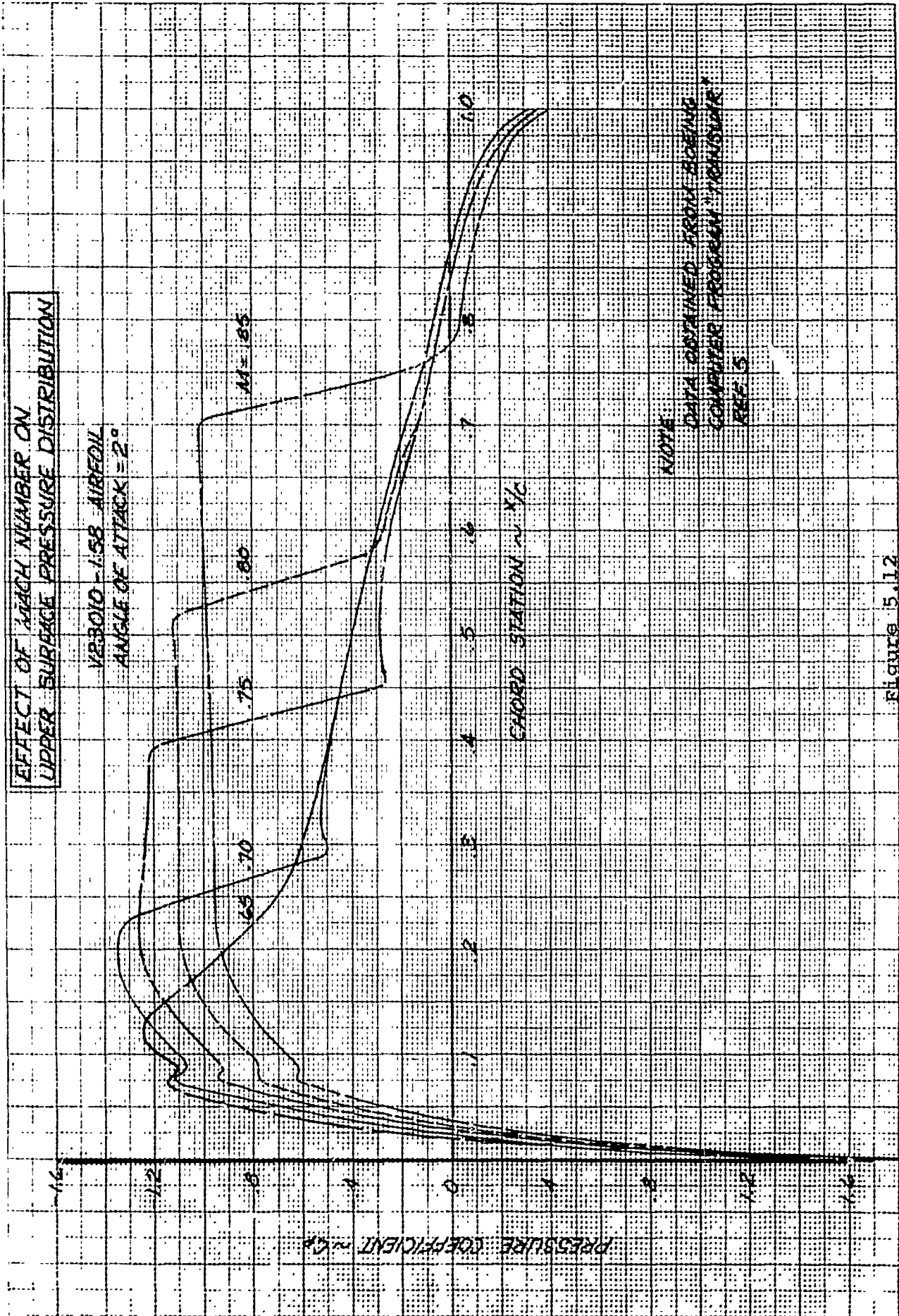


Figure 5.12

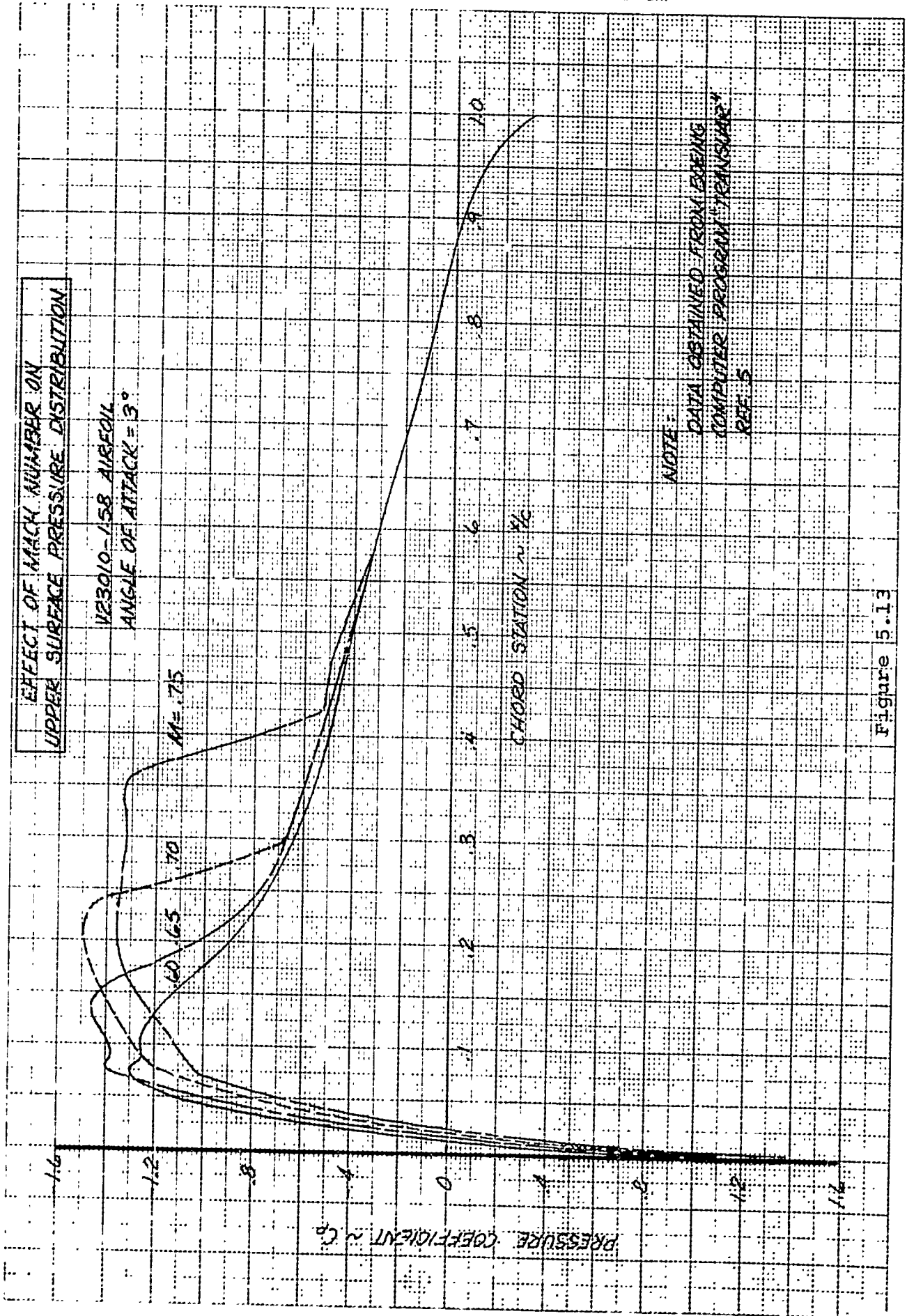


Figure 5.13

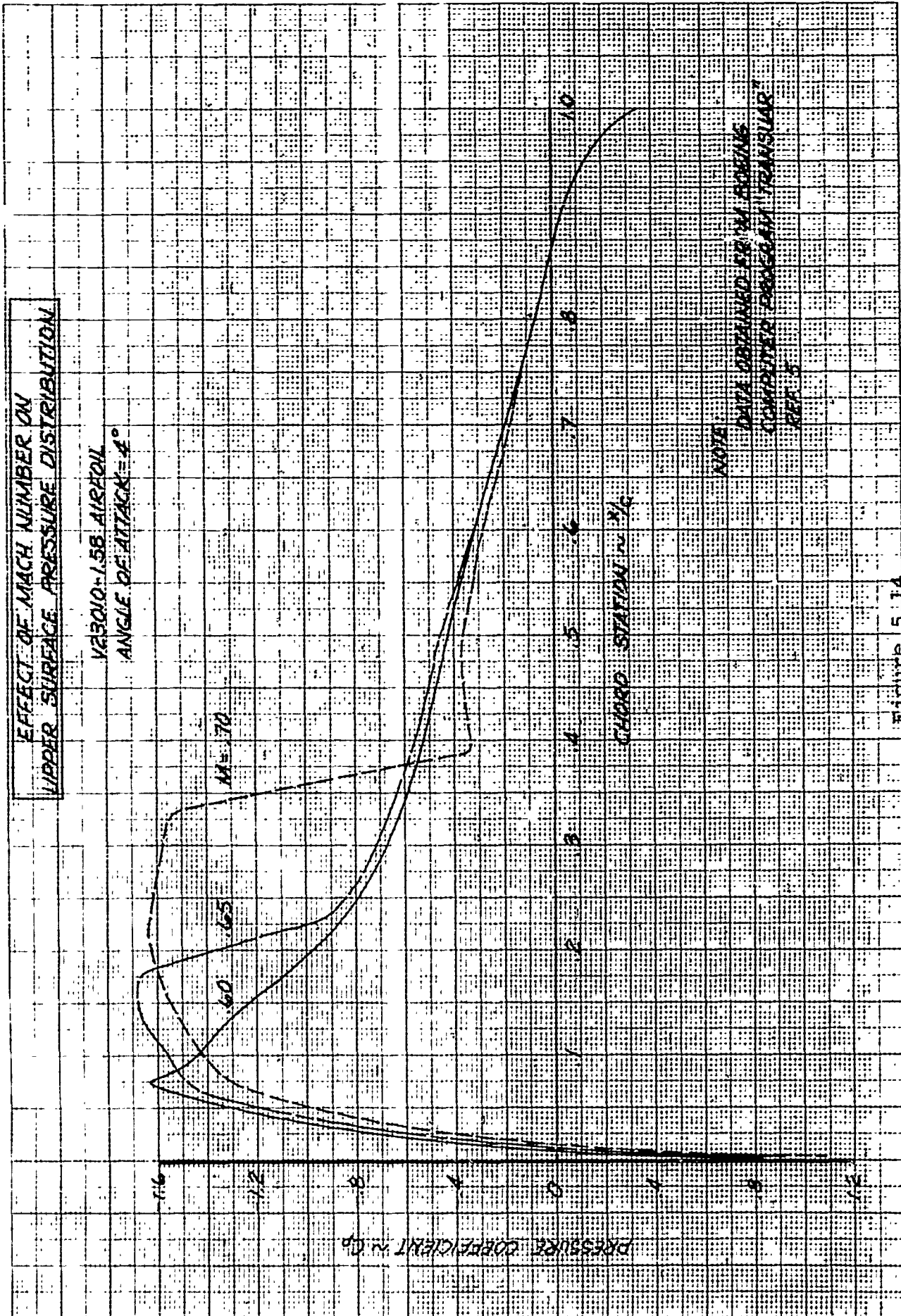


Figure 5.14

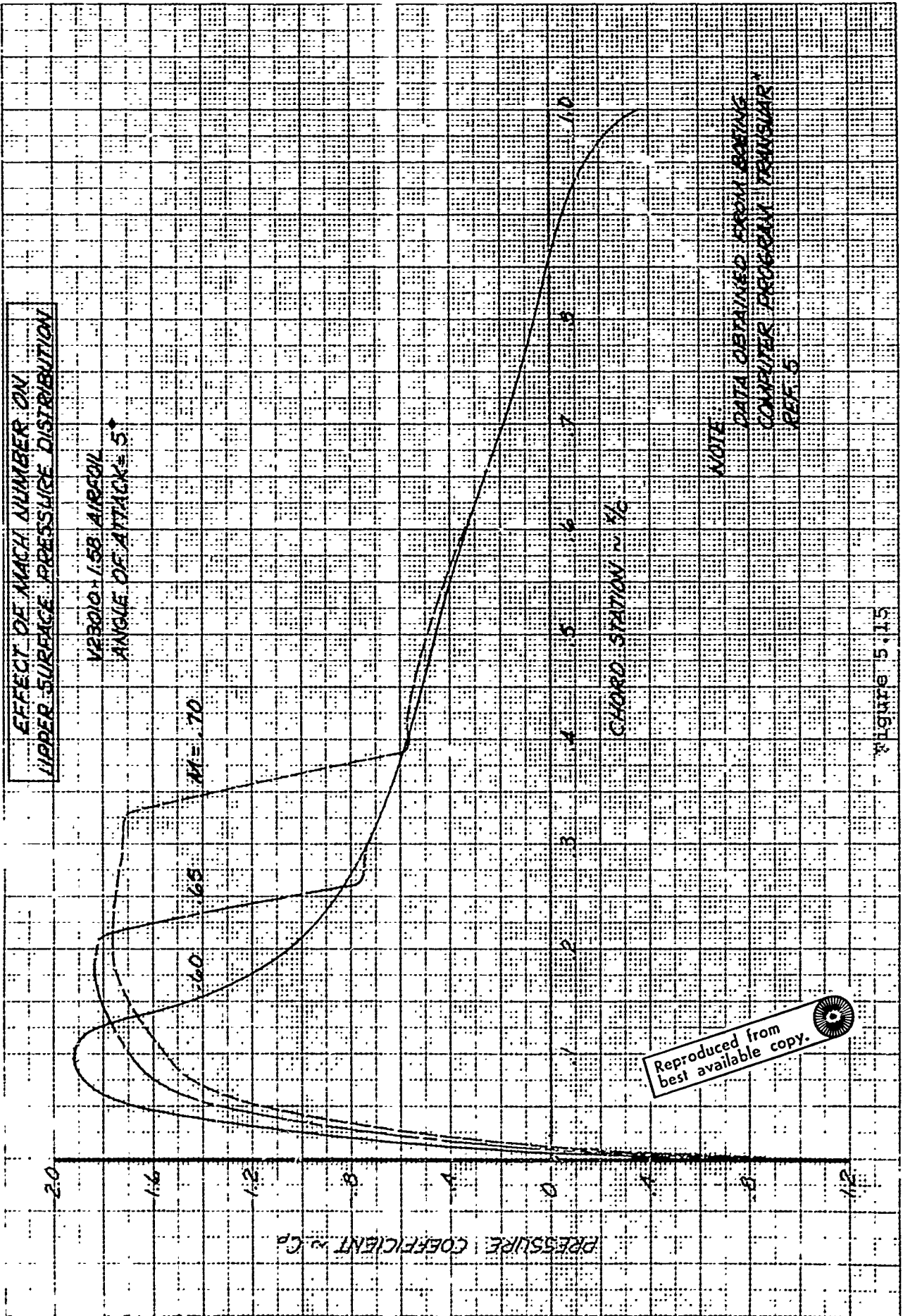


Figure 5.15

INCREMENT IN NORMAL FORCE
 COEFFICIENT DUE TO MOTION
 OF UPPER SURFACE SHOCK
 B-V 23010-1.58 AIRFOIL

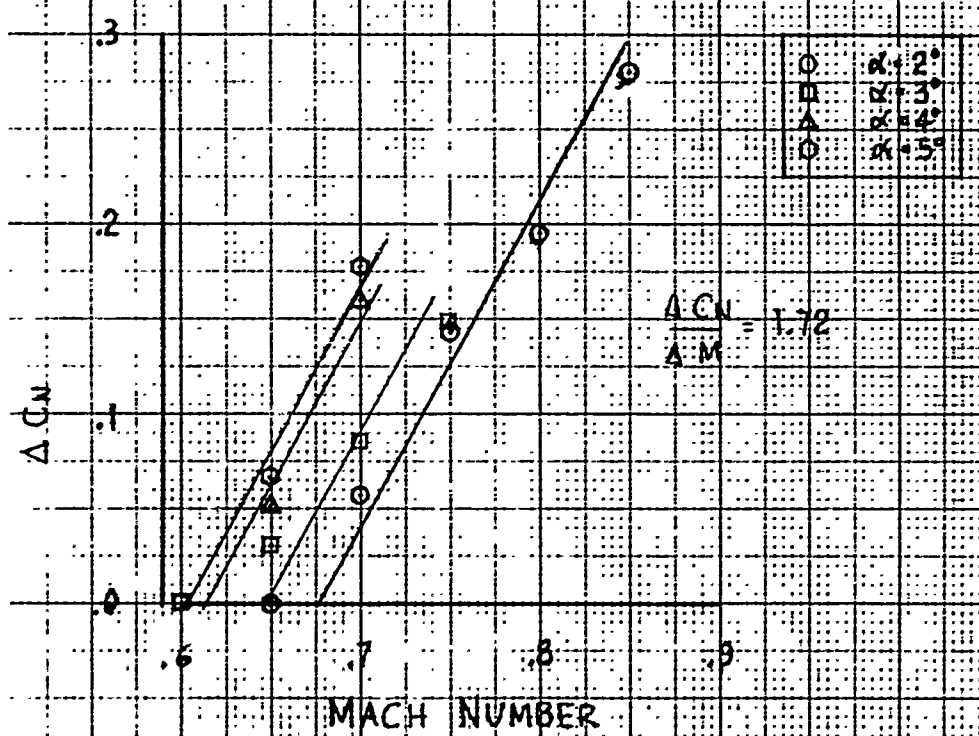


Figure 5.16

SINGLE ROTOR IMPULSIVE NOISE
REFERENCED TO LOCAL CONDITIONS AT
BLADE-VORTEX INTERSECTION POINTS

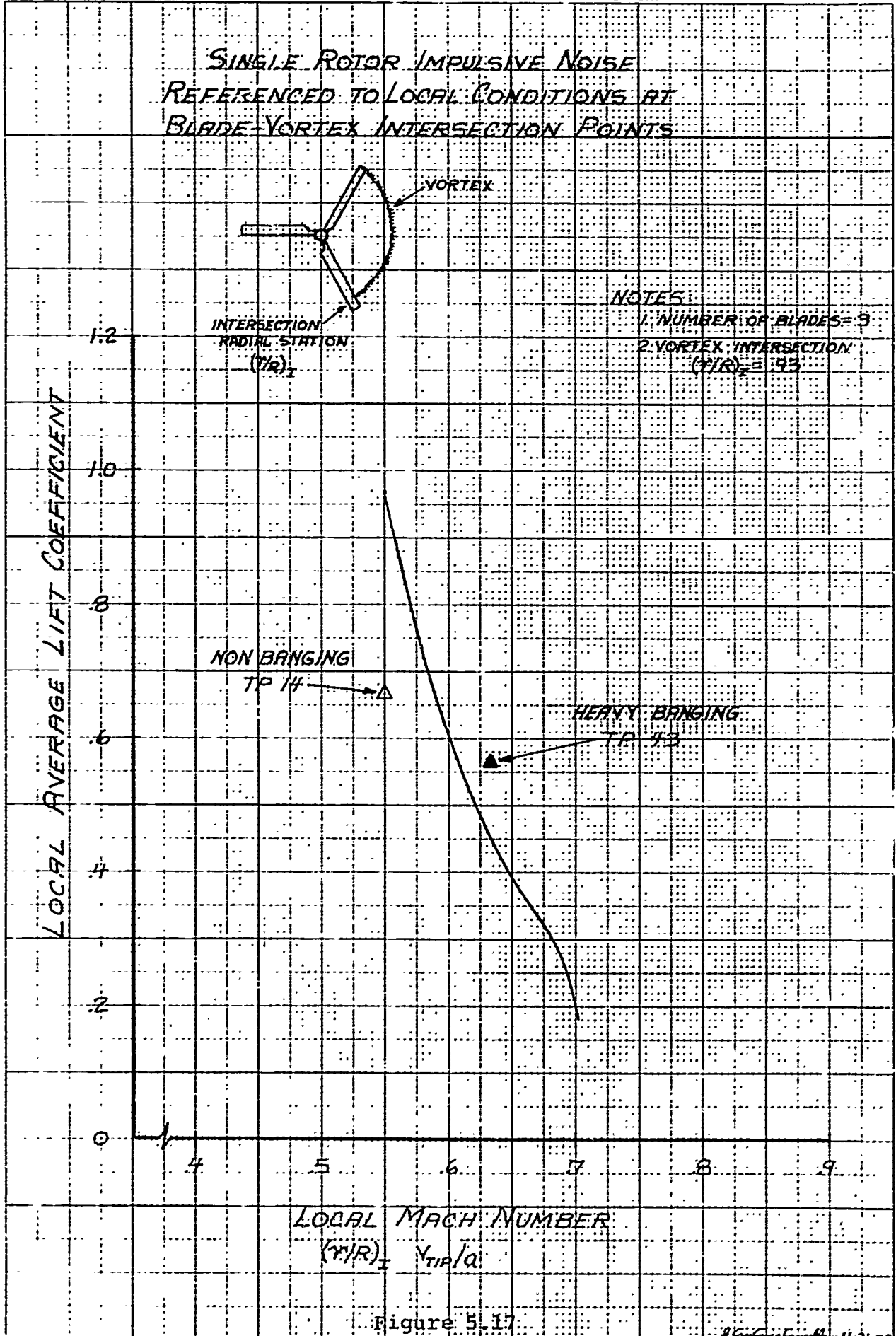


Figure 5.17

257500-11-21-72

REFERENCES

1. Sternfeld, H., Spencer, R.H., and Schairer, J.O., An Investigation of Noise Generation on a Hovering Rotor, for U.S. Army Research Office, Durham, North Carolina. Contract DAHC04-69-C-0087, January 1971.
2. Lawson, M.V., and Ollerhead, J.B., Studies of Helicopter Rotor Noise, U.S. Army Aviation Material Laboratories Report TR68-60, January 1969.
3. The Boeing Co., Vertol Division, Heavy Lift Helicopter, Advanced Technology Component Program U.S. Army Aviation Systems Command Contract DAAJ01-71-Q-0274
4. Kline, S.J., Similitude and Approximation Theory, McGraw Hill Book Company, Inc. 1965.
5. Paterson, R.W., Vogt, P.G., Amiet, R.K. Fink, M.R., Vortex Shedding Noise of an Isolated Airfoil, Helicopter Noise Symposium Proceedings, U.S. Army Research Office, Durham, Sept. 1971.
6. Beranek, L. L., Acoustics, McGraw Hill Book Company, Inc., 1954.
7. Stepniewski, W. Z., Introduction to Helicopter Aerodynamics, Rotorcraft Publishing Committee 1950.
8. Landgrebe, A.J., An Analytical and Experimental Investigation of Helicopter Rotor Hover Performance and Wake Geometry Characteristics, USAAMRDL Technical Report 71-24, June 1971.
9. Milne-Thomson, L. M., Theoretical Hydrodynamics, 4th Ed., The MacMillan Co., July 1960
10. Lindsey, W. F., and Landrun, E. J., Compilation of Information on the Transonic Attachment of Flows at the Leading Edges of Airfoils, NACA TN4204, February 1958.
11. Krupp, J. A., The Numerical Calculation of Plane Steady Transonic Flows Past Thin Lifting Airfoils, Boeing Scientific Research Laboratories, D180-12953-1, June 1971.

REFERENCES (Continued)

12. Johnson, W., Application of a Lifting-Surface Theory and the Calculation of Helicopter Airloads, Preprint No. 510, 27th Annual National V/STOL Forum of the AHS, May 1971.
13. Widnall, S., Helicopter Noise Due to Blade Vortex Interaction, The Journal of the Acoustical Society of America, Vol. 50, No. 1 (Part 2) 1971.
14. Dozanjth, D.S., Gasparek, E.D., Estrinazii, S., Decay of a Viscous Trailing Vortex, Aero Quarterly, Vol. XIII, May 1962.
15. McCormick, B.W., On The Cavitation Produced by a Vortex Trailing From a Lifting Surface, Journal of Basic Engineering, September 1962.
16. Rorke, J. B., Moffett, R. C., and Ward, J. F., Wind Tunnel Simulation of Full Scale Vortices Proceedings AHS Forum 1972.
17. Chigier, N.A., and Corsiglia, V.R., Tip Vortices - Velocity Distribution, Proceedings AHS Forum, 1971.

APPENDIX

WHIRL TOWER FREQUENCY CALIBRATION

A major concern in recording data when measurements of noise are made near the ground plane is the influence on a particular microphone of the combined wavefront from incident and reflected waves. The Reference 1 program utilized corrections to the measurements based on rotor noise as a source being similar to the impulse generated by the firing of a blank pistol cartridge. This method, while simulating impulse wavefronts, does not allow for phase changes in reflected rays based on frequency of an arriving front and does not totally explain differences between theory and data. It was desired to perform a more detailed acoustical calibration of the whirl tower by single frequency and then apply these corrections to the data prior to correlation with predictions.

The frequency calibration performed as part of this program did not explain the remaining differences between data and predictions and this may be due to the following factors. First, for simplicity the source of noise used consisted of a speaker mounted at the rotor hub and not along the blade radially where the source of the noise occurs during rotor operation. If blades had been available, mounting of a speaker along the radius might have been considered. Second, the source of noise consisting of pure tones rather than broadband impulse noise gives rise to corrections which are likely to be invalid for rotor noise which is a pulsed source consisting of a broad range of frequencies.

It must be assumed that a calibration combining the correct source location with a pulsed broadband source would achieve the desired correction for the tower data.

From the above it also appears that if data is being taken for the purpose of scientific investigation of rotor noise that microphones mounted in the ground plane may be preferable to avoid distortion.

The test setup which was used to accomplish this is shown in Figure I-1. Pure tones of noise were used for the calibration over a range of frequencies beginning at 100 Hz and extending to about 5,000 Hz. A speaker was mounted on the rotor hub and oriented toward the ground microphones. A microphone was located near this source as shown in Figure I-1 to monitor the level of the source. A microphone was placed on a tripod at the height and location where measurements were recorded for the Reference 1

program, and also as close to the ground plane as possible at the point where the reflected wavefront for the data microphone intercepted the ground plane. In addition a fourth microphone was located along the wavefront midway between the ground and data microphone. Although not required for this program, data from this latter microphone could be used to verify the calibration corrections for the data microphone, even though it contains a phase angle shift.

Tapes of pure tones were played on an Ampex SP-300 tape recorder and the output was put through a power amplifier to the tower speaker as well as to one channel of an Ampex AR-200 tape recorder. The tones generated were at the 1/3 octave band center frequencies, and were approximately 35 seconds in length. Due to limitations of the speaker, tones below 100 Hz at a suitable level were not reproducible and corrections below this frequency are not available.

Microphone 3, Figure I-1, records only the incident wavefronts from the speaker, while microphone 1 records both incident and reflected waves. Therefore the difference in data of 4-3 from 4-1 (or 1-3) is due to reflection and is, by definition, the correction which should be applied to the data microphone to obtain free field levels. A very small correction, +0.5 dB, should also be applied to the difference in level of microphone 4 to microphone 3 before it is subtracted from the level difference between microphone 4 and microphone 1 since microphone 4 is positioned 7.9 feet short of microphone 1.

Figure I-2 compares the level difference between microphones 4 and 3 with the level difference between microphones 4 and 1. Note that the ground microphone amplitude (4-3) is relatively constant with frequency while the data microphone (4-1) displays a large amplitude variation. The difference between microphones 1 and 3 is plotted in Figure I-3.

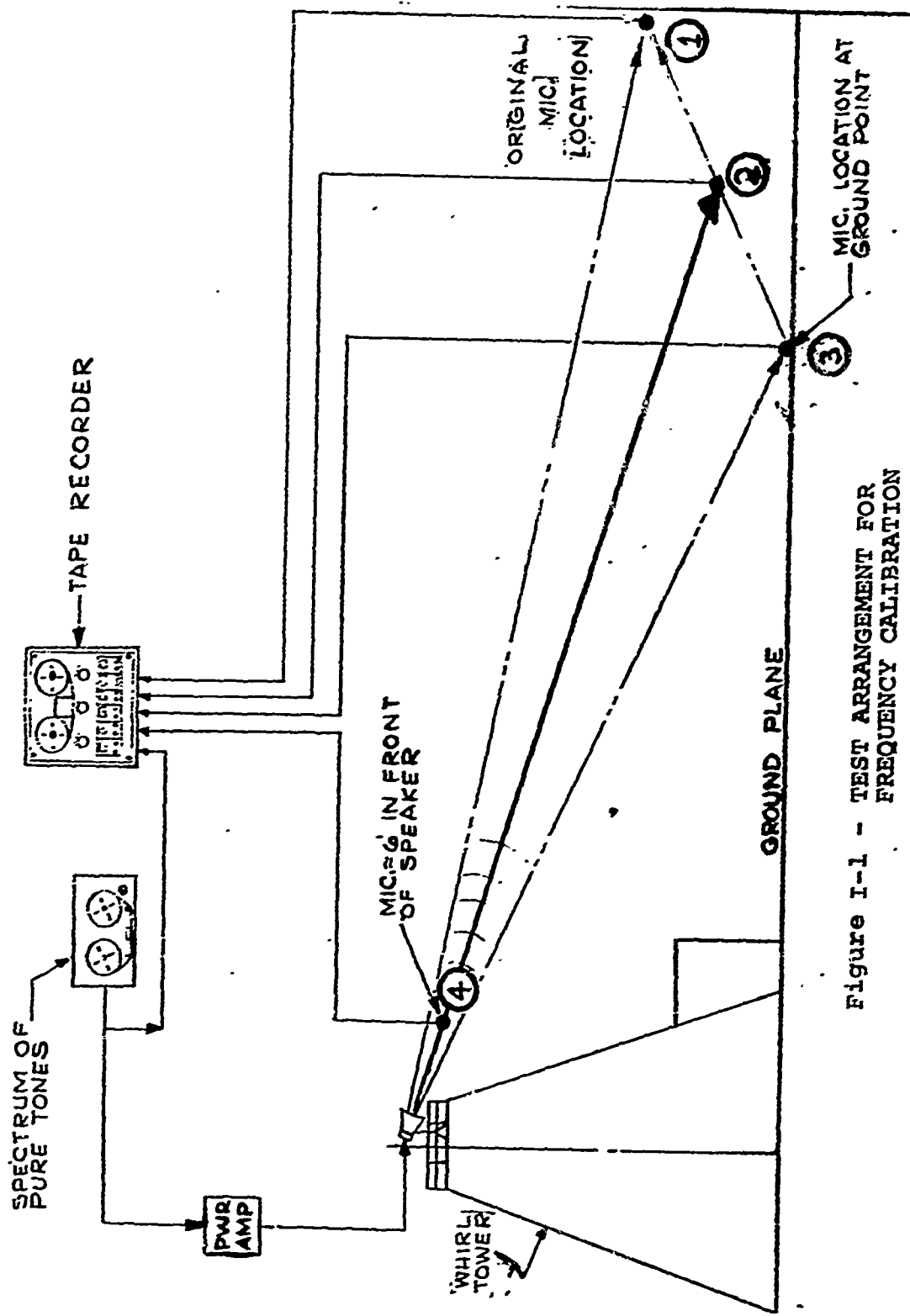
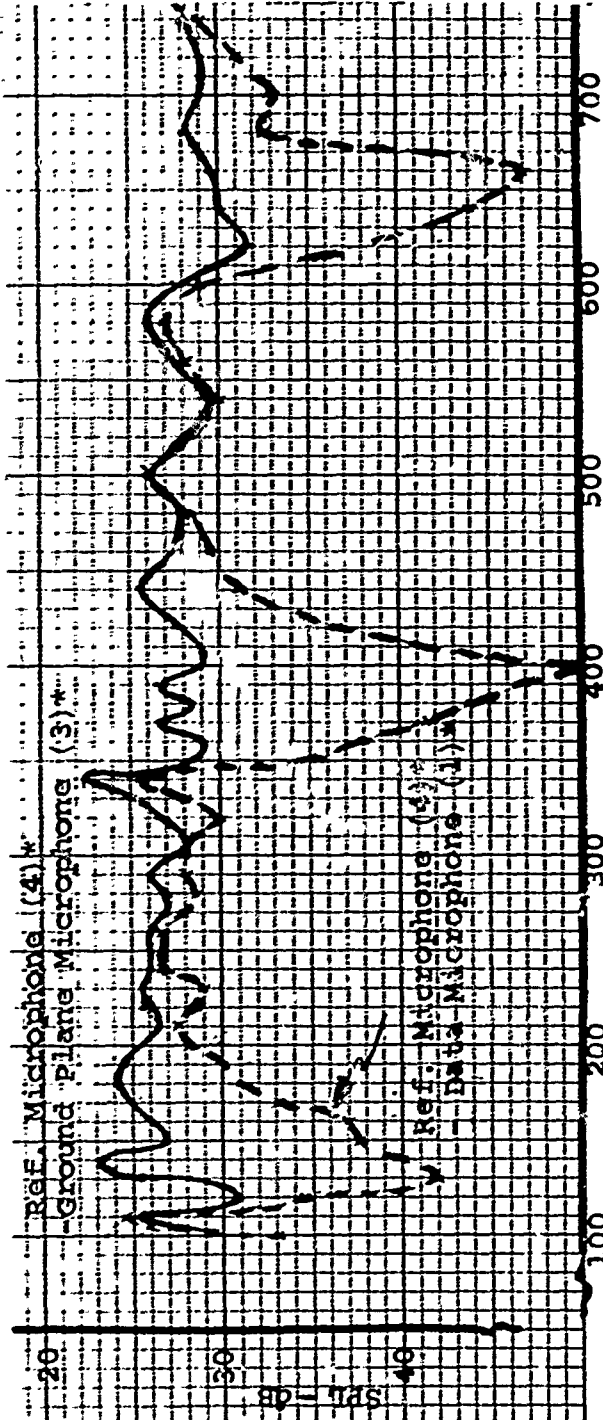
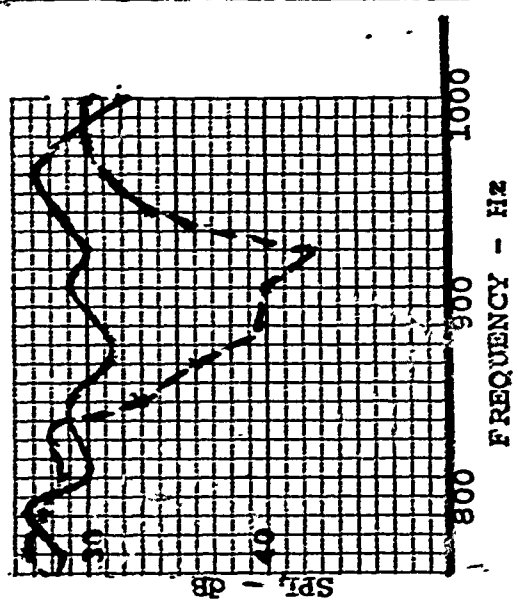


Figure I-1 - TEST ARRANGEMENT FOR FREQUENCY CALIBRATION



FREQUENCY - Hz



FREQUENCY - Hz

(*) Reference Figure I-1

Figure I-2 - COMPARISON OF MEASURED SOUND LEVEL DIFFERENCES

